SATELLITE ATTITUDE DETERMINATION BASED ON GPS CARRIER PHASE MEASUREMENTS

A THESIS SUBMITTED TO
THE GRADUATE SCHOOL OF NATURAL AND APPLIED SCIENCES
OF
MIDDLE EAST TECHNICAL UNIVERSITY

BY

EVRİM ÖZTEN

IN PARTIAL FULLFILLMENT OF THE REQUIREMENTS
FOR
THE DEGREE OF MASTER OF SCIENCE
IN
AEROSPACE ENGINEERING

AUGUST 2013

Approval of the thesis:

SATELLITE ATTITUDE DETERMINATION BASED ON GPS CARRIER PHASE MEASUREMENTS

submitted by **EVRİM ÖZTEN** in partial fulfillment of the requirements for the degree of **Master of Science in Aerospace Engineering Department, Middle East Technical University** by,

Prof. Dr. Canan Özgen
Dean, Graduate School of **Natural and Applied Sciences** _____

Prof. Dr. Ozan Tekinalp
Head of Department, **Aerospace Engineering** _____

Prof. Dr. Ozan Tekinalp
Supervisor, **Aerospace Engineering** _____

Examining Committee Members

Prof. Dr. Serkan Özgen
Aerospace Engineering Dept., METU _____

Prof. Dr. Ozan Tekinalp
Aerospace Engineering Dept., METU _____

Asst. Prof. Dr. Ali Türker Kutay
Aerospace Engineering Dept., METU _____

Prof. Dr. Bülent E. Platin
Mechanical Engineering Dept., METU _____

Prof. Dr. Kemal Leblebicioğlu
Electrical and Electronics Engineering Dept., METU _____

Date: **16.08.2013**

I hereby declare that all information in this document has been obtained and presented in accordance with academic rules and ethical conduct. I also declare that, as required by these rules and conduct, I have fully cited and referenced all material and results that are not original to this work.

Name, Last name : Evrim ÖZTEN

Signature :

ABSTRACT

SATELLITE ATTITUDE DETERMINATION BASED ON GPS CARRIER PHASE MEASUREMENTS

Özten, Evrim

M.Sc., Department of Aerospace Engineering

Supervisor: Prof Dr. Ozan Tekinalp

August 2013, 101 Pages

With the developments in the GPS receiver technology, GPS receivers have been preferable equipments also for the space applications. In the early eighties, they have been used only for position, velocity and time determination. With the further improvements, it has been proven that they can provide not only the positioning information, but also attitude knowledge with the accuracy less than 1 degree.

In this thesis, an estimation algorithm is developed in the MATLAB Simulink environment for the attitude determination using the GPS carrier phase measurements from four antennas. Because the attitude dynamics of a satellite is nonlinear, Extended Kalman Filter (EKF), a nonlinear estimator, is decided to use.

The algorithm is implemented using three quaternion and three inertial angular velocity error states. For the attitude determination, four antennas in a square shape with 1 meter inter-antenna distance are assumed to be used.

A simulation is conducted in order to evaluate the performance of the algorithm. The simulation includes a satellite in J2 perturbed orbit. The yaw stabilization of the satellite is maintained by using a momentum wheel with a spin axis perpendicular to the orbit plane.

GPS pseudorange, pseudorange rate and differential carrier phase measurements are also modeled in the simulation environment. Because most of the measurement errors are quite small in the carrier phase measurement or they mostly cancel out after the single differencing process, only the multipath error and receiver noise is modeled in the simulation.

An integrated GPS/Gyro case is also considered in this study. For the integrated GPS/Gyro case, the developed EKF is modified by adding gyro bias drift parameter to the state vector. In order to model the gyro measurements, a gyroscope error model is developed. The gyro measurements are generated by adding errors like bias, bias drift, scale factor and misalignment to the true angular rates.

The algorithms developed for GPS only and GPS/Gyro integrated cases are tested with different GPS visibility conditions.

After the simulation test, it is observed that the achieved attitude accuracy with the GPS only case is better than 0.4 degrees. Moreover, the integration with three axis gyro assembly improves the attitude performance especially for the cases with poor GPS satellite visibility.

Keywords: Spacecraft Attitude Determination, GPS Based Attitude Determination, GPS/Gyro Integration, EKF.

ÖZ

GPS TAŞIYICI FAZ ÖLÇÜMLERİNİN KULLANILARAK UYDULARIN AÇISAL KONUMUNUN BERLİRLENMESİ

Özten, Evrim

Yüksek Lisans, Havacılık ve Uzay Mühendisliği Bölümü

Tez Yöneticisi: Prof. Dr. Ozan Tekinalp

Ağustos 2013, 101 Sayfa

Gelişen GPS alıcısı teknolojisi ile bu alıcılar uzay tabanlı uygulamalarda birçok açıdan tercih edilen bir donanım halini aldılar. Seksenli yılların başlarında GPS alıcıları sadece konum, hız ve zaman bilgisi elde etmek amaçlı kullanılıyordu. Alıcı teknolojisindeki yeni gelişmelerle, GPS alıcılarının sadece konum belirleme amaçlı değil, ayrıca açısal konum belirleme amaçlı da kullanılabileceği ve bu yöntemle elde edilen açı bilgisinin 1 dereceden daha az hatayla elde edilebileceği kanıtlandı.

Bu tezde, GPS taşıyıcı faz ölçümlerinin kullanılarak açısal konum saptaması yapan bir kestirim algoritması geliştirilmiştir. Algoritmanın geliştirilmesi sırasında MATLAB Simulink programı kullanılmıştır. Uydu dinamiğinin doğrusal olmamasından dolayı, kestirim algoritması olarak Genişletilmiş Kalman Filtresi (GKF) kullanımı tercih edilmiştir.

Algoritmada durum parametreleri üç adet "quaternion" hatası ve üç adet açısal hız hatasından oluşmaktadır. Algoritmanın oluşturulması sırasında aralarında 1 metre mesafe olan ve kare şeklinde bir geometri oluşturan 4 antenden oluşan bir konfigürasyonun kullanıldığı varsayılmıştır.

Algoritmanın performansı geliştirilen benzetim çalışması test edilmiştir. Oluşturulan benzetimde, uydunun yörüngesinde ki hareketi modellenirken sadece Dünya'nın basıklık sabitinden, J2, etkilendiği varsayılmıştır. Uydunun sapma açısının kararlılığının, sisteme eklenen bir momentum tekerleği ile sağlandığı varsayılmış ve modellenmiştir.

GPS pseudorange, pseudorange rate ve taşıyıcı faz farkı ölçümlerinin modellemesi de benzetim ortamında gerçekleştirilmiştir. Birçok hata parametresinin taşıyıcı faz ölçümleri üzerindeki etkisi çok küçük olduğundan veya fark alma işlemi sırasında bu hatalarının büyük bir kısmının ortadan kaldırılmasından dolayı, sadece sinyal yansıma hatası (multipath) ve alıcı gürültüsü hataları modellenmiştir.

Bu tezde aynı zamanda tümleşik bir GPS/Dönüölçer sistemi de düşünülmüştür. Bu sitem için geliştirilen Genişletilmiş Kalman Filtresinde durum vektörüne 3 eksende dönüölçer sabit hata kayması parametresi eklenmiştir. Algoritmanın simülasyon ortamında test edilmesi

sırasında kullanılan dönüölçer verisi, modellenen dönüölçer hata modeli ile doğru veri üzerine, sabit hata, sabit hata kayması, orantı katsayısı hatası ve eksenel kaçıklık gibi hatalar eklenerek üretilmiştir.

Geliştirilen iki algoritma farklı şartlar altında test edilmiştir.

Benzetim testinden sonra elde edilen sonuçlar açı kestirimi doğruluğunun 0.4 dereceden iyi olduğunu göstermektedir. Ayrıca, üç eksenli bir dönüölçerin sisteme entegre edilmesinin, açı kestiriminin doğruluğunu, özellikle az sayıda GPS uydusunun görünür olduğu durumlarda iyileştirdiği gözlenmiştir.

Anahtar Kelimeler: Uydu Açısal Konum Belirlemesi, GPS Tabanlı Açı Belirlemesi, GPS/Dönüölçer Tümleşik Sistem, Genişletilmiş Kalman Filtresi.

ACKNOWLEDGEMENTS

I would like to express my sincere thanks to my supervisor Prof. Dr. Ozan Tekinalp for his guidance, advice and support throughout this thesis.

I am also thankful to my dear friend Zeynep Özcan for her encouragement throughout this study.

Finally, I would like to express my special thanks to my colleagues at ROKETSAN Inc. for their patience, support, encouragements and friendship.

TABLE OF CONTENTS

LIST OF FIGURES

FIGURES

LIST OF TABLES

TABLES

LIST OF ABBREVIATIONS

A/D : Analog/Digital

C/A : Coarse Acquisition

CCD : Charged-Coupled Device

DOP : Dilution of Precision

ECI : Earth Centered Inertial

ECEF : Earth Centered Earth Fixed

EKF : Extended Kalman Filter

FOG : Fiber Optic Gyroscope

FOV : Field of View

GEO : Geosynchronous Earth Orbit

GPS : Global Positioning System

Gyro : Gyroscope

MEMS : Micro Electro-Mechanical Systems

LEO : Low Earth Orbit

RMS : Root Mean Square

RLG : Ring Laser Gyro

PRN : Pseudo-Random Noise

CHAPTER 1

INTRODUCTION

1.1 BACKGROUND

The Global Positioning System (GPS) is a space-based radio positioning and time transfer system. Nowadays, GPS provides a global coverage. It is owned and operated by the U.S. Government. The rapid improvements in the GPS technology have been made it a widely used technology for the navigation purposes. Over the past years, GPS receivers have been used in the land, sea, air and even in the space applications for the position, velocity and time determination purposes.

For the applications where not only the positioning information, but also the attitude of the vehicle is required, some attitude sensors, such as star trackers, sun sensors, horizon sensors, magnetometers, gyroscopes or the combination of these sensors, can be used conventionally. The most accurate attitude information is obtained by using the star trackers, which has accuracy of several arc-seconds [1]. The least accurate one is the magnetometers. The attitude estimation obtained by the use of magnetometers has accuracy of 1 degree to several degrees [1].

By using a GPS receiver, it is also possible to determine the attitude of a vehicle, in addition to the position, velocity and timing information. There are several methods in order to calculate the attitude of the vehicle using the GPS signals. One method is based on the use of the signal to noise ratio of measurements [2]. The most common method is based on a multiple antenna GPS receiver system. In such a system, in order to obtain the attitude in three axes, at least three GPS antennas are integrated with a proper, well known distance between each other and with a proper geometry.

The knowledge of the relative positioning between antennas with high accuracy is required to obtain precise GPS based attitude estimation. In order to achieve that accuracy, the carrier phase measurements are preferred to be used in the attitude determination calculations. Moreover, because the differential measurements are used in the estimation algorithm, most of the errors like satellite clock errors, atmospheric errors, satellite position and velocity errors are cancelled out for short baselines. Then, by using the differential carrier phase measurements from the multi-antenna system, it is possible to calculate the attitude of the vehicle with the accuracy of 0.1 - 0.5 degrees [3].

The problem arising by the use of carrier phase measurements is the integer cycle ambiguity problem. This problem can be described as the unknown number of integer cycles in the received signal. Therefore, ambiguity resolution is required with high accuracy before the attitude estimation process.

Because a GPS receiver is almost certainly employed on the satellites for positioning and time determination purposes, if the attitude accuracy requirement of the mission is satisfied, using GPS receivers also for attitude determination instead of additional attitude sensors provides advantages in terms of cost and reliability.

One example of a satellite with GPS based attitude determination system is U.S. Air Force RADCAL satellite, launched in June 1993. It is the first spacecraft using GPS attitude system [4]. It is a small, gravity gradient stabilized satellite to calibrate the Space Command radars to determine orbital positions of other satellites to within a few meters. A Trimble TANS Quadrex receiver was employed for the attitude determination. Four microstrip patch antennas were mounted on the top of the spacecraft. The RADCAL data were post processed in order to determine the attitude of the satellite. The attitude accuracy of 0.75 degrees rms was obtained by using 0.67m long baselines. Also the error sources were evaluated after the experiment. It was demonstrated that the measurements errors are dominated by the multipath errors.

CRISTA-SPAS, on the other hand, was the first satellite employing a real-time GPS based attitude determination system. It was launched in November 1994. It was designed to analyze dynamical processes in the middle atmosphere and developed by Diamler-Benz Aerospace (DASA). A Trimble TANS Vector GPS receiver was used for the attitude estimation [4].

The other example of space-based experiment of GPS attitude system is the GPS Attitude and Navigation Experiment (GANE), which was launched in May 1996 by NASA. The experiment was designed to verify the attitude determination accuracy of GPS to lessen the risk of this technology for the International Space Station (ISS). A Trimble TANS Vector GPS receiver with four patch antennas was used to measure attitude, as well as navigation and overall performance on orbit. An inertial reference unit (IRU) was used as the reference for the attitude calculated in the post-processing. The experiment showed that the GPS attitude estimation accuracy is better than 0.4 degree in the presence of multipath error [5]. For this experiment, a planar, aligned antenna array with a 1.5m by 3m rectangular configuration was used [4].

Other than these examples, GPS based attitude determination systems have been employed by more missions like, Orbcomm, GADACS (GPS Attitude Determination and Control System), REX II, Globalstar and Gravity Probe B etc.

1.2 OBJECTIVES

The objective of this thesis is to develope a Global Positioning System (GPS) based attitude determination algorithm. Moreover, due to the limitations of a GPS only attitude determination system, an improvement in the reliability of the system is aimed. Therefore, integrating the GPS based system with three gyroscopes is the other objective of the thesis. In order to achieve a low cost system, the gyro performance is selected based on a low cost MEMS gyro. Based on the algorithms developed, the comparison of the GPS only system with the low-cost gyro integrated case is also aimed in the thesis. The effect of the GPS satellite visibility on the algorithm performances is also analyzed.

1.3 OUTLINE

This thesis study is composed of nine chapters.

Chapter 1 provides introduction and summary about the content of the chapters.

In Chapter 2, the fundamental information about the Spacecraft Attitude Determination Systems is presented. The basic attitude sensors used in the space applications is introduced briefly. The advantages and the disadvantages of a GPS based attitude determination system is also mentioned in this chapter.

Chapter 3 provides the basic information about the measurements obtained by a GPS receiver. The factors affecting the GPS based attitude determination system is examined. The dominant error sources and their models are presented.

In Chapter 4, the gyroscope types and the error sources that affect gyro measurements are mentioned. A gyroscope error model used in the simulation is also introduced.

Chapter 5 presents the definitions of the different coordinate frames. The rotation matrices between these frames are introduced. The satellite orbit and attitude dynamics is also provided.

In Chapter 6 and Chapter 7, the details about the extended Kalman filter algorithms developed for GPS only and GPS/Gyro integrated cases are presented.

Chapter 8 presents the simulation results and discussions about the performances of the algorithms with different GPS satellite visibility environments.

Chapter 9 provides a brief summary and conclusions of the thesis study. The comparison of the results and the future work of the thesis are mentioned.

CHAPTER 2

OVERVIEW OF SPACECRAFT ATTITUDE DETERMINATION SYSTEMS

During the attitude determination process, a combination of sensors and mathematical models are used. In this chapter of the thesis, the most commonly used attitude sensors and their selection criteria are described briefly. In addition, the benefits and drawbacks of GPS based attitude determination system over the attitude sensors are discussed.

2.1 ATTITUDE SENSORS

In this part, different types of attitude sensors and the mechanism behind them are explained briefly. The title order is from higher to lower sensor accuracy. The details about gyroscopes and GPS as an attitude determination device are mentioned in the relevant chapters instead of here.

2.1.1 Star Sensors

Star sensors measure the elevation of the line of sight to a star with respect to the plane that contains the sensor bore-sight axis. They can be divided into two categories: star scanners and star trackers. Star scanners are simpler systems than trackers. They use the satellite rotation in order to search the sky for obtaining a recognized star pattern. These types of sensors are generally used on the spinning satellites. The accuracy of star trackers is typically ranging from 0.5 to 30 arc-minutes [6].

The other type, star trackers, searches the sky over a limited field of view. The accuracy of these sensors directly depends on the field of view size and star magnitude sensitivity of the sensor. There is also a gimbaled version of star trackers. They acquire sky view by using a mechanical action. These types of trackers have very small optical FOV (Field of View). However, the gimbal gives a much larger effective FOV. Typical accuracy is on the order of 1 to 60 arc-seconds [6]. However, due to the gimbal mount assembly, the sensor weights more than a classical fixed head star tracker. Moreover, the mechanical parts reduce the long-term reliability of the sensors.

The working principle of these sensors is basically explained below. The image of the star field is captured by an image detecting system like a CCD (Charged-Coupled Device) camera. Then, the attitude is determined by the pattern recognition of the star constellation in the field of view (FOV) and by means of a star catalogue. Figure 1 shows a principle block diagram of a second-generation star tracker. The system is made up with a CCD camera, an A/D (Analog/Digital) converter and a microcomputer.

Star sensors are the most accurate sensors used in the attitude determination system. However, they are very expensive, heavy systems and they have high power requirements. They also suffer from the interference with the Sun and other bright sources. In order to prevent the stray light problem, the usage of a sunshade is critical for an improved sensor performance.

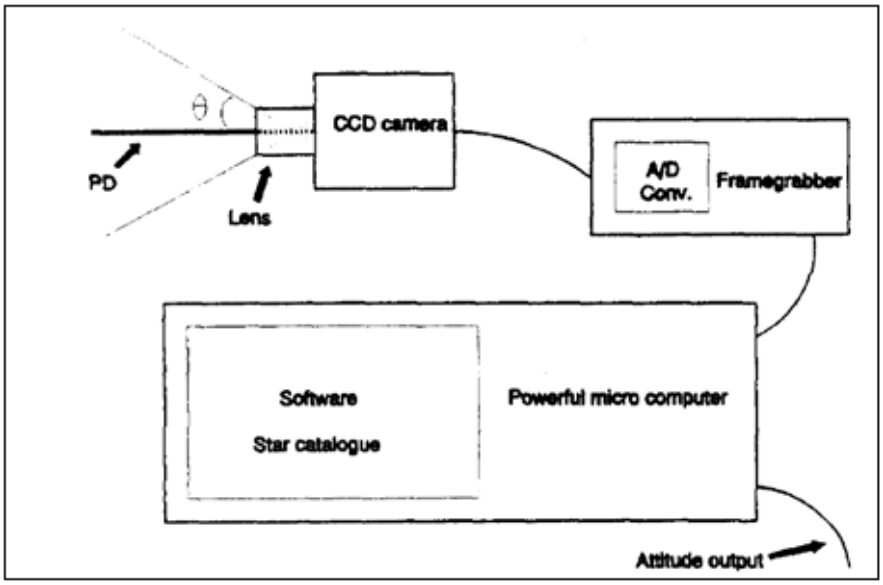

Figure 1: Principle Diagram of a Star Tracker [6]

2.1.2 Sun Sensors

One of the most common attitude determination systems is sun sensor technology. Sun sensors can be divided into three categories, which are sun presence sensors, analog sensors and digital sensors. Sun presence sensors provide a step function response depending on whether the Sun is detected or not detected within the FOV of the sensor, while analog and digital sun sensors are used in order to measure the angle between the Sun line and the normal vector to the sensor surface. The working principle of these sensors is based on materials that produce an electric signal when it is subject to sun radiation. In this way, by measuring the electrical output, it is possible to evaluate the angle between the Sun and surface normal vector.

There are wide range of sun sensors with different field of views (FOV) and resolution performances. The field of view of the sun sensors in the market is ranging from several

square arc minutes to 128x128 degrees. The resolution of them is ranging from less than an arc second to several degrees [6].

These sensors are used not just for attitude determination. Almost all satellites use solar power; therefore, it is important to orient the solar panels correctly with respect to the Sun. Moreover, some satellites have sensitive instruments that need to be protected from direct sunlight, like star trackers. In most of the satellites, sun sensors are being used in order to satisfy these requirements.

2.1.3 Horizon Sensors

Horizon Sensors are used as part of the attitude control system to determine the orientation of the satellite with respect to Earth. A horizon sensor is an optical instrument that detects the light reflected from the Earth's horizon. Moreover, thermal infrared sensing is often used in order to sense the contrast in temperature between the Earth's atmosphere and much colder cosmic background.

There is static and scanning version of horizon sensors. A static horizon sensor sense infrared radiation from the Earth's surface with a field of view which covers the entire Earth disk. They are used to determine the orientation of the satellite with respect to the nadir (i.e. Center of Earth direction). They can be used for satellites only with circular orbits. Scanning horizon sensors focus a narrow beam of light. By using these sensors, it is possible to detect when the infrared signal form Earth is received and lost. By using the time difference, the Earth's width can be determined. This information is used to determine the roll angle of the satellite.

These sensors tend to be less precise than sensors based on the stellar observation. Accuracy of systems using horizon sensors is 0.1 to 0.25 degrees [6]. By the latest technologies the accuracy is improved further.

The accuracy of these sensors highly depends on the fact that Earth is not perfectly circular. As another factor, the sensor does not detect land or ocean, but infrared in the atmosphere which can reach certain intensities due to the season and latitude.

2.1.4 Magnetometers

Magnetometers are carried on most of the satellites as a part of the attitude control system, since they are simple, inexpensive and lightweight. Moreover, they can operate over a wide range of temperatures and with low power requirements. They measure the direction and intensity of the local magnetic field expressed in the magnetometer fixed reference frame. The combination of three magnetometer sensors mounted orthogonally forms a vector sensing system. The attitude of the satellite is determined by comparing the measured magnetic field and a reference field determined by a reference model. The International

Geomagnetic Reference Field (IGRF) is the most commonly used reference model. This model is the empirical representation of the Earth's magnetic field recommended for scientific use by the International Association of Geomagnetism and Aeronomy (IAGA). However, because the magnetic field weakens with increasing altitude, these sensors can be used only at Low Earth Orbits (LEO). The average accuracy of these sensors is at the range of 0.5 to 5 degrees [1]. However, the accuracy is directly affected by the error sources they are subjected to. The main error sources are [1]:

- Disturbances in the magnetic field due to spacecraft electronics
- Errors in the reference model
- External disturbances such as ionospheric currents

A typical magnetometer is composed of two parts; sensor unit and electronic unit. Figure 2 shows a generalized magnetometer block diagram.

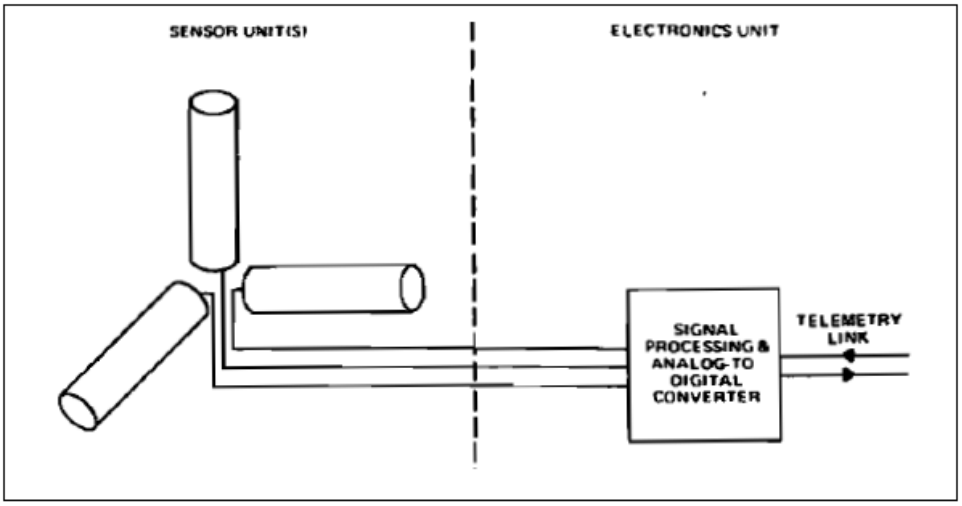

Figure 2: Generalized Magnetometer Block Diagram [6]

2.2 ATTITUDE SENSOR SELECTION

As an overview, the accuracy and the application characteristics of these sensors are compared in the table below [1]:

Table 1: Summary of Attitude Sensors and Comparison with GPS Based Attitude Determination System

Sensor	Accuracy	Mass [kg]	Power [W]	Characteristic
Star Sensors	1 to 60 arc-seconds	3-7	4-20	$\mp 6^o$ FOV . Larger FOV values can be obtained by using a gimbal mechanism.
Sun Sensors	0.005 to 4 degrees	0.5-2	0-3	FOV ranging from several square arc minutes to 128x128 degrees
Horizon Sensors	0.05^o for GEO 0.1^o for LEO	2-5	0.3-10	Horizon uncertainties affect the accuracy
Magnetometers	1^o for 5000 km altitude 5^o for 200 km altitude	0.6-1.2	<1	Magnetic field uncertainties affect the accuracy. Usable only below 6000 km
Gyroscopes	0.001 deg/hr.	3-25	10-200	Calibration is required. Error increases with time
GPS	0.5 to 1 degree	3	3.5-10	Multipath and errors in carrier phase tracking affect the accuracy

As it can be seen from Table 1, the magnetometers provide attitude measurement with about 1 to 5 degree accuracy. This type of sensors are applicable for the applications where precise attitude measurements are not crucial. An example of this application can be broad coverage communication satellites [7]. In such applications, GPS receivers are important for positioning measurements; however, the accuracy obtained by GPS based attitude determination system is far beyond the application requirements. Therefore, adding attitude measurement capability to GPS receivers may result in unnecessary additional cost for such applications.

Applications like surveillance satellites and space based astrophysical telescopes require better attitude accuracy (on the order of a few arc seconds). These applications can be supported by star sensors. This level of accuracy is beyond the capabilities of the current GPS based attitude determination technology.

Applications like most communication satellites and remote sensing satellites require attitude knowledge on the order of a few tenths of a degree [7]. This type of applications are ideal for horizon sensors or GPS receivers with attitude capability.

2.3 BENEFITS OF GPS BASED ATTITUDE DETERMINATION

Several benefits can be achieved by using GPS receivers on satellites for attitude determination purposes, instead of more conventional sensors. These benefits can be classified as cost savings and reliability improvements.

2.3.1 Cost Savings

The replacement of attitude sensors with a GPS receiver results in a considerable reduction in the amount of satellite hardware, interfaces, and ground support. A study to quantify the potential cost savings that can be achieved with the usage of GPS receiver as an attitude determination sensor is done by the NASA Goddard Space Flight Center (GSFC) Guidance Navigation and Control Technology Office (GTO) in 1997. The results obtained are presented in Table 2 [5].

Table 2: Cost Savings with Applying GPS Sensing to Spacecraft

Spacecraft System	Potential Savings	Achieved Through	Other Improvements
Operational Savings			
Ground Operations and Scheduling	$100k's-$M's/year	Autonomous vehicle operations	Hand-off operation, formation flight
Navigation Tracking	$100k's/year	On-orbit Navigation	Better accuracy, real-time positioning
Design Savings			
Precision Timing	$1M	Replaces on-board atomic clocks	Synchronization across multiple spacecraft
Attitude Determination	$100k's	Replaces other attitude sensors	Improved reliability, reduced power and mass
Spacecraft Design and Testing	$100k's	Reduces interfaces and COTS hardware	Quicker design time, less project risk

By utilizing GPS sensing technology on a satellite, the attitude measurement capability that have been divided among many sensors, such as star trackers, sun sensors, horizon sensors, magnetometers and gyroscopes, is combined into a single sensor that provides navigation solutions and precise timing information in addition to attitude determination.

Therefore, due to the reduction in the number of the sensors that are needed to be utilized on the satellite, the costs in the design process will be reduced. Moreover, because the additional hardware interfaces is eliminated, a reduction in the testing costs will also be achieved. These savings is integrated while considering a large-scale satellite constellation systems like Teledesic and GlobalStar systems.

2.3.2 Reliability Improvement

With the systems employing a single solid-state GPS receiver for the attitude determination, the reduction in the number of sensors on the satellite can be achieved. This means that the requirements for a number of components that is needed to operate properly to ensure operation success is eliminated. With the reduction in the interfaces, the design becomes simpler and this results in an improvement in the system reliability.

These benefits mentioned above are due to the employment of GPS sensing technology instead of other attitude determination sensors. However, utilizing a GPS receiver can also result in improvements in navigation tracking and ground operations. With the usage of a GPS receiver, velocity and position information can be obtained with cm level accuracy. Therefore, an autonomous orbit control may be performed on the satellite. This reduces ground operation costs dramatically over the mission life.

2.4 CHALLENGES IN THE GPS BASED ATTITUDE DETERMINATION

As it will be mentioned in Section 3.3, two types of measurements can be obtained by a GPS receiver. Due to its high accuracy, carrier phase measurements are preferred for the attitude determination. One challenge caused by the use of carrier phase measurements is called the integer ambiguity problem. In addition, due to the differences between space and ground environments, a GPS receiver designed for terrestrial applications does not operate properly in space. These differences introduce challenges in the hardware reliability and performance, satellite visibility, and signal acquisition. Because the integer ambiguity problem will be explained in Section 3.4, in this section only the drawback about the receiver design is explained.

2.4.1 Hardware Reliability and Performance

Many devices that are originally designed for terrestrial applications do not perform well in space. The electronic components used in the devices for space applications should be resistant to the severe environment in space. Radiation, temperature, and vibration are three major challenges that should be considered during the design process.

Receiver calibration is another obstacle in the space operations. For the ground applications, the calibration procedure is taken place by placing the GPS receiver on a static platform and collecting data for several hours in order to estimate the calibration parameters. However, because it is not possible to leave the GPS receiver undisturbed during launch, this calibration technique is not applicable for space applications.

2.4.2 Satellite Visibility

The other problem that arises due to using GPS technology for attitude determination purposes is the discontinuity in the satellite visibility. For the ground applications, one side of the vehicle always points toward the same direction. However, for a satellite, the varieties in the vehicle orientation can be more general due to tumbling or spinning motion. Therefore, during a period of the satellite mission, there will be a GPS signal outage problem for the cases where all the antennas point the same direction. For continuous navigation and attitude solution, it is necessary to use nonaligned antenna configuration [4]. However, this creates additional errors and a change in the algorithms to compensate them [5].

2.4.3 Signal Acquisition

By using GPS receivers in the space applications, the signal acquisition becomes a more difficult process. Due to high orbital velocity of a satellite, the time that a GPS satellite is visible decreases for space applications. For example, the time that a satellite is visible is 30 minutes for a LEO satellite, while it is 6 hours for a ground vehicle [4]. This creates cold start signal acquisition problem, due to searching for not visible GPS satellites.

The other problem is the large and rapidly changing Doppler shifts in the GPS carrier due to high orbital velocities. The relative Doppler shift is on the order of 40 kHz, while it is 5 kHz for terrestrial users [4]. Therefore, the time required for the signal acquisition increases. Moreover, signal acquisition process become more difficult. To cope with this problem, the tracking loops must be redesigned properly [4].

CHAPTER 3

GPS OBSERVATIONS

GPS receivers offer two types of measurements, namely the code phase measurements and the carrier phase measurements. By using the code phase measurements, the propagation time between the GPS satellite and the user is estimated measuring the time difference between a local replica of the C/A code and the received signal in space. Then, the pseudorange measurement is obtained. On the other hand, the phase difference between a local replica and the received signal can be evaluated by using the carrier phase measurements. However, it is not possible to distinguish one carrier period from another due to the fact that the carrier is a periodic signal. Therefore, it is possible to measure only the fraction of the carrier and the integer part must be resolved. This problem is called as the integer ambiguity problem. The mentioned fractional and integer parts of the carrier signal is represented in Figure 3.

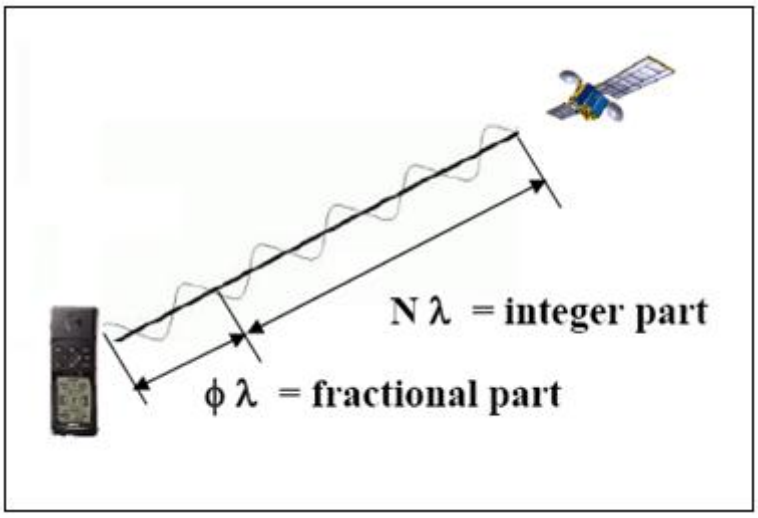

Figure 3: Carrier Phase Measurement Representation [29]

During the attitude determination process based on the GPS, all the measurements mentioned above are used to provide the related information of the satellite. Pseudorange and pseudorange rate measurements are used to estimate the position and velocity of the user satellite. The attitude of the satellite is determined using the carrier phase measurements of at least three non-collinear GPS antennas [8].

3.1 OVERVIEW OF GPS

GPS is a space-based radio positioning and time transfer system. Nowadays GPS provides a global coverage and is owned and operated by the U.S. Government. The system is composed of three segments, namely the space segment, control segment, and user segment. The space segment is made by a constellation of satellites. Initially, it was composed of 24 satellites. Recently the number of active satellites has been increased up to 31 in order to improve system capabilities and performances. The GPS satellites are positioned in six Earth-Centered orbital planes. The orbits are designed in order to obtain an optimal coverage of Earth's surface. The orbits' nominal parameters are summarized in Table 3 [9].

Table 3: GPS Orbits Parameters

Parameters	Value
Orbital Plane Spacing	6 equally spaced orbits with Ascending Node at 120 deg.
Semi-major Axis	26561.75 km
Orbital Velocity	38704 km/s
Eccentricity	less than 0.02
Angular Velocity	$2 \times 7.29211 \times 10^{-5}$
Period	~12h mean sidereal time
Inclination	55 deg. nominal

This satellite configuration guarantees that at least 4 satellites are visible considering an elevation angle of 15 degrees.

The control segment is composed of all the terrestrial reference stations including one main control station located in Colorado Springs, five monitor stations and four ground control stations around the world. The main tasks of the control stations are to coordinate the activities between satellites, to monitor the orbits, to synchronize the atomic clocks, and to exchange information for the construction of the navigation message. The control segment updates each satellites clock, ephemeris, and almanac in the navigation message once per day or as needed. The ephemeris describes the precise GPS satellite orbits and it is valid only for a time interval up to 6 hours [6].

The service by the first two segments of the system is used by the user segment, consisting of all the users equipped with a GPS receiver. Initially, the system is planned only for the military purposes; however, over the past years, the system was employed for civil applications.

During the past years, only two signals with different frequencies were continuously transmitted form each GPS satellites. These GPS signals are called as L1 and L2. The first signal L1 is at 1575.42 MHz, while the second signal L2 is at 1227.60 MHz. The Coarse Acquisition (C/A) phase ranging receivers extract and measure the carrier of the L1 signal. These receivers have a number of channels depending on the application. The position accuracy achieved by these receivers is about 8-11 m [11]. On the other hand, military

receivers encripted with Y-code, which is also called as P(Y) – code receivers, use both L1 and L2 signals. This receiver type is used for the military applications and the authorization is required by the Department of Defense (DOD) by United States. By using P(Y) – code receivers, the position accuracy can be improved up to 3-4 m [11].

With the recent increase in the satellite navigation market, a GPS modernization phase, named GPS III, have been started by the U.S. Government. The purpose of the modernization is to increase the GPS performance and flexibility for several civilian applications. For the purpose, a new carrier, L5, other than the existing carriers at L1 and L2 is introduced. This new signal is operating at 1176.45 MHz.

3.2 RELATING GPS OBSERVATIONS TO ATTITUDE

The GPS based attitude determination is based on the phase difference measurements, $\Delta\varphi$, between the signals received by a master antenna and one or more slave antennas.

The phase difference is related to the range difference as follows:

$$\Delta r = \Delta\varphi + n - \beta + \nu \qquad 3.1$$

where Δr is the range difference in cycles, $\Delta\varphi$ is the phase difference, n is the integer number of carrier cycles in the phase difference, β is the constant hardware delay between two antennas and ν is the measurement noise.

Therefore, the range difference can be calculated using the measured phase difference, after resolving the integer ambiguity n, and the constant hardware delay, β.

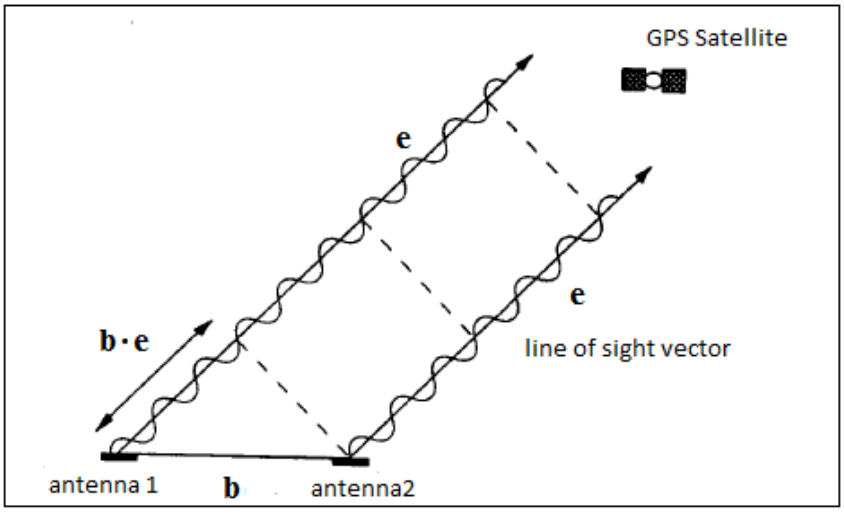

Figure 4: GPS Carrier Phase Geometry

The range difference can be described as the projection of the baseline vector $\boldsymbol{b}$ onto the line of sight vector from the antenna to the GPS satellite as it is shown in Figure 4. Therefore, in the simulation environment, range difference measurements, Δr, can be modeled as below, assuming that integer ambiguity and hardware delay problems are solved.

$$\Delta r = \boldsymbol{b} \cdot \boldsymbol{e} \tag{3.2}$$

where $\boldsymbol{b}$ is the baseline vector, and $\boldsymbol{e}$ is the line of sight vector between user antenna and GPS satellite.

It is more convenient to obtain the baseline vector in the Satellite Body Frame, and the line-of-sight vector is known in the ECI (Earth Centered Inertial) frame. Then the range difference equation in the matrix form becomes as follows:

$$\Delta r = (\boldsymbol{b}^B)^T \boldsymbol{R}_I^B \boldsymbol{e}^I \tag{3.3}$$

where $\boldsymbol{\alpha}^\beta$ representation is used to show that the vector α is resolved in the β-Coordinate System and $\boldsymbol{R}_I^B$ is the transformation matrix from the ECI frame to the satellite body frame. $\boldsymbol{R}_I^B$ is obtained by the following equation:

$$\boldsymbol{R}_I^B = \boldsymbol{R}_L^B \boldsymbol{R}_I^L \tag{3.4}$$

,where $\boldsymbol{R}_I^L$ is the transformation matrix from ECI to orbit level frame, and $\boldsymbol{R}_L^B$ is the transformation matrix from orbit level frame to the satellite body frame. The details about these transformation matrices are explained in Chapter 5.1.

Then the final form of the equation becomes:

$$\Delta r = (\boldsymbol{b}^B)^T \boldsymbol{R}_L^B \boldsymbol{R}_I^L \boldsymbol{e}^I \tag{3.5}$$

Because the satellite attitude is defined as the orientation of the satellite body frame with respect to the orbit level frame, the term $\boldsymbol{R}_L^B$ in the equation above relates the range difference with the attitude of the satellite.

3.3 PERFORMANCE OF GPS ATTITUDE DETERMINATION

As it is mentioned before, two types of measurements, which are code phase and carrier phase measurements, are obtained by GPS signals. Using carrier phase measurements, GPS can achieve centimeter-level precision, provided that the initial integer ambiguity set is solved correctly. This level of accuracy allows using GPS sensors for attitude determination applications.

In this section of the thesis, the reasons of choosing carrier phase measurements and the factors that affect the attitude determination performance are explained with more details.

3.3.1 Advantages of Carrier Phase Measurements

The most important reason for preferring carrier phase measurements over code measurements for some applications is the measurement accuracy. Although the working principle is the same for both measurements, the carrier phase measurements offers cm level accuracy in the positioning, while for code measurements the positioning accuracy is on the order of a few meters.

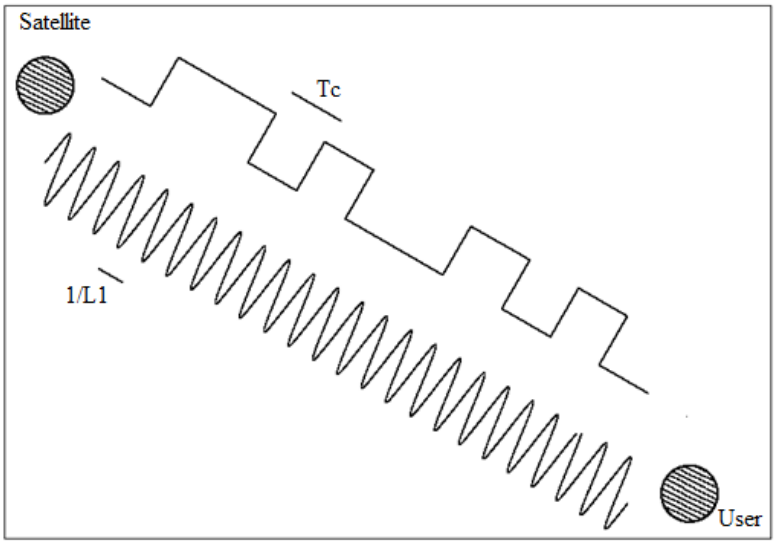

Figure 5: The Comparison between Code Period (Tc) and Carrier Period [29]

It is easier to understand the difference in the accuracy level of these two measurements, by comparing their periods. In order to measure the pseudorange between a GPS satellite and the user antenna, a GPS receiver should first determine the signal travel time by comparing the pseudo random code generated by the GPS satellite with a local replica generated at the receiver. The receiver slides its local code until it synchronizes with the GPS satellite's code. The amount it slides the code represents the signal travel time. It is important to note that even the signals look matched, one signal can still be ahead of the other one. The standard deviation of the synchronization is usually about 1% of the cycle [10]. Then the accuracy can be calculated by multiplying the speed of light with the non-synchronized part of the signal period. The period of code measurements is about 1μs, while the carrier period is around 634.8×10^{-12}s (1/L1). Figure 5 shows the character of the code and carrier phase signals. Because the period of the pseudo random code (code measurement) is quite wide, the synchronization error can cause almost 3m error considering 1% of the cycle synchronization error. On the other hand, the accuracy for carrier phase measurements can be calculated as 1.9 mm.

The other advantage of the carrier phase measurement is the low measurement noise level, which is usually less than 1 mm, and the low multipath effects which are less than 0.25λ [8], where λ is the wavelength of the carrier signal.

Despite of these advantages, the most challenging problem arising due to using the carrier phase measurement is the integer ambiguity problems, which will be described in Chapter 3.4.

3.3.2 Measurement Errors

The errors affecting GPS measurements can be classified as satellite clock errors, receiver clock error, ephemeris error, ionospheric error, tropospheric error, multipath error, antenna phase center variation, and receiver noise. These error sources affect both code and carrier phase measurements; however, the impact of the errors on the code and carrier measurement accuracy is different. In this part of the thesis, these sources of errors are defined briefly.

It should be noted that, for the attitude determination, the carrier phase measurements are not used directly. Instead of that, the measurements are used after the single differencing (e.g. this concept is discussed in Section 3.3.3 with more detail). Therefore, some of the error sources are eliminated for attitude determination, but not for positioning purposes. The most dominant error sources affecting carrier phase measurements are the multipath, receiver noise, and antennas phase center variations.

In order to illustrate the errors on the code and carrier phase measurements, the observation equations for both measurements are given below [8]:

$$\rho = \rho_T + c(\Delta t_s - \Delta t_r) + E_\rho + I_\rho + T_\rho + \epsilon_{m,\rho} + \epsilon_{r,\rho} \quad 3.6$$

$$\lambda\phi = \rho_T + c(\Delta t_s - \Delta t_r) + \lambda N + E_\rho - I_\rho + T_\rho + \epsilon_{m,\phi} + \epsilon_{r,\phi} \quad 3.7$$

where

ρ : Measured pseudorange, [m]

ρ_T : True distance between the user receiver and the GPS satellite, [m]

c : Speed of light, [m/s]

Δt_s : Satellite clock correction, [s]

Δt_r : Receiver clock correction, [s]

E_ρ : Ephemeris error, [m]

I_ρ : Ionospheric error, [m]

T_ρ : Tropospheric error, [m]

$\epsilon_{m,\rho}$: Multipath error on the code phase measurement, [m]

$\epsilon_{r,\rho}$: Receiver noise error on the code phase measurement, [m]

ϕ : Measured cycles

λ : Carrier wavelength, [m]

N : Integer cycles ambiguity

$\epsilon_{m,\phi}$: Multipath error on the carrier phase measurements

$\epsilon_{r,\phi}$: Receiver noise error on the carrier phase measurements

3.3.2.1 Clock Errors

The satellite clock error is the difference between the time maintained by a satellite and the GPS time. Although satellites contain highly stable atomic clocks for all the timing operations, they can still deviate from the GPS system time. The pseudorange error due to satellite clock errors is in the order of 2m [11]. It is possible to compensate this error by using the clock correction parameters determined and transmitted by the Master Control Station (MCS). These parameters are contained in the broadcasted navigation message.

$$\delta t = a_{f0} + a_{f1}(t - t_{oc}) + a_{f2}(t - t_{oc})^2 + \Delta t_r \qquad 3.8$$

where a_{f0} is the clock bias (s), a_{f1} is the clock drift, a_{f2} is the frequency drift (1/s), t_{oc} is the clock data reference time (s) and Δt_r is the correction due to the relativistic effects (s).

Similarly, receiver clock error is due to the deviation of receiver time from GPS system time.

3.3.2.2 Tropospheric Error

The troposphere is a zone of dry gases and vapor extended up to 50 km from the Earth surface. Therefore, it is negligible even for LEO satellites.

Since satellite receiver error can be compensated using the ephemeris data, the receiver clock error can be estimated using measurements from at least four GPS satellites, and the tropospheric error is negligible in space, the most dominant error sources are ionospheric errors, ephemeris error, multipath, and receiver noise.

3.3.2.3 Ionospheric Error

The ionosphere error is the delay due to the ionized gases in that zone of the atmosphere. The ionosphere is ranging from 50 to 1000 km from the Earth surface. The density of the ions and free electrons varies from day to day and with particular solar conditions. The error in the pseudorange caused by the ionosphere is represented as below [27]:

$$I_\rho = \frac{40.3\ TEC}{f^2} \tag{3.9}$$

where f is the carrier frequency and TEC is the total electron content defined as the number of electrons in a tube of 1 m^2 cross section from the receiver to satellite.

For the attitude determination, the differences of carrier measurements from different antennas are used; therefore if the effect of ionosphere is the same for all the antennas, this error is eliminated after the single differencing of the carrier phase measurements. Therefore, for short baselines with a few meter lengths, the error caused by the ionosphere can be neglected for the attitude determination process. However, it should be considered when using the pseudorange measurements for the positioning purposes. In order to compensate this error, the parameters broadcasted by the GPS satellites can be used.

3.3.2.4 Ephemeris Error

The ephemeris error is generated when the navigation message does not transmit the correct satellite position and velocity. The effect of this error in the pseudorange measurement is on the order of 2 m [11]. The effect of ephemeris error in differential mode depends upon the distance between the two antennas. For short baselines with a few meter lengths, this error can be neglected.

3.3.2.5 Multipath Error

The multipath error is the result of interference between signals through the direct path from the GPS satellite and signals reflected by the surfaces near the antenna. The code multipath error is typically in the order of several meters in normal conditions. There are several methods to compensate the code multipath error, such as Narrow Correlator Spacing, Multipath estimating delay lock loop (MEDLL), TrEC and carrier-code smooth methods [3]. On the other hand, the carrier phase multipath error is more difficult to isolate. The multipath effect on the carrier phase measurements is less than 0.25λ in meters [8]. The error in the attitude due to multipath can be calculated roughly as below [7]:

$$\epsilon_{m,\phi} = 8 \cdot 10^{-3}/(b \cdot T^{1/2}) \quad 3.10$$

where b is the baseline length, T is the receiver integration time interval, and $\epsilon_{m,\phi}$ is the RMS error in the attitude due to multipath (in radians).

For instance, for a 1 m baseline and 1 second integration time, the error is about 0.5 degree RMS.

3.3.2.6 Receiver Noise

The receiver noise represents the measurement error in the tracking loops of a GPS receiver. The dominant source of error is the thermal noise. The other error sources include hardware and software resolution, and oscillator stability. The attitude error due to the receiver noise can be calculated approximately by using the equation below [7]:

$$\epsilon_{r,\phi} = 4 \cdot 10^{-4}/(b \cdot T^{1/2}) \quad 3.11$$

where b is the baseline length, T is the receiver integration time interval, and $\epsilon_{r,\phi}$ is the RMS error in the attitude due to receiver noise (in radians)

For instance, for a 1 m baseline and 1 second integration time, the error is about 0.02 degree RMS.

3.3.2.7 Antenna Phase Center Variation

The other large error source is due to the antenna phase center variations. The antenna phase center is considered as a physical point, such as the geometric center of the antenna. However, the phase center can change with the direction of the receiving signal. The attitude error due to antenna phase center variations is typically on the order of 1×10^{-3}rad (0.06 degree) RMS [7]. Because GPS based attitude determination systems requires high accuracy measurements, these variations in the antenna phase center should be considered when examining the error sources. In order to reduce this error, all antennas should point the same direction. After the differencing the measurements, the effect of this error can be significantly reduced.

The phase center changes also depending on the antenna type and design. Therefore, in the multiple antenna GPS based attitude determination system, the same type of antennas should be used in order to avoid the errors caused by the antenna design differences [12].

3.3.3 Carrier Phase Single Differencing

In this thesis, the observations used for the attitude determination are the carrier phase measurement differences for different two antenna configurations. After the differencing of the measurements simultaneously collected by two antennas with respect to the same satellite, some of the errors affecting the measurement cancel out for the short baselines (Figure 6).

For short baselines, the satellite clock errors, the ephemeris errors, ionospheric errors and tropospheric errors are highly correlated. Therefore, after single differencing the residual errors can be assumed to be zero.

The single differenced equation for the carrier phase measurement between antenna 1 and antenna 2 is given below:

$$\lambda\phi_{12}^{j} = \lambda\phi_{1}^{j} - \lambda\phi_{2}^{j} \tag{3.12}$$

$$\begin{aligned}\lambda\phi_{12}^{j} = {} & \left(\rho_{T,1}^{j} - \rho_{T,2}^{j}\right) + c\left(\Delta t_{s,1}^{j} - \Delta t_{s,2}^{j}\right) - \left(\Delta t_{r,1}^{j} - \Delta t_{r,2}^{j}\right) + \lambda\left(N_{1}^{j} - N_{2}^{j}\right) + \\ & \left(E_{\rho,1}^{j} - E_{\rho,2}^{j}\right) - \left(I_{\rho,1}^{j} - I_{\rho,2}^{j}\right) + \left(T_{\rho,1}^{j} - T_{\rho,2}^{j}\right) + \left(\epsilon_{m,\phi,1}^{j} - \epsilon_{m,\phi,2}^{j}\right) + \\ & \left(\epsilon_{r,\phi,1}^{j} - \epsilon_{r,\phi,2}^{j}\right)\end{aligned} \tag{3.13}$$

After the cancellations the equation becomes:

$$\begin{aligned}\lambda\phi_{12}^{j} = {} & \left(\rho_{T,1}^{j} - \rho_{T,2}^{j}\right) - \left(\Delta t_{r,1}^{j} - \Delta t_{r,2}^{j}\right) + \lambda\left(N_{1}^{j} - N_{2}^{j}\right) - \left(\epsilon_{m,\phi,1}^{j} - \epsilon_{m,\phi,2}^{j}\right) + \\ & \left(\epsilon_{r,\phi,1}^{j} - \epsilon_{r,\phi,2}^{j}\right)\end{aligned} \tag{3.14}$$

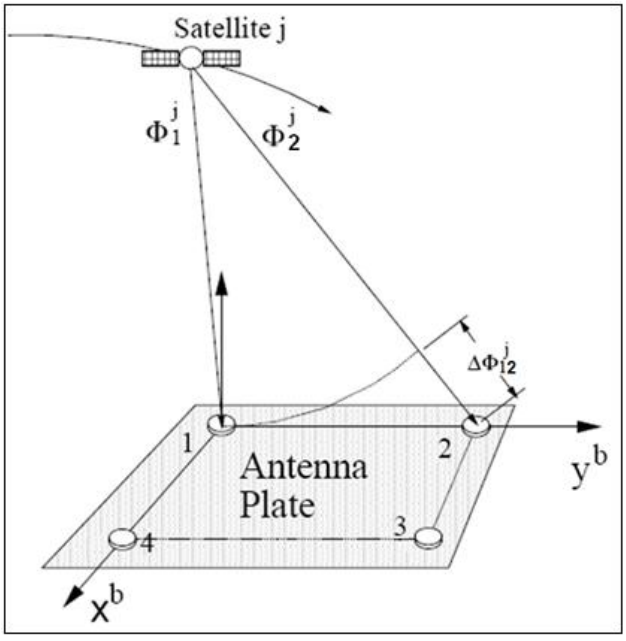

Figure 6: Single Differencing between Antenna 1 and Antenna 2

For systems with multiple receivers such that each receiver has a single antenna, the receiver clock error cannot be cancel out with single differencing. Therefore, in order to obtain accurate attitude or positioning estimations, the receiver clock should be carefully calibrated for each receiver and should be considered in the data processing [8]. In some spacecraft attitude determination applications, the system consists of a single receiver and multiple antennas connected to that the same receiver. For example, the U.S. Air Force RADCAL satellite is equipped with a Trimble Quadrex receiver and four antennas. For such systems, because the receiver clock error affects all of the measurements from different antennas, this error can also be assumed to be zero after differencing.

The other error sources discussed in the previous section is the antenna phase center variations. However, as it is stated before, if the same kinds of antennas pointing the same direction are used in a GPS attitude determination system, this error also cancels out after single differencing.

3.3.4 Errors Modeled in the Simulation

It should be noted that multipath and receiver noise cannot be cancelled after differencing. However, because the impact of receiver noise on the attitude estimation is very small, the performance of the attitude determination system is highly influenced by the accuracy of the multipath mitigation algorithms.

In this thesis, models for receiver noise and multipath error are developed. The receiver noise is assumed to have a Gaussian white noise distribution. In the model, the effects of receiver noise on the pseudorange, pseudorange rate and delta range measurements are modeled with zero mean and the following standard deviations respectively:

$$\sigma_{\rho} = 6\ m$$

$$\sigma_{\dot{\rho}} = 0.025\ m/s$$

$$\sigma_{\Delta r} = 1\ mm$$

On the other hand, a first order Gauss-Markov process is usually used in order to represent the multipath error [13]. The first order Gauss-Markov process is described by the following continuous time equation [14]:

$$\frac{dx}{dt} = -\frac{1}{\tau_c}x + w \qquad 3.15$$

where t is time, τ_c is the correlation time, w is the driven white noise, and x is any random process, which is multipath error for this case.

In discrete time, it can be written as:

$$x_k = e^{-\Delta t/\tau_c} x_{k-1} + w_k \quad (3.16)$$

And the variance of the driven noise can be written as:

$$\sigma_{w_k}^2 = \sigma_{x_k}^2 \left(1 - e^{-2\Delta t/\tau_c}\right) \quad (3.17)$$

where Δt is the measurement sampling time, x_k and w_k represents the multipath error and the driven noise respectively at the k^{th} time interval.

The model for the multipath error is only an approximation and the correlation time changes with time and satellite elevation. However, for the simplicity, it is assumed that all the satellites have the same correlation time and the same variance for the driven noise. The correlation time is chosen as 300 seconds due to the values given in the reference [13].

3.3.5 Operational Factors

Besides the measurement errors discussed above, the attitude estimation accuracy also affected by the operational factors like the number of visible satellites, their geometry, antenna baseline length, and antenna configuration.

3.3.5.1 Satellite Number and Geometry

Each range difference measurement obtained between user antennas and GPS satellites is considered as an observation and included to the estimation algorithm. Therefore, as the number of visible satellites increases, the accuracy of the attitude estimation increases as well.

The locations of the GPS satellites also affect the accuracy of the attitude determination system. The effect of the satellite relative geometry on the accuracy can be measured through the DOP (Dilution of Precision) concept. There are several types of DOP showing the satellite geometry effect on different parameters. The most commonly used one is the Geometric Dilution of Precision (GDOP), which is used to select the best satellites for user position and time determination. It depends on where the satellites are relative to the user. GDOP has two components: PDOP (Position DOP) and TDOP (Time DOP) [10]. TDOP determines the uncertainty in the clock solution, and PDOP determines the uncertainty of the three-dimensional position solution. For the attitude determination applications, there are several parameters analogous to the position and timing related DOP concept. The widely used one is the ADOP (Attitude Dilution of Precision), which is a figure of merit to measure the effect of satellite geometry on the attitude determination. AZ-DOP (Azimuth DOP) and El-DOP (Elevation DOP) are the other two concept used to identify the effect of satellite geometry on the attitude accuracy [3].

A lower ADOP value leads to better attitude estimation accuracy. Therefore, this value should be considering while selecting the measurements which are used in the attitude estimation algorithm. Moreover, with the decrease in the available number of satellites, AZ-DOP and El-DOP values increase and this again leads to low attitude estimation accuracy [3].

3.3.5.2 Antenna Configuration

The attitude accuracy also highly depends on the baseline length, the antenna number, and the position of the antennas relative to each other.

Figure 7 illustrates the impact of baseline length onto the estimation accuracy of heading and pitch angles [3]. The results show that the estimation accuracy of heading and pitch angle improves with the increasing baseline length.

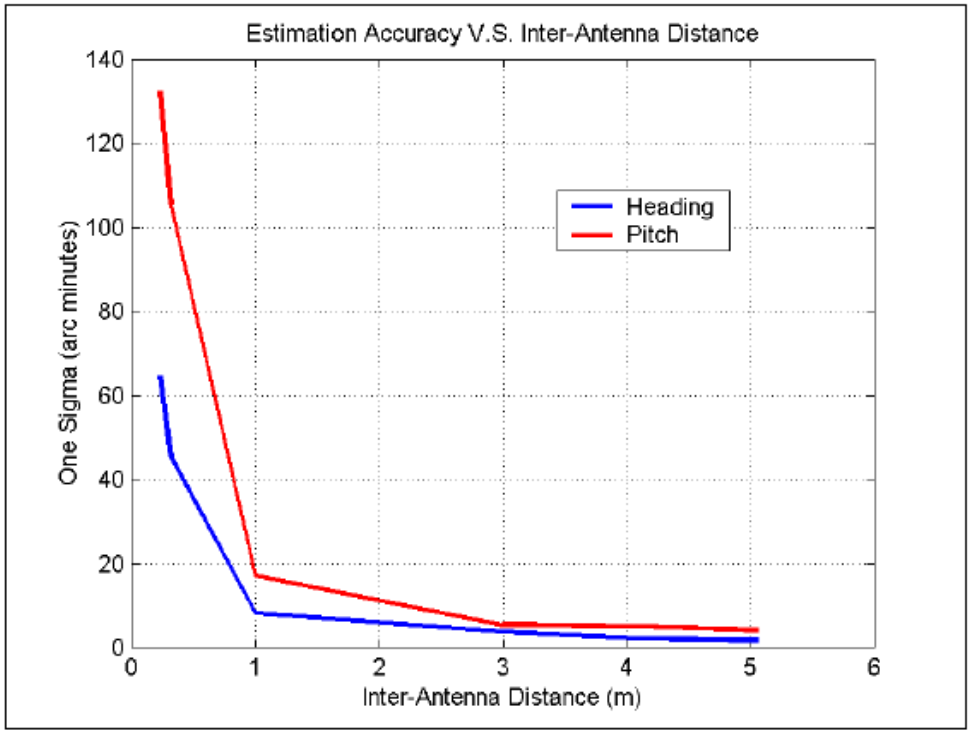

Figure 7: The Effect of Baseline Length on the Attitude Estimation Accuracy [3]

However, it is important to note that these results are obtained with only theoretical point of view. In reality, with the increase in the baseline length, the errors due to multipath and structural flexing are likely to increase [15]. Therefore, it is important to place the antennas with an optimal distance.

The other factor affecting the attitude accuracy is the number of GPS antennas. For a 3-dimensional attitude determination system, at least three non-collinear antennas are required [8]. Adding redundant antennas may increase the availability and reliability of the system; however, the increase in the attitude estimation accuracy is negligible compared to the additional hardware cost [3]. Therefore, there should be a balance between the attitude accuracy and the hardware cost. A four-antenna attitude system is found to be the optimal configuration [3], which is also implemented in this thesis.

Besides the number of antennas, the geometry of antenna array also affects the accuracy of the attitude estimation. In the literature, this effect has been analyzed several times. One research has focused on a system with three and four antennas in planar and three dimensional configurations [15]. In the results of that research, it has been concluded that for a three-antenna system, the optimal configuration is placing the antennas in order to form two orthogonal baselines. For a four-antenna system, forming an orthogonal triad, meaning that the three baseline vectors from the master antenna to the slave ones have the same length and are orthogonal to each other, gives the best attitude estimation results. However, it has been also noted that the accuracy does not change significantly for a planar distribution of the four antennas in a square shape [15]. In practice, an orthogonal triad antenna configuration is applicable due to the location limitations on the platform [3]. Therefore, in this thesis, a square-shaped antenna configuration is implemented.

3.4 INTEGER AMBIGUITY RESOLUTION

In order to estimate the attitude accurately using GPS measurement, carrier phase measurements are highly required due to its cm level accuracy. The carrier phase measurements from a GPS receiver contain the total number of integer cycles and the fractional part. The problem arises with the carrier phase measurements is the fact that the integer number of cycles are unknown for this type of measurements. This problem can be described better by comparing with the code measurements. The pseudorange information obtained by the code measurements is calculated by using the known time phase difference between the signal transmitted and the signal received. This time phase is estimated by comparing the pseudo-random noise (PRN) code generated by the GPS satellite with a local replica generated at the receiver side. Using the PRN codes received, the time difference can be detected by shifting the local replica. However, for the carrier phase measurements, because all the cycles are identical, it is not possible to distinguish one from other. This problem is called as the integer ambiguity problem.

The accuracy of ambiguity resolution is very important for the high precision GPS attitude determination. More precisely, the error left after the resolution is the most important drawback in the attitude accuracy. For the GPS based attitude determination systems used on the moving platforms for real-time applications, fast and reliable on-the-fly ambiguity resolution techniques are required. There are several methods developed in order to overcome this problem. The integer ambiguity resolution of the carrier phase measurements

is beyond the topic of this thesis; however, some of the methods are summarized here briefly.

One category of these methods is known as the search method. In this method, the set of all the possible values are considered to resolve the integers and the solution minimizing the solution residual is selected [16]. An ambiguity resolution algorithm based on this method is developed in reference 17. The advantage of such a technique is that if the measurement quality is high (i.e. not noisy measurement), the solution can be achieved very quickly. However, the computational effort required for search methods is high. Moreover, under poor measurement conditions, the solution can converge to incorrect number of integers [16].

Another method for the resolution of the integer ambiguities is known as motion-based methods. Carrier phase measurements are collected over a period of time and used by the algorithms in order to resolve the ambiguity through a batch filter. The possibility of obtaining incorrect solutions is very small for motion method compared to the search method. However, the solution procedure might be longer, several minutes typically. This may not be acceptable for real time applications.

There are also some additional techniques trying to minimize the computation effort and the solution time. An example is given in reference 18. The algorithm offers fast and reliable integer ambiguity resolution for real-time GPS attitude determination. This algorithm requires minimal computational effort compared to both search method and the motion-based method. Moreover, the integer ambiguity resolution is achieved faster than the motion-based methods.

CHAPTER 4

GYROSCOPE TECHNOLOGY

4.1 GYROSCOPE TYPES

Gyroscopes are used to determine the attitude of a vehicle by measuring either the angular displacement or angular rate of the rotation about the gyro axis. There are different gyroscope technologies. Three main types of gyroscopes are spinning mass, optical and vibratory gyroscopes.

4.1.1 Spinning Mass Gyroscopes

Gimbaled spinning mass gyros operate based on the conservation of angular momentum principle. However, strapdown systems are usually used for the navigation purposes. For such systems, the angular rate about an axis that is fixed with respect to the case is measured. This type of systems operates based on the gyroscopic theory. This concept is illustrated in Figure 8, where a disc is rotating about the spin axis (y-axis) with some angular momentum. When a torque is applied in an axis perpendicular to the spin axis (z-axis), the disc starts to rotate in an axis which is both perpendicular to the spin axis and torque axis (x-axis).

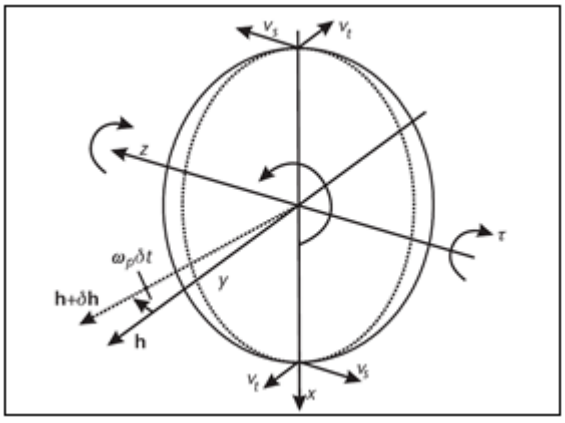

Figure 8: Orthogonal Torque Effect on the Spinning Disc [20]

There are two basic types of single axis, spinning mass gyros: the rate gyro and the rate integrating gyro. Rate gyros measure the angular rates of a vehicle, while rate integrating gyros measures the angular displacement directly [6].

Rate gyros are open loop systems; therefore, they can suffer from limitations due to pickoff resolution and nonlinearities in the spring system. Closed loop version of the rate gyros are rate integrating gyros. In such systems, the spring system is replaced by an electromagnetic torque.

4.1.2 Optical Gyroscopes

The optical gyroscopes detect the path length difference between two beams of light travelling a closed path. By measuring the changes in the path length, the angular rate with respect to the inertial frame is determined. Two main types of optical gyroscopes are ring laser gyros (RLG) and fiber optic gyros (FOG).

RLG's development started in the 1960s. The bias repeatability range of RLGs varies from 0.001 deg/h to 5 deg/h [19]. It operates based on the fact that "an optical frequency oscillator can be assembled as a laser using three or more mirrors to form a continuous path" [19]. Two beams are generated travelling opposite directions. If the sensor is fixed with respect to the inertial space, the beams have the same optical frequency. If the sensor rotates about an axis perpendicular to the enclosed tube plane, the optical path lengths of the beams changes with respect to each other. This path difference is used in order to measure the angular rate of the rotation. The principle diagram of a ring laser gyro is given in Figure 9.

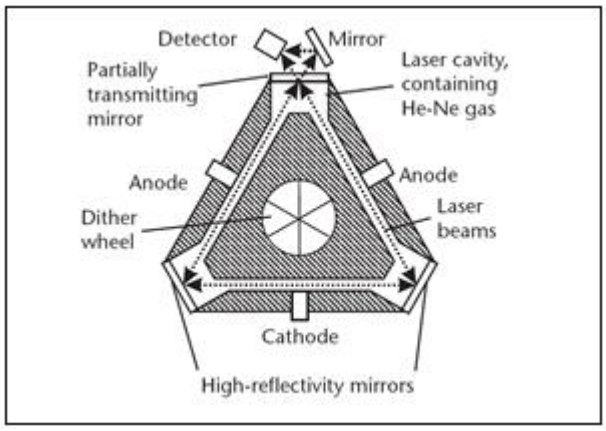

Figure 9: Ring Laser Gyro [20]

On the other hand, FOGs developed in the 1970s. This type of sensors was developed as a cheaper alternative to the RLGs with bias performance from 50 deg/h to 0.5 deg/h and bias stability better than 0.0003 deg/h [19]. The FOGs operates based on the Sagnac effect principle. A light beam from a source is split into two beams that travel in the opposite directions around an optical fiber coil. When the two beams are combined, the interference between them is observed by a detector. When the fiber coil is rotated about an axis

perpendicular to its plane, a phase change is introduced between the two light paths. This phase difference is used in order to measure the angular rate.

4.1.3 Vibratory Gyroscopes

All vibratory gyroscopes operate based on the same principle, which is to detect the Coriolis acceleration of the vibrating elements when the gyro is rotated [20]. The vibrating part may be a string, beam, ring, cylinder or hemisphere. The most common design technology for these sensors is using a stable quartz resonator with piezoelectric driver circuits [19].

MEMS (Micro Electro-Mechanical Systems) gyros are also classified as vibratory gyroscopes. This type of technology offers low size, low cost sensors to the market.

4.2 GYROSCOPES IN SPACE APPLICATIONS

Currently, optical gyroscope technologies still dominate the market by a wide margin as it can be seen in Figure 10 [21]. In that figure, the use of different gyroscope technologies in the market depending on the gyro bias stability performance requirements is illustrated. In particular, RLGs are largely used in space applications due to high bias stability and robustness. The ring laser gyroscope today is well established in the medium and high performance markets. However, the big size and weight, high power requirements and most importantly high cost of these systems are limiting factors to its use.

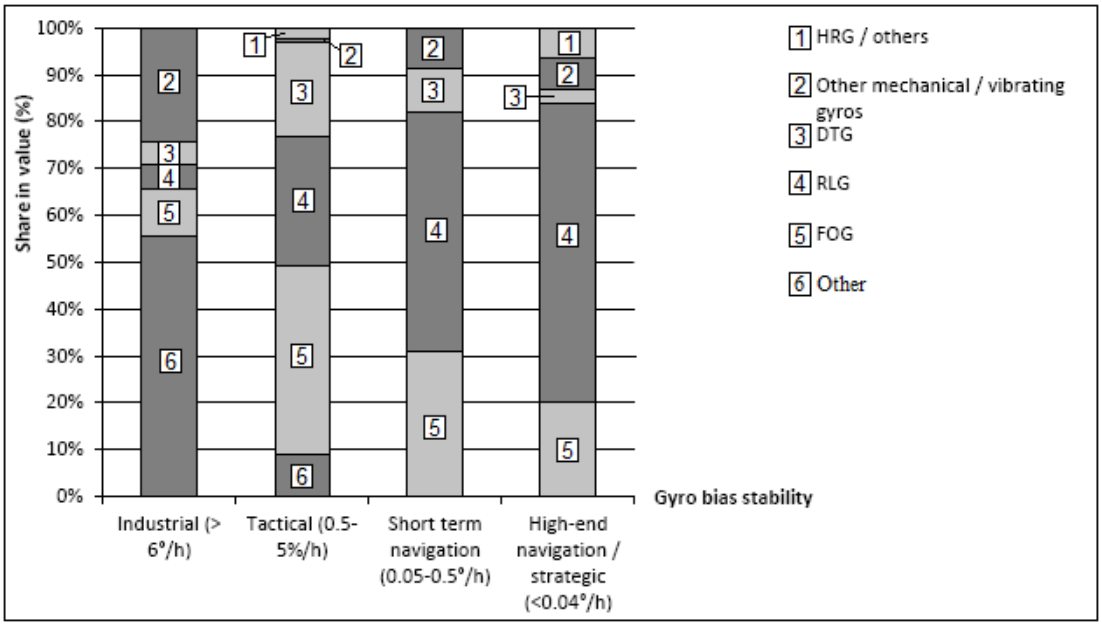

Figure 10: Trends in the Gyroscope Market depending on the Gyro Bias Stability Performance Requirements [21]

On the other hand, FOGs are much more flexible in terms of design and packaging. Mass production of fiber components results in a significant cost advantages over the ring laser and mechanical gyroscopes in many applications. FOGs are suitable for low to medium performance range applications. For many applications, these type of sensors offer a solid state, low cost, highly reliable, lightwieghted alternative with low power requirements [22].

Table 4: ISC Gyro Properties

Parameter	Value
1σ Values	
Bias Stability [deg/h]	1.0
Scale Factor Repeatability [ppm]	30
Misalignment [μrad]	100
Angular Random Walk [deg/$\sqrt{h}$]	0.01
Budget	
Mass [kg]	1.9
Volume [cm^3]	1050
Power [W]	3.5

MEMS gyros are low-cost devices and their performance is usually lower than the RLGs and FOGs. Applications of these types of sensors include small, low cost spacecraft and satellites. With the recent improvements, the drift performance of 1 deg/h is achieved with the sensor called micro inertial reference system (μIRS) [23]. The other example of MEMS gyros used in the space applications is Inertial Stellar Compass (ISC) used in the CubeSat program with 1 deg/h bias drift [24]. The properties of ISC gyro is given in Table 4.

Gyro measurements are subject to some errors like bias, drift and wide band noise. The attitude estimations computed by integrating the gyro angular rate measurements result in increasing and unbounded errors. Because long term operation is reqiured for the space applications, high performance gyros like RLGs are used in most of the currently operating systems. However, the bias of gyroscopes can be estimated by aiding with some other attitude sensors. For such systems, FOGs or MEMS gyros can be good alternatives to use. For example, magnetometers and GPS sensors are used to calculate the absolute altitude solutions. However, their output frequency are quite low and can not be used to estimate the attitude of a vehicle performing high maneuver. For such systems, gyroscopes can be used due to their high output frequency, while magnetometers and GPS measurements can be used to estimate the gyro bias and bound gyro based attitude estimation errors.

4.3 ERROR SOURCES

The outputs of gyroscopes are affected by errors like bias, scale factor, misalignment and random noise. Each of these errors has a fixed contribution, a temperature dependent variation, a run-to-run variation and an in-run variation [20]. The fixed contribution and temperature dependent parts can be compensated using the calibration data. The run-to-run variation error is different each time the sensor is used. However, the amount of the error remains constant within any run. This type of error can be calibrated by integrating the sensor with some aiding sensors, like GPS aiding in this thesis. Finally, the in-run variation is a slowly changing error during the course of a run. Since the duration of operations are quite long in space applications, this type of error is quite important while determining the performance of a gyroscope.

4.3.1 Bias

The gyroscope bias can be defined as a constant error present in the gyro output. It is independent of the underlying angular rate. The bias error remains after the calibration has a static and a dynamic part. The static bias is also known as the run-to-run bias or the bias repeatability, while the dynamic part can be also called as the in-run bias or bias instability. The bias repeatability stays constant during an operation, but changes at every run. However, the bias instability defines the error slowly varies during the operation. This type of error can be represented by a 1^{st} order Gauss-Markov process. Error due to this drift limits the quality of the gyro output severely for long-term operations like space applications. Therefore, this error should be calibrated periodically.

4.3.2 Scale Factor

The scale factor error is defined as the departure of the input-output ratio of a gyroscope from unity. This type of error is dependent on the amount of the angular rate that the instrument is underlying. In other words, the scale factor error is proportional to the true angular rate about the sensitive axis.

4.3.3 Misalignment

The gyroscope package is strapped to the body and should be aligned with the body axis. However, due to manufacturing limitations, a small misalignment of the sensitive axis of the inertial sensors with respect to the orthogonal axes of the body frame causes this type of error in the sensor output.

4.3.4 Random Noise

Gyroscopes are affected by this type of error due to various sources. Spinning mass gyros exhibit random noise due to mechanical instabilities, while an RLG exhibits due to the residual lock-in effects. Moreover, vibratory gyros can exhibit high frequency resonances. This type of error cannot be calibrated and compensated, because the past and future values are uncorrelated. Random noise can be modeled as a zero mean, Gaussian white noise in the gyroscope error models [20]. The conventional units are deg/$\sqrt{h}$ or deg/h/$\sqrt{Hz}$.

4.4 ERROR MODEL

The major error sources for a gyroscope which is operated in the space applications are the bias repeatability, bias instability, scale factor repeatability, misalignment and random noise. Equation 4.1 illustrates these error sources affecting the three gyro system outputs. A gyroscope error model is developed within the scope of this thesis based on this equation.

$$\begin{bmatrix}\widetilde{\omega}_x\\ \widetilde{\omega}_y\\ \widetilde{\omega}_z\end{bmatrix} = \left\{\begin{bmatrix}B_x+\delta B_x\\ B_y+\delta B_y\\ B_z+\delta B_z\end{bmatrix} + \begin{bmatrix}1 & M_{xy} & M_{xz}\\ M_{yx} & 1 & M_{yz}\\ M_{zx} & M_{zy} & 1\end{bmatrix}\begin{bmatrix}\omega_x\\ \omega_y\\ \omega_z\end{bmatrix}\right\}\begin{bmatrix}1+S_x & 0 & 0\\ 0 & 1+S_y & 0\\ 0 & 0 & 1+S_z\end{bmatrix} + \begin{bmatrix}n_x\\ n_y\\ n_z\end{bmatrix} \quad (4.1)$$

where

$\widetilde{\omega}_x, \widetilde{\omega}_y, \widetilde{\omega}_z$: measured angular rates with respect to the inertial frame in the body frame in x, y and z directions respectively.

$\omega_x, \omega_y, \omega_z$: true angular rates with respect to the inertial frame in the body frame in x, y and z directions respectively.

S : Scale factor repeatability error

M : Misalignment error

B : Bias repeatability

δB : Bias instability

n : Random noise

CHAPTER 5

ATTITUDE DETERMINATION

5.1 ATTITUDE REPRESENTATION

Various mathematical representations can be used in order to define the attitude of a body with respect to a reference coordinate system. Two attitude representations are described here namely, Euler angles and quaternions.

5.1.1 EULER ANGLES

A transformation from one coordinate frame to another can be carried out by three successive rotations about different axes.

The transformation can be expressed as follows:

1st rotation: Rotation about the reference z-axis by an amount of ψ, called yaw angle.

2nd rotation: Rotation about the new y-axis by an amount of θ, called pitch angle.

3rd rotation: Rotation about the new z-axis by an amount of ϕ, called roll angle.

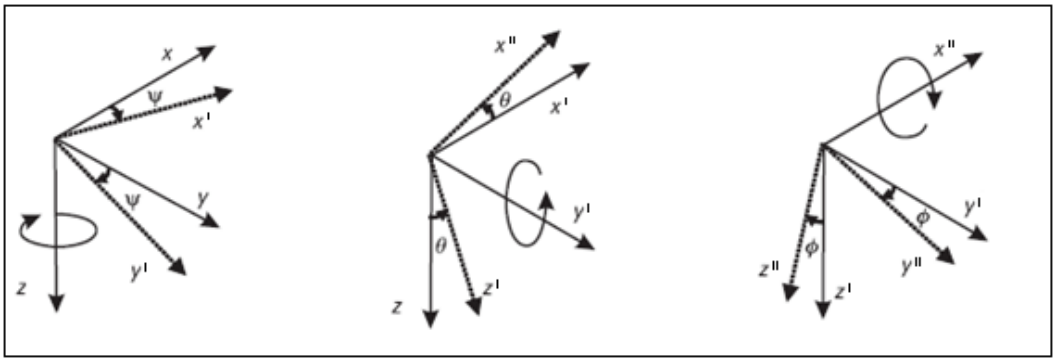

Figure 11: Three Basic Rotations about z-axis, y-axis and x-axis

For this study, the Euler angles describe the satellite body attitude relative to the Orbit Level frame. The 3-2-1 rotation sequence is applied as expressed above.

The Euler angle representation is one of the simplest techniques in terms of the physical interpretation. However, Euler angles exhibit a singularity at $\pm 90^o$ for the second rotation angle. Because of this difficulty, Euler angles are not commonly used for the spacecraft attitude computations.

5.1.2 QUATERNIONS

The quaternion attitude representation allows a transformation from one coordinate frame to another by a single rotation about a unit vector $\boldsymbol{u}$ by an amount of . The quaternion is a four-element-vector representation. However, as the Euler angle representation, only three components are independent. The elements of a quaternion are functions of the orientation of this vector and the magnitude of the rotation:

$$q = \begin{bmatrix} q_0 \\ q_1 \\ q_2 \\ q_3 \end{bmatrix} = \begin{bmatrix} \cos(\mu/2) \\ u_x \sin(\mu/2) \\ u_y \sin(\mu/2) \\ u_z \sin(\mu/2) \end{bmatrix} \quad 5.1$$

where u_x, u_y, u_z are the components of the unit vector $\boldsymbol{u}$ representing the rotation axis.

A quaternion can also be expressed as a four parameter complex number with a real component and three imaginary components as follows:

$$\boldsymbol{q} = q_0 + q_1\boldsymbol{i} + q_2\boldsymbol{j} + q_3\boldsymbol{k} \quad 5.2$$

The quaternions satisfy the constraint $\boldsymbol{q}^T\boldsymbol{q} = 1$.

In this study, in order to overcome the singularity problem in the attitude representation, quaternions are used during the computations; however, the results are converted to the Euler angles for easy interpretation.

5.2 COORDINATE SYSTEMS AND ROTATION MATRICES

The attitude of a spacecraft is the orientation of its body frame coordinate system with respect to a reference coordinate system in space. Each coordinate system can be transformed to another by three rotations. The matrix obtained by these rotations is defined as the rotation matrix. Therefore, the concept of coordinate system and rotation matrix are two basic elements during the attitude estimation process.

5.2.1 COORDINATE SYSTEMS

The main coordinate frames used in this thesis are defined briefly in this Chapter.

During the attitude estimation process, the attitude is propagated by using the angular velocity of the spacecraft. The angular velocity is propagated by using the Euler's equation, which is defined in inertial reference frame. Therefore, ECI frame is an important frame for this study.

Almost for all the GPS receivers, the GPS satellite position and velocity measurements are given in the ECEF (Earth-Centered Earth Fixed) coordinate system. Therefore, it is the other frame that is described in this chapter.

The Earth-Centered orbit frame is used just as an intermediate frame while transformation between ECI - orbit level and ECEF - orbit level frames.

Because the main scope of this thesis is the attitude determination, the main reference frames are satellite body and orbit level frames. The attitude of the satellite is defined between these reference frames.

5.2.1.1 Earth Centered Inertial Coordinate System

The Earth Centered Inertial (ECI) frame is considered as a non-accelerated, non-rotated reference frame in which Newton's laws is valid. It is centered at the Earth's center of mass and oriented with respect to the Earth's spin axis and vernal equinox direction. The z-axis is aligned with the Earth's spin axis, the x-axis is pointing towards vernal equinox. Vernal equinox is the point where ecliptic (the plane of Earth's orbit about the Sun) crosses the equatorial plane going from south to north. The y-axis completes the right-handed orthogonal set. The frame is denoted by I.

5.2.1.2 Earth Centered Earth Fixed Coordinate System

The Earth Centered Earth Fixed (ECEF) frame is similar to the ECI frame, except that all axes are fixed with respect to the Earth. The ECEF frame has also its origin at the Earth's center of mass. The z-axis points along the Earth's spin axis, the x-axis points from the center to the intersection of the equator with the conventional zero meridian (CZM), which defines 0 degree longitude. The y-axis completes the right-handed orthogonal set. This frame is denoted by E.

5.2.1.3 Earth Centered Orbital Coordinate System

This is the frame in which the Keplerian elements are defined. The origin is located at the Earth's center of mass. The x-axis points the perigee, the z-axis is perpendicular to the orbital plane and y-axis completes the orthogonal right-handed system. The frame is denoted O.

Although the orbit rotates slowly because of the perturbations due to non-spherical central body, gravitational attraction of other bodies, etc., this frame can be considered as an inertial frame.

5.2.1.4 Orbit Level Coordinate System

The orbit level coordinate system is a system of coordinates that maintain its orientation relative to the Earth as the satellite moves along its orbit. It is used as the reference to measure the attitude of the satellite. The origin is located at the satellite's center of mass. The z-axis is directed toward the nadir (i.e. toward the mass center of the Earth), y-axis is along the negative orbit normal and the x-axis completes the orthogonal right-handed system. Therefore, in a circular orbit, the x-axis will be along the negative velocity vector. The orbit level frame is denoted by L. The representation of this coordinate system is given in Figure 12.

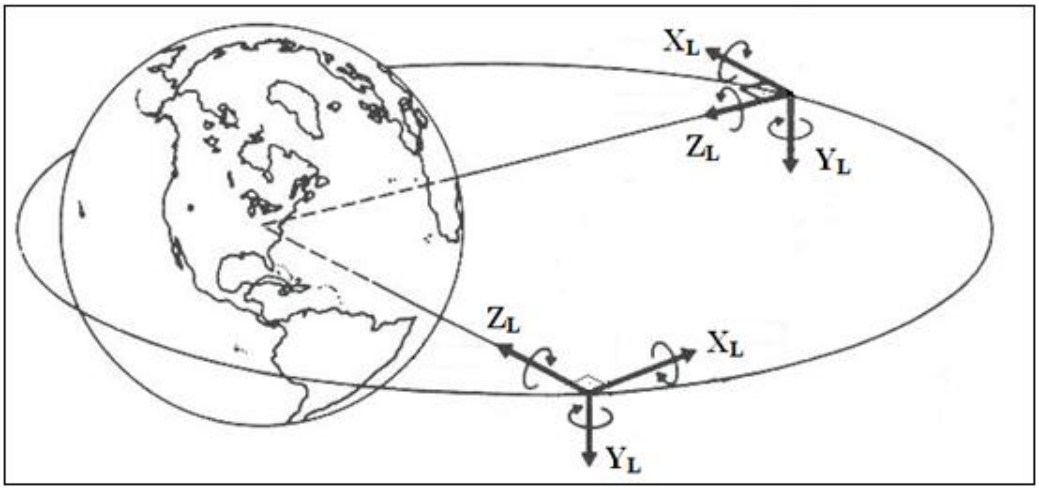

Figure 12: X-Y-Z Axis in the Orbit Level Coordinate System [6]

5.2.1.5 Satellite Body Coordinate System

This frame is fixed relative to the satellite's body, and its origin is placed at the satellite's center of mass. The orientation of the satellite is described relative to the orbit level frame, while angular velocities are expressed in the Body frame. The axes of body frame coincide with the principle axes of satellite. It is assumed that the roll, pitch and yaw angles are zero when the body frame is perfectly aligned with the orbit level frame. This frame is denoted by B. The representation of satellite body coordinate system is given in Figure 13.

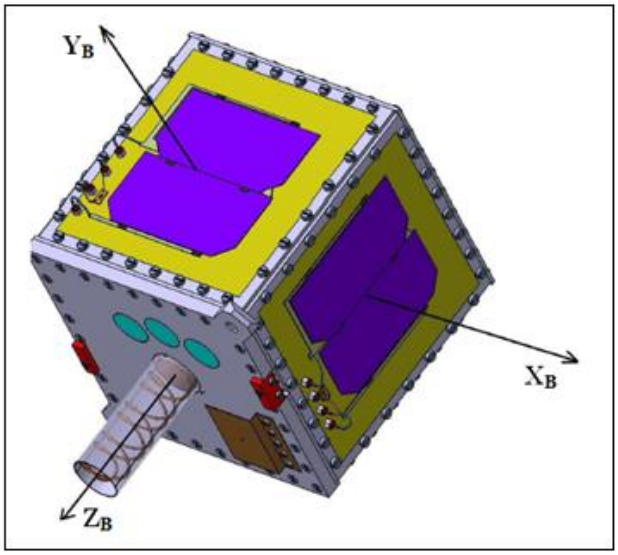

Figure 13: X-Y-Z Axis in the Satellite Body Coordinate System [30]

5.2.2 ROTATION MATRICES

The rotation matrix is a 3x3 matrix and denoted by $\mathbf{R}_{\alpha}^{\beta}$. The lower index represents the coordinate system which is transformed and the upper index represents the final coordinate system after the transformation. The rotation of a vector, $\boldsymbol{v}$, from α to β coordinate systems can be represented with the following notation:

$$\boldsymbol{v}^{\beta} = \boldsymbol{R}_{\alpha}^{\beta}\boldsymbol{v}^{\alpha} \tag{5.3}$$

The rotation matrix satisfies:

$$\boldsymbol{R}_{\alpha}^{\beta} = \left(\boldsymbol{R}_{\beta}^{\alpha}\right)^{-1} = \left(\boldsymbol{R}_{\beta}^{\alpha}\right)^{T} \tag{5.4}$$

The rotations about x-y-z axes may be expressed as three separate rotation matrices:

$$\boldsymbol{R}_x(\phi) = \begin{bmatrix} 1 & 0 & 0 \\ 0 & cos\,\phi & sin\,\phi \\ 0 & -sin\,\phi & cos\,\phi \end{bmatrix} \quad 5.5$$

$$\boldsymbol{R}_y(\theta) = \begin{bmatrix} \cos\theta & 0 & -\sin\theta \\ 0 & 1 & 0 \\ \sin\theta & 0 & \cos\theta \end{bmatrix} \quad 5.6$$

$$\boldsymbol{R}_z(\psi) = \begin{bmatrix} \cos\psi & \sin\psi & 0 \\ -\sin\psi & \cos\psi & 0 \\ 0 & 0 & 1 \end{bmatrix} \quad 5.7$$

where

$\boldsymbol{R}_x(\phi)$ represents the rotation about the x-axis by an amount of ϕ degrees.

$\boldsymbol{R}_y(\theta)$ represents the rotation about the y-axis by an amount of θ degrees.

$\boldsymbol{R}_z(\psi)$ represents the rotation about the z-axis by an amount of ψ degrees.

5.2.2.1 Transformation from ECI to Earth Centered Orbital Coordinate System

The Earth-Centered orbital coordinate system is related geometrically to the ECI frame through the angles ω, i and Ω as shown in Figure 14.

$$\boldsymbol{R}_I^O = \boldsymbol{R}_z(\omega)\boldsymbol{R}_x(i)\boldsymbol{R}_z(\Omega) \quad 5.8$$

where ω is the argument of perigee, i is the inclination of the satellite orbit and Ω is the right ascension of the ascending node.

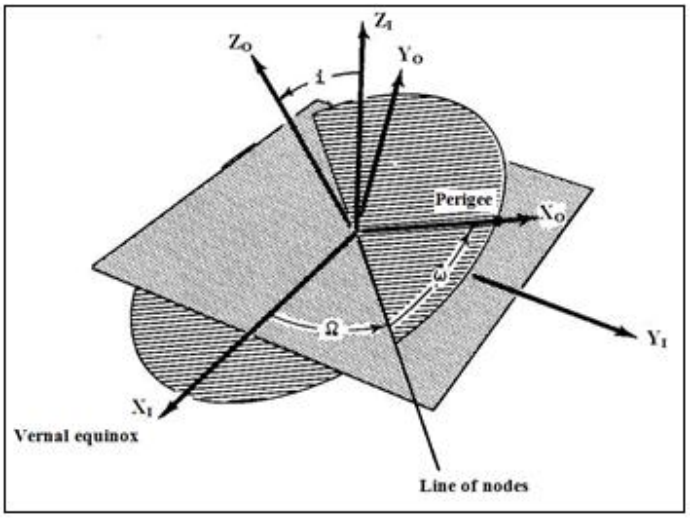

Figure 14: Rotation Angles for ECI to Earth Centered Orbital Frame Transformation [30]

5.2.2.2 Transformation from Earth Centered Orbital Coordinate System to Orbit Level Coordinate System

The rotation matrix depends on only the true anomaly of the satellite. According to the definitions of the related reference frames, the rotation matrix can be expressed as follows:

$$\boldsymbol{R}_O^L = \boldsymbol{R}_y(-\nu)\boldsymbol{R}_x(-90^o)\boldsymbol{R}_z(90^o) \tag{5.9}$$

where ν is the true anomaly of the satellite.

This transformation is an intermediate state in order to obtain the rotation matrix between ECI and orbit level coordinate system. Then, the rotation matrix between these reference frames can be obtained as follows:

$$\boldsymbol{R}_I^L = \boldsymbol{R}_O^L \boldsymbol{R}_I^O \tag{5.10}$$

5.2.2.3 Transformation from Orbit Level Coordinate System to Satellite Body Coordinate System

The rotation matrix used for the transformation between orbit level and satellite body coordinate systems is used extensively in this report. This rotation depends on the attitude of the satellite. In this study, the rotation matrix parameterized by the Euler angles is defined based on a 3-2-1 rotation sequence and it is represented by R_L^B

$$\boldsymbol{R}_L^B = \boldsymbol{R}_x(\phi)\boldsymbol{R}_y(\theta)\boldsymbol{R}_z(\psi) \tag{5.11}$$

$$\boldsymbol{R}_L^B = \begin{bmatrix} \mathrm{c}\,\theta\,\mathrm{c}\,\psi & \mathrm{c}\,\theta\,\mathrm{s}\,\psi & -\mathrm{s}\,\theta \\ -\mathrm{c}\,\phi\,\mathrm{s}\,\psi + \mathrm{s}\,\phi\,\mathrm{s}\,\theta\,\mathrm{c}\,\psi & \mathrm{c}\,\phi\,\mathrm{c}\,\psi + \mathrm{s}\,\phi\,\mathrm{s}\,\theta\,\mathrm{s}\,\psi & \mathrm{s}\,\phi\,\mathrm{c}\,\theta \\ \mathrm{s}\,\phi\,\mathrm{s}\,\psi + \mathrm{c}\,\phi\,\mathrm{s}\,\theta\,\mathrm{c}\,\psi & -\mathrm{s}\,\phi\,\mathrm{c}\,\psi + \mathrm{c}\,\phi\,\mathrm{s}\,\theta\,\mathrm{s}\,\psi & \mathrm{c}\,\phi\,\mathrm{c}\,\theta \end{bmatrix} \tag{5.12}$$

where ϕ is the roll angle, θ is the pitch angle, ψ is the yaw angle of the Satellite, c represents the cosine, and s represents the sine of the related angle.

However, in this study, the quaternion representation is used during the calculations. The rotation matrix expressed in terms of quaternions is as follows:

$$\boldsymbol{R}_L^B = \begin{bmatrix} {q_0}^2 + {q_1}^2 - {q_2}^2 - {q_3}^2 & 2(q_1q_2 + q_0q_3) & 2(q_1q_3 - q_0q_2) \\ 2(q_1q_2 - q_0q_3) & {q_0}^2 - {q_1}^2 + {q_2}^2 - {q_3}^2 & 2(q_2q_3 + q_0q_1) \\ 2(q_1q_3 + q_0q_2) & 2(q_2q_3 - q_0q_1) & {q_0}^2 - {q_1}^2 - {q_2}^2 + {q_3}^2 \end{bmatrix}$$

5.13

5.3 SATELLITE ORBIT AND ATTITUDE DETERMINATION

Although the primary interest of this study is the satellite attitude determination, the knowledge of the satellite's position and velocity is also required due to the fact that the orbit level frame depends on the position and the velocity of the satellite. The position of the satellite is also necessary for the calculation of the gravity gradient torque. In order to analyze the performance of the attitude filter, the true position and velocity of the satellite is modeled as well as the attitude dynamics. In order to obtain simulated GPS data, the position and velocity of the GPS satellites are also calculated analytically. The details on the models are described in this chapter.

5.3.1 ORBIT DYNAMICS

5.3.1.1 User Satellite Orbit Dynamics

The motion of the satellite is described by assuming that it is a two-body problem with the effects of the second zonal harmonics, J_2. The two-body problem assumption can be expressed as:

- The bodies are spherically symmetric. In other words, their masses were concentrated at their centers.
- There are no external or internal forces acting on the system other than the gravitational forces which act along the line joining the centers of the two bodies.

The second zonal harmonic, J_2, is a zonal harmonic coefficient in an infinite Jacobi Polynomial series representation of the Earth's gravity field. It represents the dominant effects of Earth oblateness and has the value of 1.082629×10^{-3}. The other harmonics are at least 1000 times smaller than J_2. The J2 propagator includes only the dominant first-order secular effects, but it does not model atmospheric drag, solar or lunar gravitational forces.

The equations of the motion are [28]:

$$\begin{aligned}
\ddot{x} &= \frac{-\mu x}{r^3}\left[1 - \frac{3}{2}J_2\left(\frac{R_e}{r}\right)^2\left(5\frac{z^2}{r^2} - 1\right)\right] \\
\ddot{y} &= \frac{-\mu y}{r^3}\left[1 - \frac{3}{2}J_2\left(\frac{R_e}{r}\right)^2\left(5\frac{z^2}{r^2} - 1\right)\right] \\
\ddot{z} &= \frac{-\mu z}{r^3}\left[1 - \frac{3}{2}J_2\left(\frac{R_e}{r}\right)^2\left(5\frac{z^2}{r^2} - 3\right)\right]
\end{aligned} \qquad 5.14$$

where $r = \sqrt{x^2 + y^2 + z^2}$ and x, y, z are satellite position coordinated with respect to the Earth centered inertial reference frame, R_e is the Earth radius, μ is the Earth's gravitational constant, and J_2 is the Earth's 2nd order zonal harmonics.

5.3.1.2 GPS Satellite Orbit Dynamics

The position and velocity of the GPS satellites are calculated by considering only the two-body effects. This is the simplest form of the unpertubed satellite motion in an elliptic orbit about a perfect sphere of uniform density. Under these assumptions, a satellite will obey Kepler's laws of planetary motion and Newton's law of universal gravitation. The equation obtained considering these assumtions is in the form of:

$$\ddot{\mathbf{r}} = \frac{-\mu \cdot \mathbf{r}}{r^3} \tag{5.15}$$

The properties for the GPS satellite orbits are obtained by using a Two Line Element (TLE) file, which are published in a particular format. It includes the orbital elements, which gives information about the shape, size and orientation of the orbit. Then, by using the orbital elements, the initial condition in ECI frame is obtained. The details about the transformation from orbital elements to the Cartesian coordinates in ECI frame are given in Appendix C.

5.3.2 ATTITUDE KINEMATICS

The quaternion, q, propagates with the following equation [19]:

$$\dot{\boldsymbol{q}} = 0.5\, \boldsymbol{q} \otimes \boldsymbol{p}_{LB}^{B} \tag{5.16}$$

where $\boldsymbol{p}_{LB}^{B} = \begin{bmatrix} 0 & \boldsymbol{\omega}_{LB}^{B\,T} \end{bmatrix}^T$ and the operator '$\otimes$' refers to the quaternion multiplication.

This equation can be expressed in the matrix form as follows:

$$\dot{\boldsymbol{q}} = \begin{bmatrix} \dot{q}_0 \\ \dot{q}_1 \\ \dot{q}_2 \\ \dot{q}_3 \end{bmatrix} = 0.5 \begin{bmatrix} q_0 & -q_1 & -q_2 & -q_3 \\ q_1 & q_0 & -q_3 & q_2 \\ q_2 & q_3 & q_0 & -q_1 \\ q_3 & -q_2 & q_1 & q_0 \end{bmatrix} \begin{bmatrix} 0 \\ \omega_x \\ \omega_y \\ \omega_z \end{bmatrix} \tag{5.17}$$

where $\omega_x, \omega_y, \omega_z$ refers to the x-y-z components of the vector $\boldsymbol{\omega}_{LB}^{B}$ respectively.

Since in the dynamics equations below, the angular velocity of the satellite with respect to an inertial frame ($\boldsymbol{\omega}_{IB}^{B}$) is used, it is more convenient to remove the angular velocity of orbit level frame with respect to the inertial frame ($\boldsymbol{\omega}_{IL}^{B}$):

$$\boldsymbol{\omega}_{LB}^{B} = \boldsymbol{\omega}_{IB}^{B} - \boldsymbol{\omega}_{IL}^{B} \tag{5.18}$$

where $\boldsymbol{\omega}_{IL}^{B} = \boldsymbol{R}_{L}^{B}\boldsymbol{\omega}_{IL}^{L}$ and $\boldsymbol{\omega}_{IL}^{L} = [0 \quad -\dot{u} \quad 0]^{T}$.

u in Equation 5.18 refers to the argument of latitude. The calculation of the arguments of latitude is given in the Appendix C.

Then the quaternion differential equations become:

$$\begin{aligned}
\dot{q}_0 &= -0.5[q_1\omega_1 + q_2(\omega_2 + \dot{u}) + q_3\omega_3] \\
\dot{q}_1 &= \quad 0.5[q_0\omega_1 + q_2\omega_3 - q_3(\omega_2 - \dot{u})] \\
\dot{q}_2 &= \quad 0.5[q_0(\omega_2 + \dot{u}) - q_1\omega_3 + q_3\omega_1] \\
\dot{q}_3 &= \quad 0.5[q_0\omega_3 + q_1(\omega_2 - \dot{u}) - q_2\omega_1]
\end{aligned} \tag{5.19}$$

5.3.3 ATTITUDE DYNAMICS

The satellite body is assumed to be a rigid body, which means the distance between any two points in the body remains constant in any motion. The rotational equations of motion for a rigid body can be expressed by Euler's equation.

$$\dot{\boldsymbol{h}} + \boldsymbol{\omega} \times \boldsymbol{h} = \boldsymbol{M} \tag{5.20}$$

where $\boldsymbol{h}$ is the angular momentum vector of the satellite, $\boldsymbol{\omega}$ is the angular velocity of the satellite with respect to the inertial frame and $\boldsymbol{M}$ is the net applied torque about the mass center.

In order to ensure the yaw stabilization of the satellite, it is assumed that a constant speed momentum wheel with a spin axis perpendicular to the orbit plane is attached to the satellite. Then the total angular momentum, $\boldsymbol{h}$, can be expressed as:

$$\boldsymbol{h} = \boldsymbol{I}\boldsymbol{\omega} + \boldsymbol{h}_{\boldsymbol{w}} \tag{5.21}$$

where $\boldsymbol{I}$ is the mass moment of inertia and $\boldsymbol{h}_{\boldsymbol{w}}$ is the angular momentum vector due to the momentum wheel and it is equal to $\boldsymbol{h}_{\boldsymbol{w}} = -h_w\boldsymbol{j}^{\boldsymbol{B}}$.

During this study, it is assumed that the net torque acting on the satellite body is only the gravity gradient torque, $\boldsymbol{M}_{GG}$, and it is equal to the equation below [6].

$$\boldsymbol{M} = \boldsymbol{M}_{GG} = \frac{3\mu}{r^3}\boldsymbol{u_r} \times (\boldsymbol{I}\boldsymbol{u_r}) \tag{5.22}$$

,where r is the satellite orbit radius in a circular orbit, $\boldsymbol{u_r}$ is the unit vector in the radial direction, $\boldsymbol{I}$ is the mass moment of inertia, μ is Earth's gravitational constant and its value is $398600.4415\ km^3/s^2$.

After inserting Equations 5.21 and 5.22 to the Euler's equation given in Equation 5.20:

$$\boldsymbol{I}\dot{\boldsymbol{\omega}} + \boldsymbol{\omega} \times (\boldsymbol{I}\boldsymbol{\omega} + \boldsymbol{h_w}) = \frac{3\mu}{r^3}\boldsymbol{u_r} \times (\boldsymbol{I}\boldsymbol{u_r}) \tag{5.23}$$

Since $\boldsymbol{I}$ is constant in the satellite body frame, it is convenient to write the matrix form of the above equation in the body frame. It is also assumed that the body frame axes are aligned with the principle axes; therefore, the moment of inertia matrix is a diagonal matrix. Then the matrix form of Equation 5.23 can be expressed as:

$$\boldsymbol{I^B}\dot{\boldsymbol{\omega}}_{IB}^{B} + [\boldsymbol{\omega}_{IB}^{B} \wedge]\left(\boldsymbol{I^B}\boldsymbol{\omega}_{IB}^{B} + \boldsymbol{h_w}^{B}\right) = \frac{3\mu}{r^3}[\boldsymbol{u_r}^{B} \wedge]\left(\boldsymbol{I^B}\boldsymbol{u_r}^{B}\right) \tag{5.24}$$

,where $[\boldsymbol{\omega}_{IB}^{B} \wedge]$ is the skew-symmetric form of the vector $\boldsymbol{\omega}_{IB}^{B}$, $\boldsymbol{u_r}^{B} = \boldsymbol{R}_L^B\boldsymbol{u_r}^{L}$ and $\boldsymbol{u_r}^{L} = [1 \quad 0 \quad 0]^T$. Therefore; $\boldsymbol{u_r}^{B} = \begin{bmatrix}\boldsymbol{R}_L^B(1,1)\\ \boldsymbol{R}_L^B(2,1)\\ \boldsymbol{R}_L^B(3,1)\end{bmatrix}$

Then the right hand side of the equation becomes as:

$$\boldsymbol{M}_{GG}^{B} = \frac{3\mu}{r^3}\begin{bmatrix}(I_3 - I_2)\boldsymbol{R}_L^B(2,1)\boldsymbol{R}_L^B(3,1)\\ (I_1 - I_3)\boldsymbol{R}_L^B(1,1)\boldsymbol{R}_L^B(3,1)\\ (I_2 - I_1)\boldsymbol{R}_L^B(1,1)\boldsymbol{R}_L^B(2,1)\end{bmatrix} \tag{5.25}$$

Finally, the final form of the Euler's equation (Equation 5.24) becomes:

$$\begin{bmatrix}I_1\dot{\omega}_1\\ I_2\dot{\omega}_2\\ I_3\dot{\omega}_3\end{bmatrix} + \begin{bmatrix}0 & -\omega_3 & \omega_2\\ \omega_3 & 0 & -\omega_1\\ -\omega_2 & \omega_1 & 0\end{bmatrix}\begin{bmatrix}I_1\omega_1\\ I_2\omega_2 - h_w\\ I_3\omega_3\end{bmatrix} = \frac{3\mu}{r^3}\begin{bmatrix}(I_3 - I_2)\boldsymbol{R}_L^B(2,1)\boldsymbol{R}_L^B(3,1)\\ (I_1 - I_3)\boldsymbol{R}_L^B(1,1)\boldsymbol{R}_L^B(3,1)\\ (I_2 - I_1)\boldsymbol{R}_L^B(1,1)\boldsymbol{R}_L^B(2,1)\end{bmatrix} \tag{5.26}$$

$$\dot{\omega}_1 = \frac{(I_2 - I_3)}{I_1}\left[\omega_2\omega_3 - \frac{3\mu}{r^3}\boldsymbol{R}_L^B(2,1)\boldsymbol{R}_L^B(3,1)\right] - \omega_3\frac{h_w}{I_1}$$

$$\dot{\omega}_2 = \frac{(I_3 - I_1)}{I_2}\left[\omega_1\omega_3 - \frac{3\mu}{r^3}\boldsymbol{R}_L^B(1,1)\boldsymbol{R}_L^B(3,1)\right] \tag{5.27}$$

$$\dot{\omega}_3 = \frac{(I_1 - I_2)}{I_3}\left[\omega_1\omega_2 - \frac{3\mu}{r^3}\boldsymbol{R}_L^B(1,1)\boldsymbol{R}_L^B(2,1)\right] + \omega_1\frac{h_w}{I_3}$$

The transformation matrix from orbit level to satellite body coordinate system, R_L^B, is given in Equation 5.13.

CHAPTER 6

EXTENDED KALMAN FILTER

Instead of using only GPS observations, known dynamics can be integrated to the system in order to get a better solution. For this purpose, a Kalman Filter is designed as the estimation algorithm.

The Kalman filter is an optimal, recursive estimation algorithm developed by R. E. Kalman in 1960 and has been improved further by numerous researchers [20]. It is supplied by an initial estimate of the states and then operates recursively. It updates the unknown states as a weighted average of their previous values and new values derived from latest measurements [20]. The measurements must be the functions of the parameters to be estimated. The Kalman filter was designed under the assumption that the measurement noise has a zero mean Gaussian distribution.

In a standard Kalman filter, the measurement model and the system model is assumed to be linear. In other words, the measurement model and the time derivatives of the states are a linear function of the state vector. However, this is not the case for the GPS based attitude determination system. In such a system, the GPS differential carrier phase observations are related with the state parameters (quaternion and inertial angular velocity vector) by nonlinear equations. The attitude dynamic equations are also nonlinear. Therefore, the extended Kalman filter, which is a nonlinear version of the standard Kalman filter, is preferred to be used. The continuous time, nonlinear system model and measurement model can be described as:

$$\dot{x}(t) = f(\mathrm{x}, \mathrm{t}) + \mathrm{w}(t) \tag{6.1}$$

$$\mathrm{z}(t) = h(\mathrm{x}, \mathrm{t}) + v(t) \tag{6.2}$$

where $x(t)$ is the state vector and f is the nonlinear system model, w is the process noise, z is the measurement vector, h is the nonlinear measurement model and v is the measurement noise.

In the EKF, it is assumed that the error in the state vector is much smaller than the states themself. Therefore, by using error states, the problems due to the linearization process lessen. Then the system model and its linearized version become as:

$$\delta\dot{x}(t) = F(x,t)\delta\mathrm{x}(t) + w(t) \tag{6.3}$$

where δx is the error state vector, F is the linearized system model and it can be calculated as in Equation 6.4.

$$F(x,t) = \left.\frac{\partial f(x,t)}{\partial x}\right|_{\hat{x}(t)} \tag{6.4}$$

Moreover, in the EKF, the measurement innovation is used instead of the measurement's itself in order to reduce the linearization errors. The measurement innovation can be calculated as:

$$\delta z(t) = H(x,t)\,\delta x(t) + v(t) \tag{6.5}$$

,where H is the linearized measurement matrix and it can be calculated as:

$$H(x,t) = \left.\frac{\partial h(x,t)}{\partial x}\right|_{\hat{x}(t)} \tag{6.6}$$

The derivation of Equations 6.3, 6.4 and 6.5 is given in Appendix D.

In order to construct a discrete Kalman filter, it is necessary to express the system error equation (Equation 6.3) and the measurement innovation equation (Equation 6.5) in the discrete form.

$$\delta x_k = \Phi_{k-1}\delta x_{k-1} \tag{6.7}$$

$$\delta z_k = H_k\delta x_k + v_k \tag{6.8}$$

,where Φ is the state transition matrix and it is calculated using Equation 6.22.

After the linearized system model and measurement model is obtained, the standard Kalman filter equations can be applied in order to obtain the optimal estimates.

6.1 GENERAL KALMAN FILTER EQUATIONS

The Kalman filter is composed of three steps. The first step is the state and error covariance propagation in time. Then, the Kalman gain calculation is performed using the propagated state vector and covariance matrix. Finally, the measurements are used in order to correct the propagated states and their covariance.

The general equations for a discrete Kalman filter are presented below:

Time update equations

$$x_k^- = \Phi_{k-1} x_{k-1}^+ \tag{6.9}$$

$$P_k^- = \Phi_{k-1} P_{k-1} \Phi_{k-1}^T + Q_{k-1} \tag{6.10}$$

Kalman filter gain calculation

$$K_k = P_k^- H_k^T \left(H_k P_k^- H_k^T + R_k \right)^{-1} \tag{6.11}$$

Measurement update equations

$$x_k^+ = x_k^- + K_k (Z_k - H_k x_k^-) \tag{6.12}$$

$$P_k^+ = P_k^- - K_k H_k P_k^- \tag{6.13}$$

where

x : State vector

P : State covariance matrix

Φ : State transition matrix

Q : Process noise covariance matrix

R : Measurement noise covariance matrix

Z : Measurement

H : Measurement matrix

After the error state vector is estimated, the quaternion and the inertial angular velocity vector should be corrected as:

$$\boldsymbol{q}_{corrected} = \boldsymbol{\delta q} \otimes \boldsymbol{q}_{estimated} \tag{6.14}$$

$$\boldsymbol{\omega}_{corrected} = \boldsymbol{\delta \omega} + \boldsymbol{\omega}_{estimated} \tag{6.15}$$

6.2 STATE VECTOR SELECTION

The state vector is a set of parameters to be estimated in the Kalman filter algorithm. In this thesis the error state vector is composed of three quaternion and three inertial angular velocity parameters in body frame.

$$\boldsymbol{\delta x} = [\delta q_1\ \delta q_2\ \delta q_3\ \delta\omega_1\ \delta\omega_2\ \delta\omega_3]^T \tag{6.16}$$

,where

$$\boldsymbol{\delta q} = \boldsymbol{q_{true}} \otimes \boldsymbol{q_{estimated}}^{-1} \tag{6.17}$$

$$\boldsymbol{\delta\omega} = \boldsymbol{\omega_{true}} - \boldsymbol{\omega_{estimated}} \tag{6.18}$$

Traditionally, Euler angles may be preferred in the land, sea or air applications in order to describe the attitude of the vehicle. However, calculations of kinematic equations with Euler angles result in high computational load. Moreover, by using Euler angles, the singularity problem may arise when the second rotation angle is ∓ 90 degrees (pitch angle in this case). Because the maneuver characteristic of a satellite may be highly dynamic, the quaternions are preferred in the space applications in order to represent the attitude of the vehicle.

As it is described in Section 5.1.2, a quaternion is composed of four parameters. However, only the three of them is independent. Therefore, in this thesis, only the three of them (vector part) are included to the state vector in order to decrease the computational load. After the three components are estimated, the forth one is calculated as:

$$\delta q_4 = \sqrt{1 - {\delta q_1}^2 - {\delta q_2}^2 - {\delta q_3}^2} \tag{6.19}$$

6.3 LINEARIZED SYSTEM MODEL

In order to obtain the discrete time system transition matrix, Φ_k, the continuous time system model should be linearized firstly. The linearized system model, F, and the derivation process are given in Appendix E.

Then the discrete time state transition matrix, Φ_k, can be calculated by using the equation below:

$$\boldsymbol{\Phi_k} = e^{\Delta t \boldsymbol{F}} \tag{6.20}$$

This exponential matrix can be computed as a power-series expansion.

$$\boldsymbol{\Phi_k} = \sum_{r=0}^{\infty} \frac{\Delta t^r \boldsymbol{F}^r}{r!} = I + \Delta t \boldsymbol{F} + \frac{1}{2}\Delta t^2 \boldsymbol{F}^2 + \frac{1}{6}\Delta t^3 \boldsymbol{F}^3 + \cdots \tag{6.21}$$

In this thesis, the state transition matrix calculated as taking only the first two terms of the expansion considering the fact that Δt is a small number, which is 0.01 sec. Then,

$$\boldsymbol{\Phi_k} = \boldsymbol{I} + \Delta t \boldsymbol{F} \tag{6.22}$$

6.4 LINEARIZED MEASUREMENT MODEL

In order to update the state vector estimate with the measurements, it is necessary to know how the measurements change with the states. In other words, the function of measurement model should be driven. The measurement matrix, H, represents this relation of the range difference measurements to the quaternion and angular velocity states such that:

$$\boldsymbol{H} = [\boldsymbol{H_q} \quad \boldsymbol{H_\omega}] \tag{6.23}$$

From Equation 6.5, the elements of the H matrix can be calculated using the equations below:

$$\boldsymbol{H_q} = \frac{\partial \delta r}{\partial \boldsymbol{\delta q}} \tag{6.24}$$

$$\boldsymbol{H_\omega} = \frac{\partial \delta r}{\partial \boldsymbol{\delta \omega}} \tag{6.25}$$

In the equations above δr represents the measurement innovation and it is equal to:

$$\delta r = \Delta r - \Delta \hat{r} \tag{6.26}$$

where Δr represents the delta range measured by the GPS receiver and $\Delta \hat{r}$ represent the estimated delta range. The equation for the Δr is derived in Chapter 3.2 and it is equal to:

$$\Delta r = (\boldsymbol{b}^B)^T \boldsymbol{R}_I^B \boldsymbol{e}^I \tag{6.27}$$

$$\Delta \hat{r} = (\boldsymbol{b}^B)^T \widehat{\boldsymbol{R}}_I^B \boldsymbol{e}^I \tag{6.28}$$

where $\boldsymbol{R}_I^B = \boldsymbol{\delta R}_I^B \widehat{\boldsymbol{R}}_I^B$

By definition, the quaternion error δq is just one half of the small Euler rotations. Then the rotation matrix difference, δR_I^B, can be approximated as:

$$\boldsymbol{\delta R}_I^B \approx \boldsymbol{I}_{3\times 3} - 2[\boldsymbol{\delta q} \wedge] \tag{6.29}$$

Then, the final form of the measurement innovation becomes:

$$\delta r = -2(\boldsymbol{b}^B)^T [\boldsymbol{\delta q} \wedge] \widehat{\boldsymbol{R}}_I^B \boldsymbol{e}^I \tag{6.30}$$

This equation can be rearranged as:

$$\delta r = \left\{-2\left(\widehat{\boldsymbol{R}}_I^B \boldsymbol{e}^I\right)^T [\boldsymbol{b}^B \wedge]\right\} \boldsymbol{\delta q} \tag{6.31}$$

Finally, the measurement matrix is found as:

$$\boldsymbol{H} = \left[-2\left(\widehat{\boldsymbol{R}}_I^B \boldsymbol{e}^I\right)^T [\boldsymbol{b}^B \wedge] \quad \boldsymbol{0}_{3\times 3}\right]_{3\times 6} \tag{6.32}$$

This matrix should be calculated for every baseline and for each satellite during the flight.

CHAPTER 7

GPS/GYRO ENTEGRATED EXTENDED KALMAN FILTER

As it is mentioned before, the fundamental problem of using GPS based attitude determination system is its low output rate. The other problem might be the low GPS signal visibility. This problem might be arisen for the high altitude satellites. For such cases, GPS based systems cannot meet the high accuracy requirement. Therefore, an integrated system with some high rate aiding sensors should be considered for such systems. Therefore, an integrated GPS receiver and three-axis gyro assembly is considered in this thesis in order to overcome the problems mentioned above. In this chapter, the details about the developed extended Kalman filter by using the GPS differential carrier phase measurements and three gyro measurements are given.

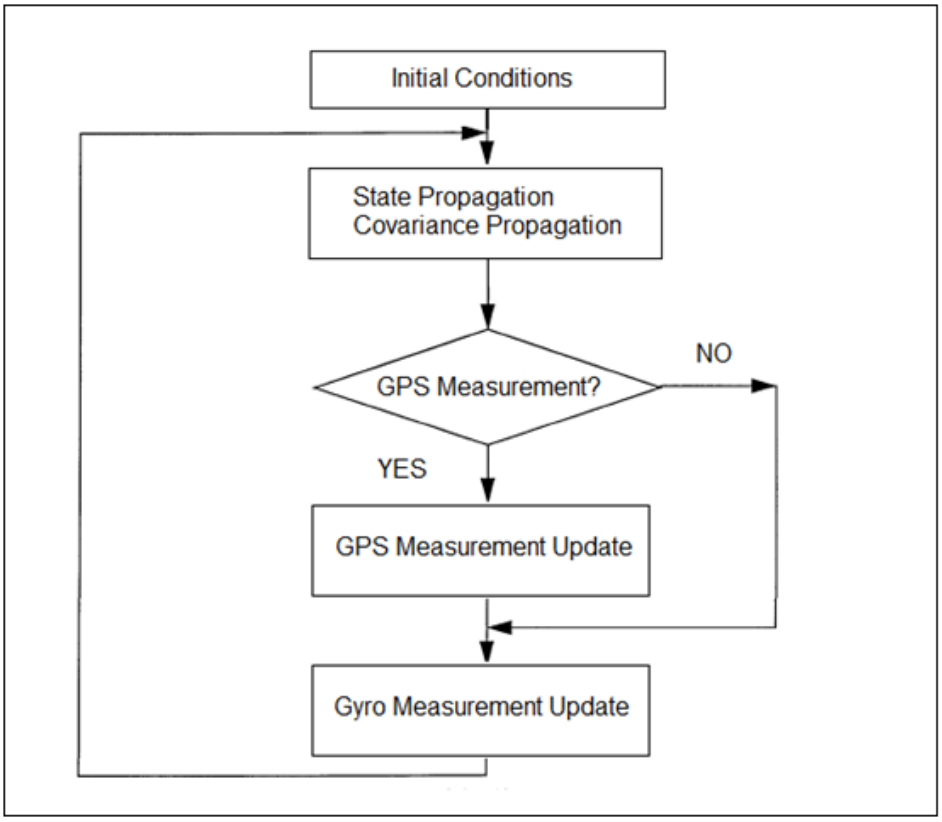

Figure 15: GPS/Gyro Integration Filter Algorithm

The same Kalman filter equations as the ones given in Chapter 6 are used. One of the differences with the GPS only EKF solution is the addition of three more states into the state vector.

The other difference is in the measurement model. In this filter, not only GPS differential phase measurements but also the gyro measurements in three axes are used in the measurement model.

The algorithm flow chart is given in Figure 15. The algorithm again is composed of time update and measurement update phases. Note that the Kalman gain is calculated in the measurement update phase. As it can be seen from the algorithm flow chart, the states are updated for both GPS and gyroscope measurements. However, the GPS measurement update is carried out at 1 Hz, while the gyro measurement update is at 100 Hz. Moreover, the algorithm checks whether the GPS measurements is available or not. If there is no GPS measurement at that time interval, the states are updated only with the gyro measurements.

7.1 STATE VECTOR SELECTION

In the GPS/Gyro integrated solution, the error state vector is composed of three quaternion components, three inertial angular velocities in body axis and three gyro bias drift states.

$$\boldsymbol{\delta x} = [\delta q_1\ \delta q_2\ \delta q_3\ \delta\omega_1\ \delta\omega_2\ \delta\omega_3\ b_1\ b_2\ b_3]^T \tag{7.1}$$

The other gyro errors, namely scale factor and misalignment error, are not included in the state vector due to the observability issues. These errors are not observable for most of the air, land, sea and space applications [20]. Therefore, including them to the Kalman filter states increases the computational load without any accuracy improvement.

7.2 LINEARIZED SYSTEM MODEL

The quaternion error and inertial angular velocity error propagation equations are derived in Chapter 6. For the integrated Kalman filter algorithm, only the gyro bias drift time propagation equation should be derived additionally. As it is mentioned in Chapter 4.3, the bias drift error of a gyroscope can be represented by a 1st order Gauss-Markov process [20].

$$\dot{b}_{Gyro} = -\frac{1}{\tau_{Gyro}} b_{Gyro} + w_{Gyro} \tag{7.2}$$

where w_{Gyro} is the zero mean Gaussian white noise. This term is also called as the driven noise.

Then the new continuous time system model can be written as:

$$\begin{bmatrix} \dot{\boldsymbol{x}}_{\boldsymbol{old}} \\ \dot{b}_1 \\ \dot{b}_2 \\ \dot{b}_3 \end{bmatrix} = \begin{bmatrix} \boldsymbol{F}_{\boldsymbol{old}} & 0 & 0 & 0 \\ 0 & -1/\tau_{Gyro,1} & 0 & 0 \\ 0 & 0 & -1/\tau_{Gyro,2} & 0 \\ 0 & 0 & 0 & -1/\tau_{Gyro,3} \end{bmatrix} \begin{bmatrix} \boldsymbol{x}_{\boldsymbol{old}} \\ b_1 \\ b_2 \\ b_3 \end{bmatrix} \tag{7.3}$$

where $\boldsymbol{x}_{old}$ and $\boldsymbol{F}_{old}$ represents the states and state transition matrix in Appendix E.

The discrete time state transition matrix is again calculated by using Equation 6.22

7.3 LINEARIZED MEASUREMENT MODEL

7.3.1 GPS Measurement Model

The measurement matrix, H_{GPS}, represents the relation between the range difference measurements and the Kalman filter states, namely, quaternions, inertial angular velocity and the gyro measurement bias drift.

$$\boldsymbol{H}_{\boldsymbol{GPS}} = [\boldsymbol{H}_{\boldsymbol{q,GPS}} \quad \boldsymbol{H}_{\boldsymbol{\omega,GPS}} \quad \boldsymbol{H}_{\boldsymbol{b,GPS}}]_{3\times 9} \tag{7.4}$$

The relation with quaternions and the inertial angular velocities is given in the previous Chapter. Because there is no relation between the gyro measurement bias drift and the GPS measurements, the new term $H_{b,GPS}$ is equal to zero for all three axes.

$$\boldsymbol{H}_{\boldsymbol{b,GPS}} = \boldsymbol{0}_{3\times 3} \tag{7.5}$$

7.3.2 Gyro Measurement Model

The measurement matrix, H_{Gyro}, represents the relation between the range difference measurements and the Kalman filter states:

$$\boldsymbol{H}_{\boldsymbol{Gyro}} = [\boldsymbol{H}_{\boldsymbol{q,Gyro}} \quad \boldsymbol{H}_{\boldsymbol{\omega,Gyro}} \quad \boldsymbol{H}_{\boldsymbol{b,Gyro}}]_{3\times 9} \tag{7.6}$$

where

$$\boldsymbol{H_{q,Gyro}} = \frac{\partial \boldsymbol{\delta\omega_{Gyro}}}{\partial \boldsymbol{\delta q}} \tag{7.7}$$

$$\boldsymbol{H_{\omega,Gyro}} = \frac{\partial \boldsymbol{\delta\omega_{Gyro}}}{\partial \boldsymbol{\delta\omega_{IB}^{B}}} \tag{7.8}$$

$$\boldsymbol{H_{b,Gyro}} = \frac{\partial \boldsymbol{\delta\omega_{Gyro}}}{\partial \boldsymbol{b_{Gyro}}} \tag{7.9}$$

In order to determine the elements of the gyro measurement matrix, the measurement innovation should be determined firstly. The measurement innovation, $\delta\omega_{Gyro}$, is the difference between the measured angular velocity and the estimated angular velocity.

$$\boldsymbol{\delta\omega_{Gyro}} = \left(\boldsymbol{\omega_{IB}^{B}} + \boldsymbol{b_{gyro}}\right) - \boldsymbol{\hat{\omega}_{IB}^{B}} \tag{7.10}$$

where $\left(\omega_{IB}^{B} + b_{gyro}\right)$ represents the measured angular velocity, while $\hat{\omega}_{IB}^{B}$ represents the estimated one.

After rearranging the equation, the measurement innovation is found as:

$$\boldsymbol{\delta\omega_{Gyro}} = \boldsymbol{\delta\omega_{IB}^{B}} + \boldsymbol{b_{Gyro}} \tag{7.11}$$

Then by using this equation, the elements of the measurement matrix are found as:

$$\boldsymbol{H_{q,Gyro}} = \mathbf{0_{3\times3}}$$

$$\boldsymbol{H_{\omega,Gyro}} = \boldsymbol{I_{3\times3}}$$

$$\boldsymbol{H_{b,Gyro}} = \boldsymbol{I_{3\times3}}$$

Finally,

$$\boldsymbol{H_{Gyro}} = [\mathbf{0_{3\times3}} \quad \boldsymbol{I_{3\times3}} \quad \boldsymbol{I_{3\times3}}]_{3\times9} \tag{7.12}$$

CHAPTER 8

RESULTS AND DISCUSSION

Two attitude estimation algorithms are developed in this thesis. One of them is based on a standalone GPS receiver. The other one includes a system with integrated GPS and three axis gyroscope. As the estimation algorithm, an extended Kalman filter algorithm is developed for both of the systems mentioned. The performance of each system is analyzed under with or without GPS outage conditions. The performances of algorithms are also compared for a case with only three GPS satellites are visible, which is the case for a middle/high altitude satellite.

The flow chart of the simulation developed is given in Figure 16. In the first step of the simulation, an initialization process is required. The parameters required in this step are given in Table 5. As a second step, the "User Satellite Attitude & Orbit Dynamics" part in Figure 16 is performed. In this step, the true position, velocity and attitude of the user satellite are calculated using Equations 5.14, 5.19 and 5.27. The related Simulink block is given in Figure 29 (Appendix F). Then, "GPS Satellites Orbit Dynamics" part are performed in order to obtain the GPS measurements. The position and velocity of the GPS satellites are calculated by integrating Equation 5.15. The pseudorange and the pseudorange rate measurements are also calculated in this step. The related Simulink block is given in Figure 30 (Appendix F).

Then, the "Delta Range Measurement Calculation" is performed by using Equation 3.3. The measurement errors like multipath error and receiver noise are added to the calculated delta ranges. Multipath error is modeled as a 1^{st} order Markov process as given in the Equation 3.16, while the receiver noise is assumed to be Gaussian white noise with zero mean. The Simulink block of this step is given in Figure 31.

After the GPS measurements are generated, a model is designed including a navigation filter and an attitude filter. The related Simulink model is given in Figure 33. In the navigation filter, the position and velocity of the user satellite is estimated by using the GPS pseudorange and pseudorange rate measurements. The details about the navigation filter are given in Appendix G. In the Attitude Filter part, an EKF is designed in order to estimate the attitude and angular rate of the satellite based on standalone GPS or GPS/Gyro measurements.

Finally, the estimated attitude solutions are compared with the true solutions in order to analyze the filter performance. The performances of the algorithms are analyzed under various GPS visibility conditions.

For the case where gyro measurements are also input to the simulation, a gyro measurement error model is modeled by using Equation 4.1. The Simulink model is given in Figure 32.

In this thesis, a low rate GPS receiver is assumed to be used. Therefore, in the simulation, the measurement rate of the GPS receiver is assumed to be 1 Hz. On the other hand, the measurement rate for the gyro measurement is selected as 100 Hz.

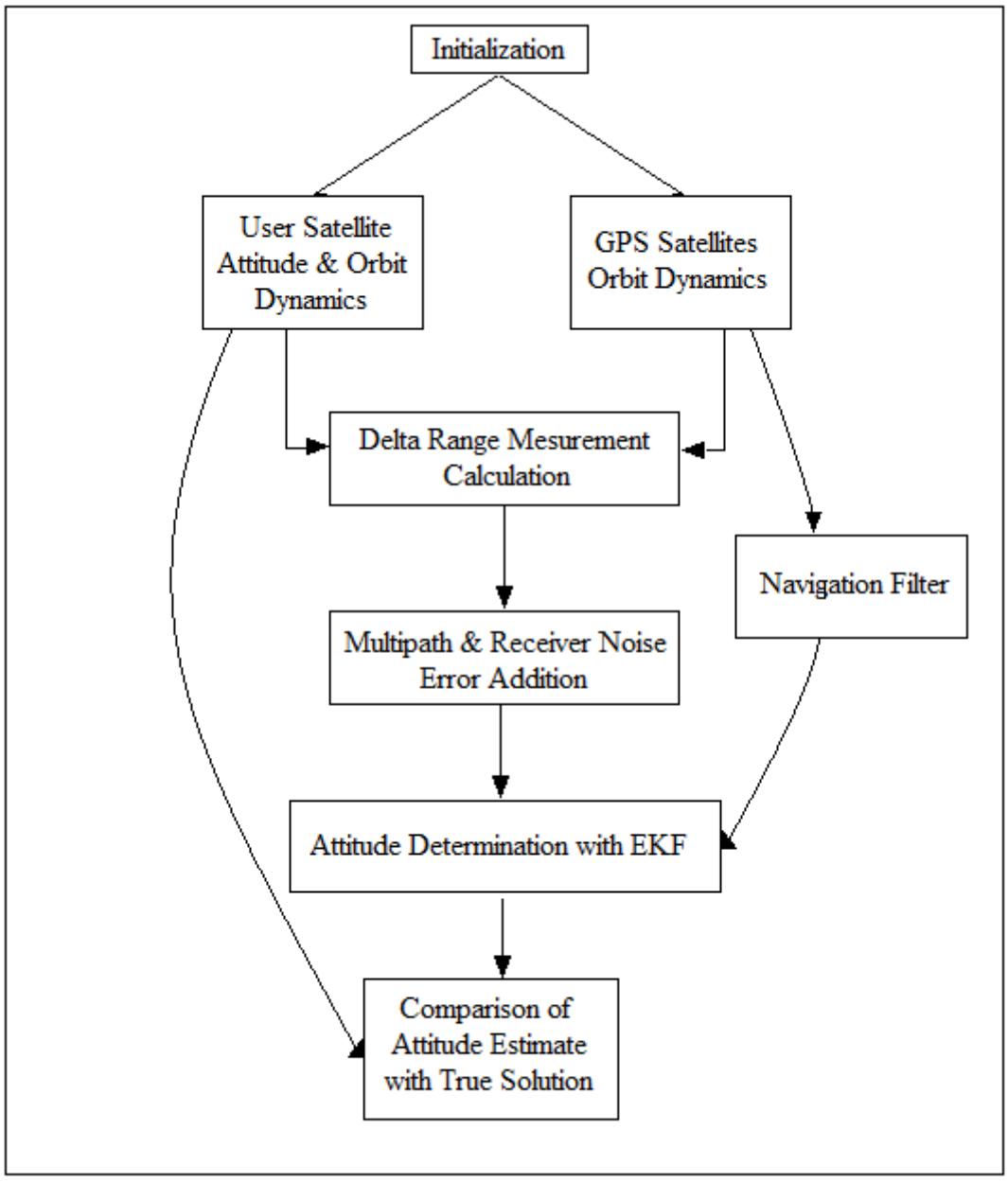

Figure 16: Flow Chart of the Simulation

The user satellite parameters and the initial conditions for the simulation are summarized in Table 5, while Figure 17 shows the true attitude solution of the satellite.

Table 5: User Satellite Parameters and Initial Conditions

USER SATELLITE PARAMETERS	
ORBITAL ELEMENTS	
Semi-major axis	7057 km
Eccentricity	0.00145
Inclination	98.1474 degrees
Argument of Perigee	236.6817 degrees
Right Ascension of Ascending Node	8.8030 degrees
True Anomaly	0
SATELLITE CONFIGURATION	
Moment of Inertia	I_1=1000 kg m^2 I_2=1500 kg m^2 I_3=2000 kg m^2
Momentum wheel	50 kg m^2/s
Antenna Configuration	4 antennas with 1m inter-antenna distance
SIMULATION INITIALIZATION	
INITIAL CONDITIONS	
Initial Euler Angles	3 degrees for three axes
Initial Euler Angle Error	3 degrees for three axes
Initial Angular Velocity	0.005 deg/s for three axes
Initial Angular Velocity Error	0.005 deg/s for three axes
Initial Position Error	1 m for three axes
Initial Velocity Error	0.01 m/s for three axes
MEASUREMENT ERRORS	
Pseudorange	σ = 6 m
Pseudorange rate	σ = 0.25 m/s
Receiver Noise on the Range Difference	σ = 1 mm
Multipath on the Range Difference	σ = 2 mm with 300 sec. time constant

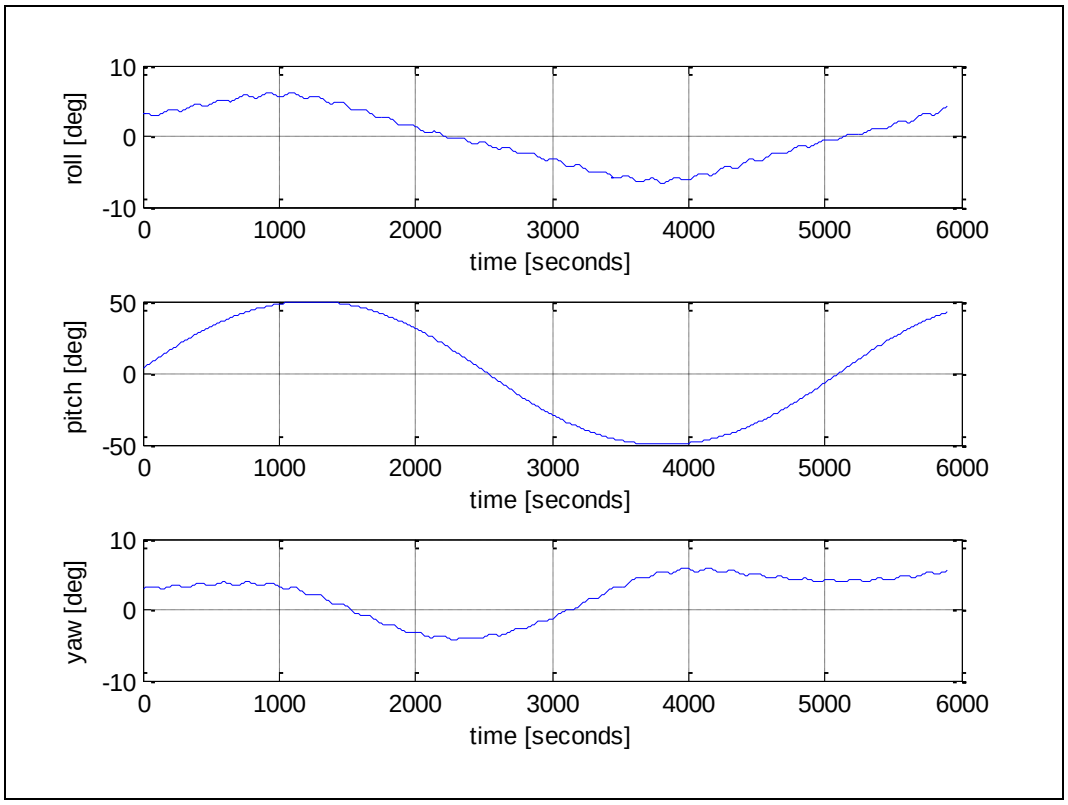

Figure 17: True Euler Angles

8.1 NO GPS OUTAGE CASE

For this test case, it is assumed that the GPS receiver on the satellite obtains measurements from at least 5 satellites throughout its flight. The results include the attitude estimation for one period of the satellite, which is about 5900 seconds for the orbital parameters chosen.

GPS Only Case

This test case analyzes the performance of the GPS based attitude determination system under the measurement errors, namely receiver noise and multipath error.

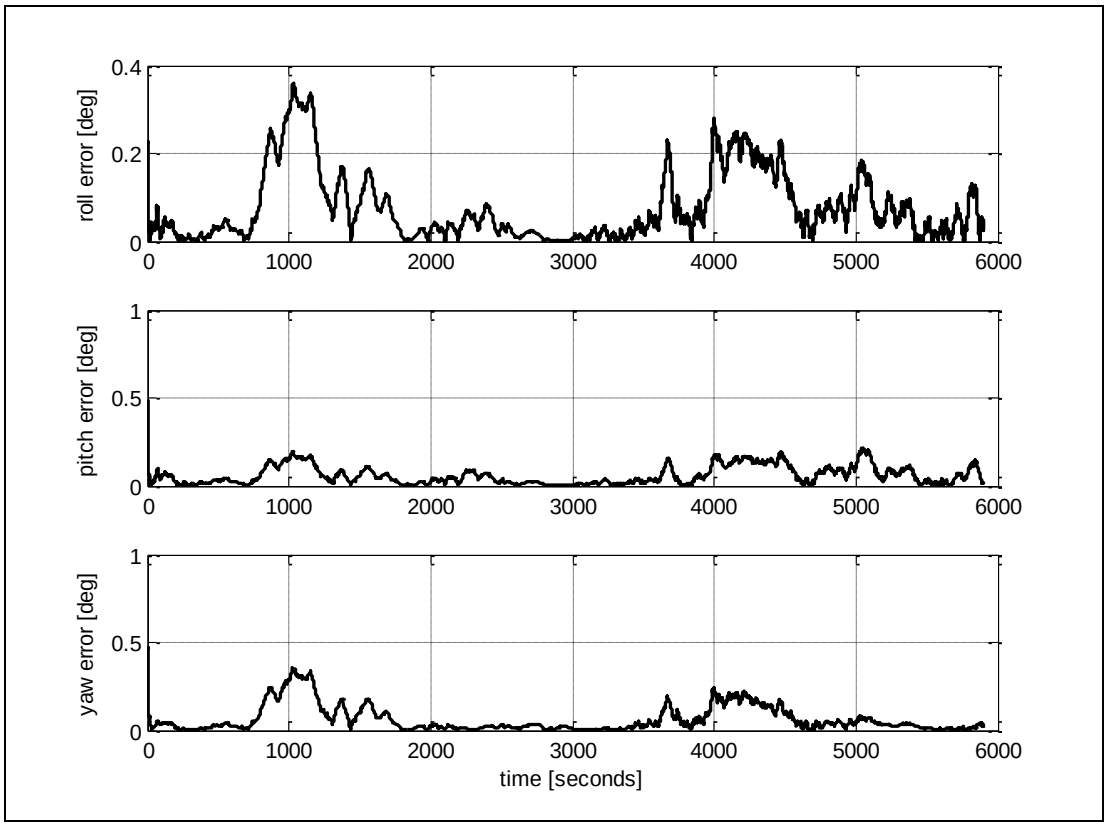

Figure 18: Estimated Euler Angle Error Magnitude for the GPS only Case with no GPS Outages

Table 6: Performance Parameters Obtained with GPS only Case with no GPS Outages

	Roll	Pitch	Yaw
RMS [degrees]	0.1111	0.0790	0.0983
3 sigma [degrees]	0.2394	0.1556	0.2263
Maximum Error [degrees]	0.3560	0. 2110	0.3616

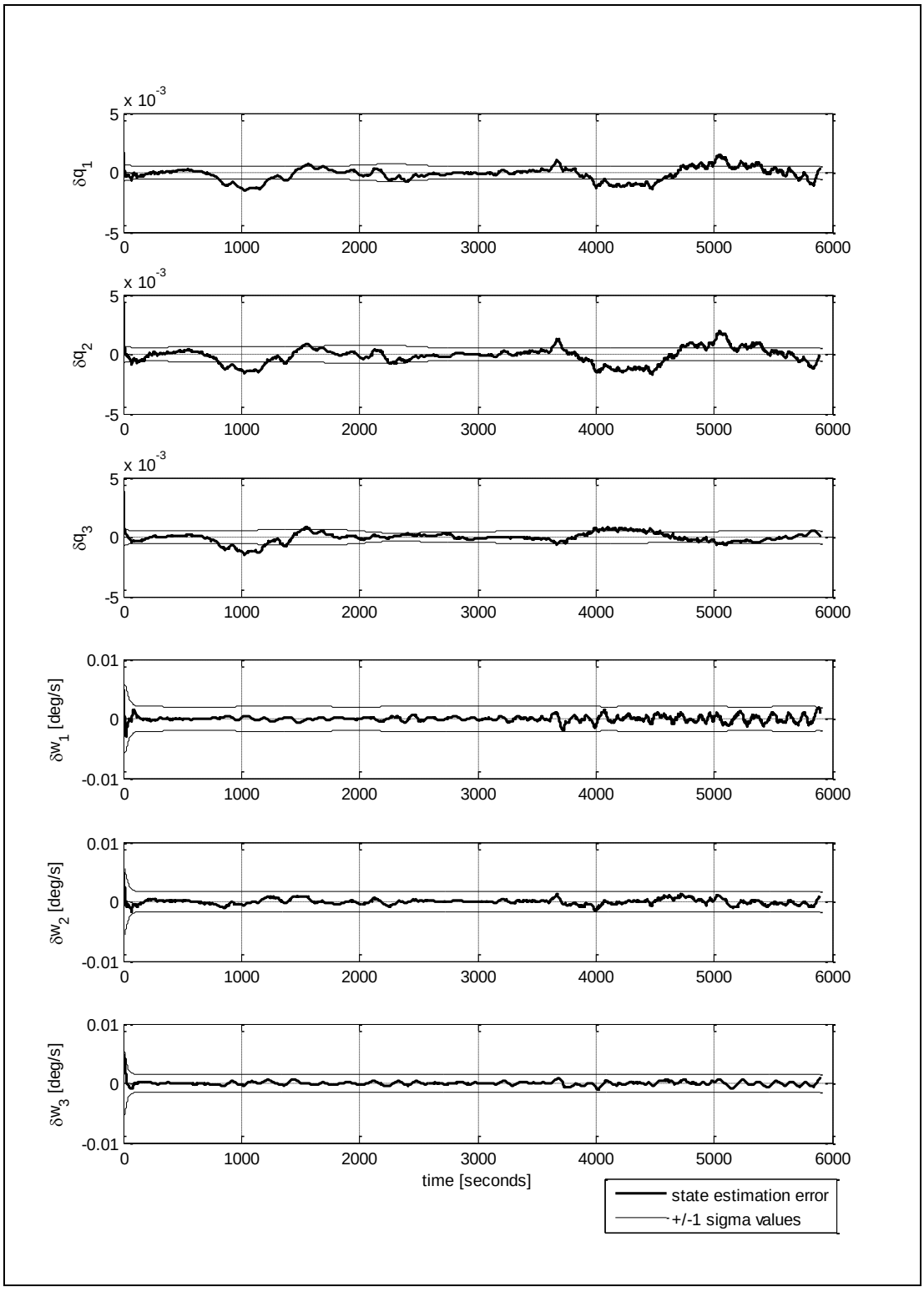

Figure 19: Kalman Filter State Estimation Error and Corresponding Standard Deviation for the GPS only Case with no GPS Outages

The results obtained for the GPS only attitude determination system is illustrated in Figure 18 and Figure 19. The results are summarized in Table 6. It is seen that the RMS values for the roll, pitch and yaw angles are 0.1111, 0.0790 and 0.0983 degrees respectively. Moreover, the maximum errors in these angles are 0.3560, 0.2110 and 0.3616 degrees. By considering these values, it can be concluded that the attitude accuracy obtained by using a GPS based attitude determination system is below 0.4 degrees.

Figure 19 also illustrates that the quaternion and angular velocity estimates remains in the +/- 1 standard deviation limits throughout the flight

GPS/Gyro Integrated Case

This test case analyzes the effect of gyro integration on the filter performance. Conditions during the test are identical to those of the GPS only case. The only difference is that the gyro measurements are also used in addition to the GPS range difference measurements.

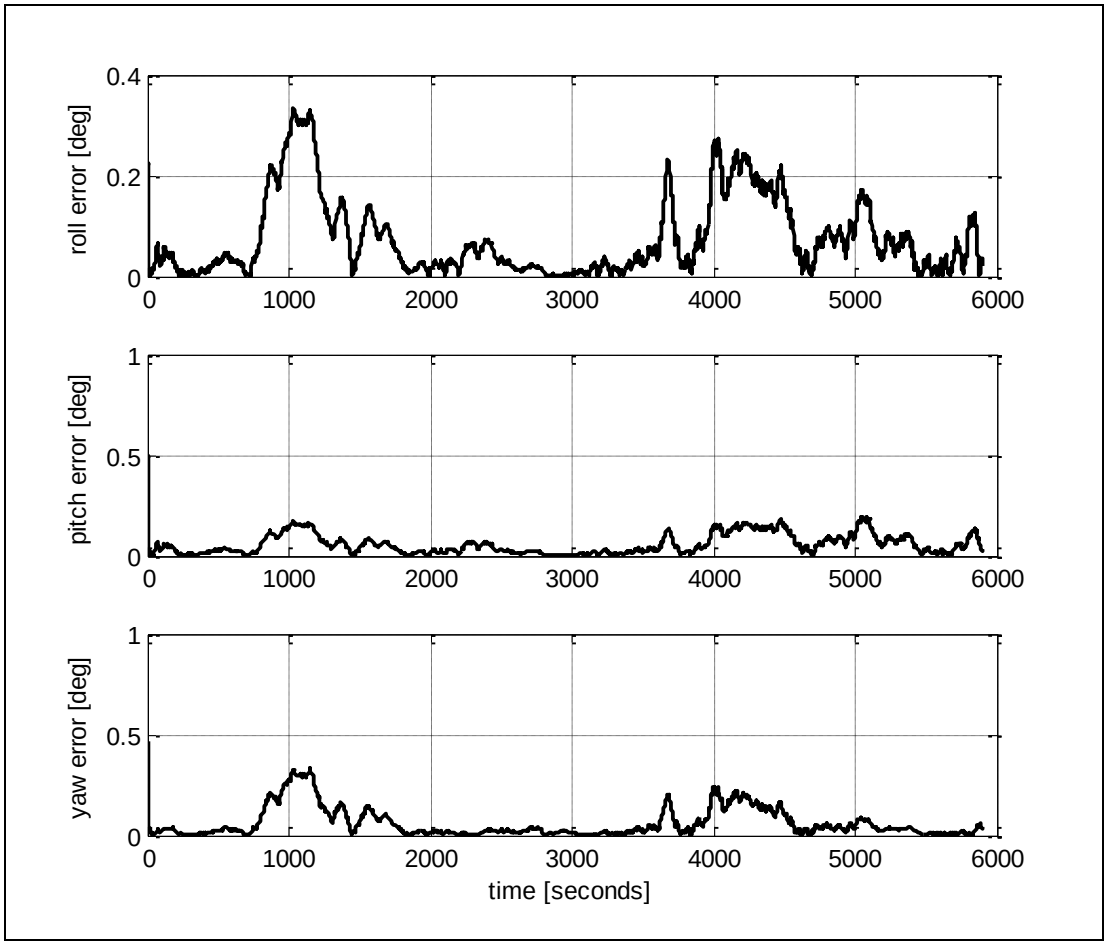

Figure 20: Estimated Euler Angle Error Magnitude for the GPS/Gyro Integrated Case with no GPS Outages

Table 7: Performance Parameters Obtained with GPS/Gyro Integrated Case with no GPS Outages

	Roll	Pitch	Yaw
RMS [degrees]	0.1094	0.0750	0.0953
3 sigma [degrees]	0.2356	0.1468	0.2192
Maximum Error [degrees]	0.3339	0.1922	0.3313

Comparing the results summarized in Table 6 and Table 7, it is seen that there is an improvement in the attitude accuracy for the gyro integrated case. The RMS of the attitude error shows a small decrease for the gyro aided case. However, the effect of the gyro aiding is seen mostly in the attitude error peaks. The lower maximum error obtained with the GPS/Gyro integrated solution shows that the GPS only solution exhibits more noisy estimation than the gyro aided system. The maximum error for the roll angle is improved around 6%, while this improvement is almost 9% for the pitch and yaw angles. This result show that the gyro aiding in the GPS based attitude determination system improves the attitude estimation performance slightly for the case without GPS outages.

In Figure 21, it is seen that, the quaternion and angular velocity estimates are again remain in the 1 sigma uncertainty limits.

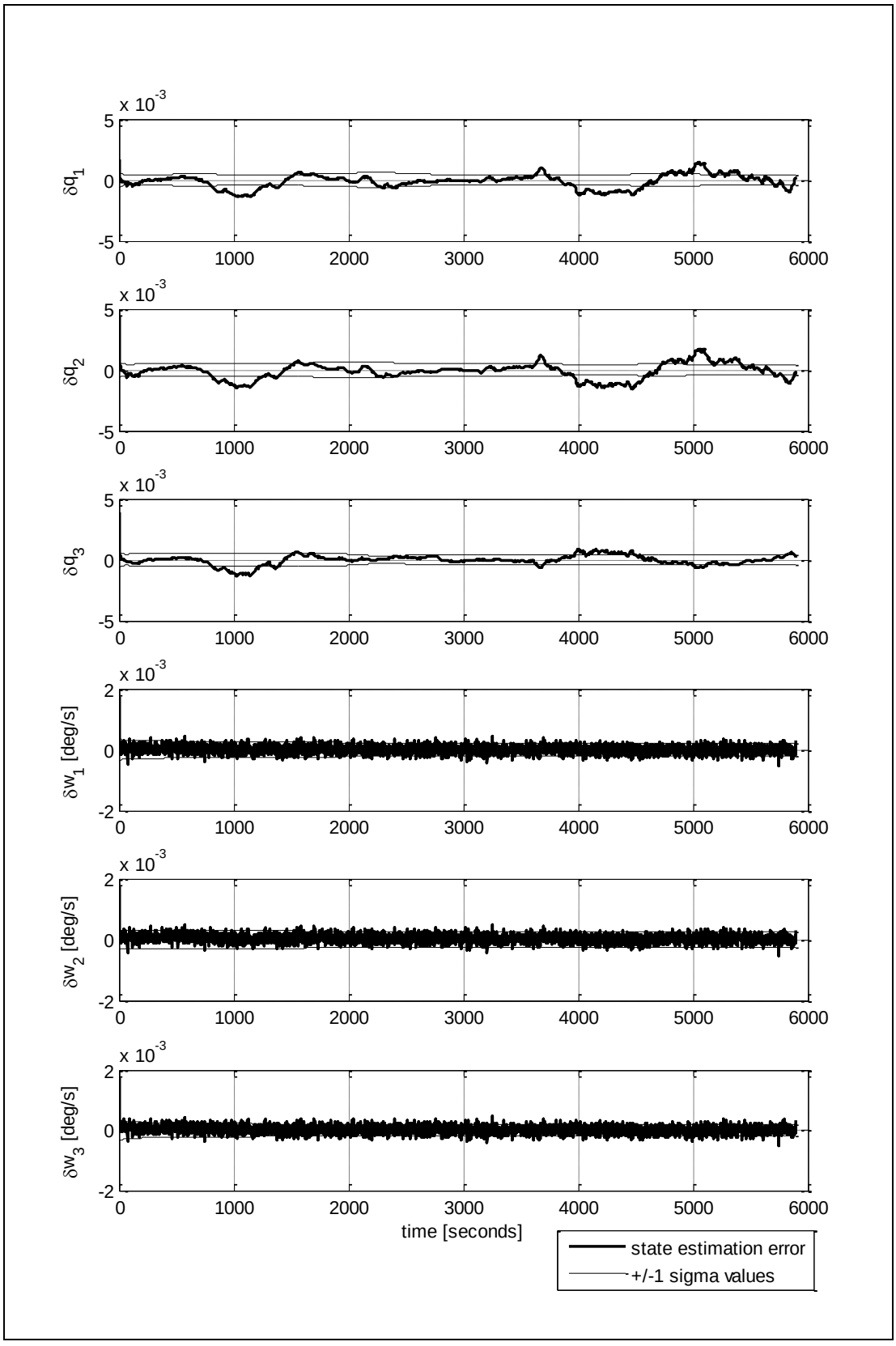

Figure 21: Kalman Filter State Estimation Error and Corresponding Standard Deviation for the GPS/Gyro Integrated Case with no GPS Outages

8.2 GPS OUTAGE CASE

For this test case, it is assumed that the GPS receiver is unable to obtain measurements from any satellite at some periods of its flight. In the simulation, the periods with GPS outages is applied in the periods between 1500 – 1800 and 4000 – 4300 seconds. Other than these time intervals, the GPS measurements from 5 satellites are obtained in the flight.

This test measures the possible attitude error under the condition with loss of GPS satellite visibility. Such a case might happened for satellites with all the antennas pointing the same direction. Results are compared for GPS only and GPS/Gyro integrated cases.

GPS Only Case

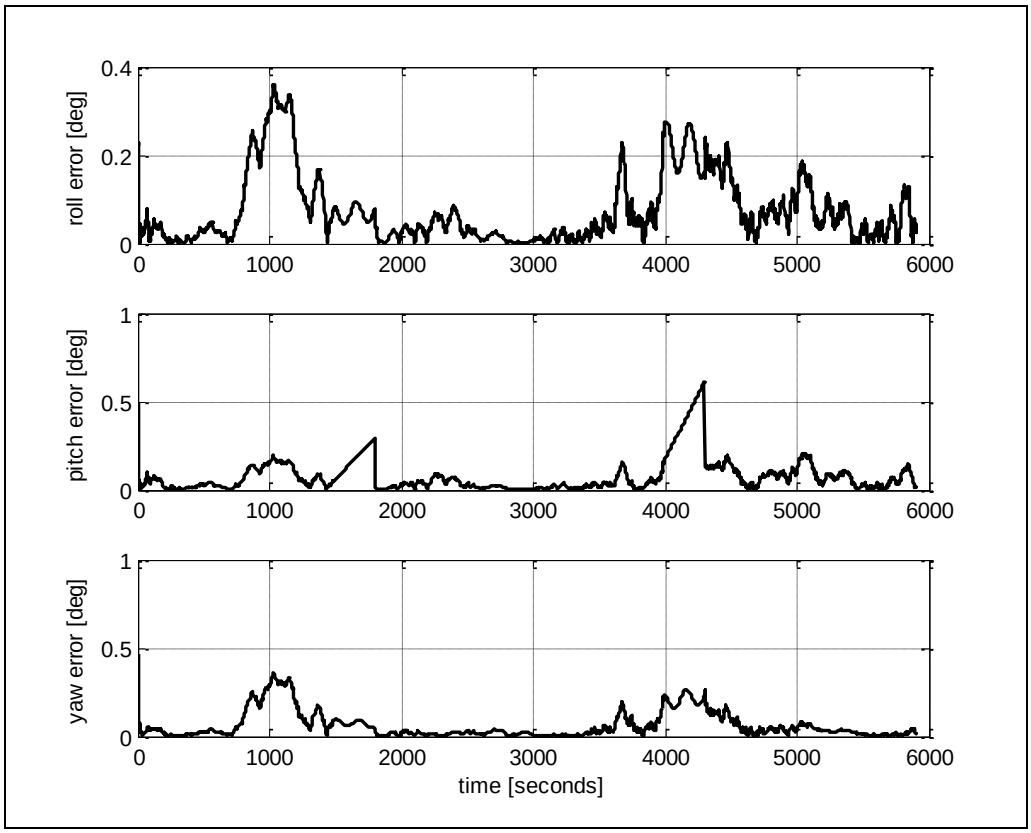

Figure 22: Estimated Euler Angle Error Magnitude for the GPS only Case under GPS Outages

Table 8: Performance Parameters Obtained with the GPS only Case under GPS Outages

	Roll	Pitch	Yaw
RMS [degrees]	0.1103	0.1246	0.0997
3 sigma [degrees]	0.2391	0.2909	0.2309
Maximum Error [degrees]	0.3590	0.6112	0.3616

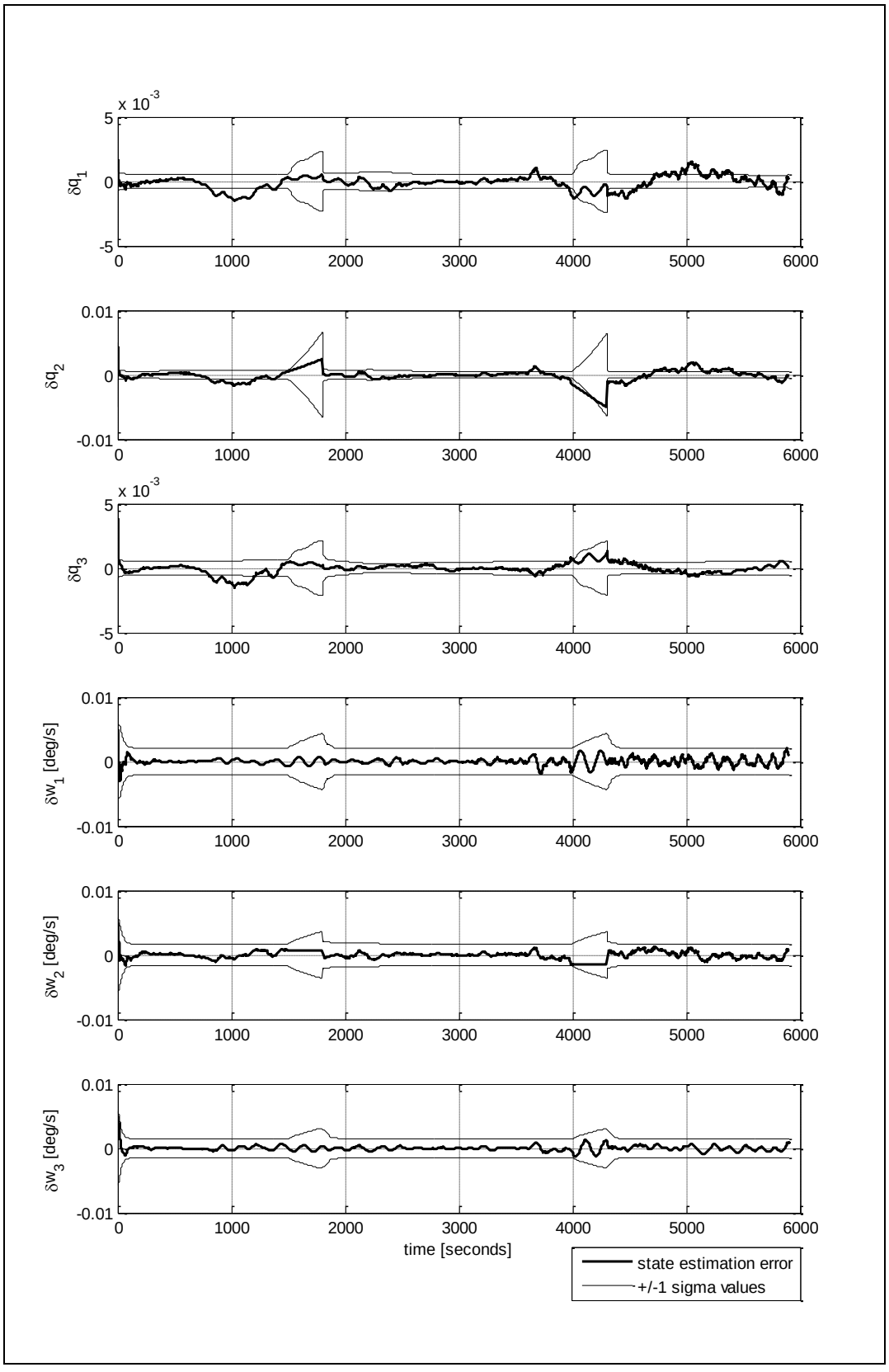

Figure 23: Kalman Filter State Estimation Error and Corresponding Standard Deviation for the GPS only Case under GPS Outages

The results obtained for the GPS only attitude determination system under GPS outages is illustrated in Figure 22 and Figure 23. The maximum errors in the attitude estimations are 0.3590, 0.6112 and 0.3616 degrees respectively. The error increase during the GPS outages is highly affected by the satellite attitude dynamics. This effect can be seen from the high pitch error peaks when the GPS measurements are not available (Figure 22). The maximum error in the pitch angle is about 0.6 degrees, while it is around 0.36 degrees for the other angles. This high difference is due to the rapid change in the pitch angle. In a one period of the satellite flight, the pitch angle varies between +/-50 degrees, while this values is +/-10 degrees for the roll and yaw angles.

The other effect on the maximum attitude error during the GPS outages is the initial condition error (the error at the beginning of the outage period). This effect is seen again in Figure 22. The pitch angle error is lower for the first outage period; therefore, the pitch error after the same amount of time is lower for that outage period.

The RMS results are also summarized in Table 8.

GPS/Gyro Integrated Case

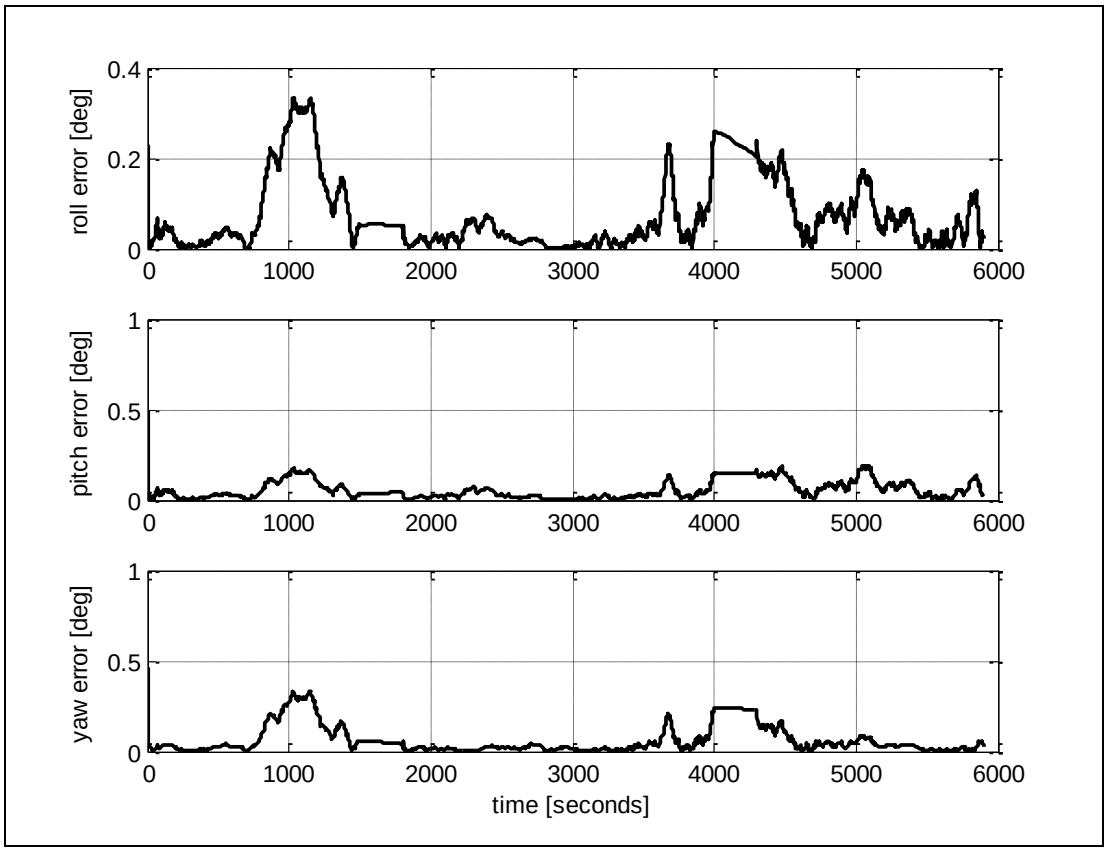

Figure 24: Estimated Euler Angle Error Magnitude for the GPS/Gyro Integrated Case under GPS Outages

Table 9: Performance Parameters Obtained with GPS/Gyro Integrated Case under GPS Outages

	Roll	Pitch	Yaw
RMS [degrees]	0.1100	0.0749	0.0994
3 sigma [degrees]	0.2402	0.1483	0.2328
Maximum Error [degrees]	0.3339	0.1922	0.3313

Comparing Table 8 and Table 9, the effect of gyro integration is seen especially on the pitch angle. As it is mentioned before, the pitch angle is rapidly changing throughout the flight. Therefore, during the GPS outage, the pitch angle is subjected to more error. However, aiding the system with the gyroscopes improves the pitch angle accuracy significantly. The improvement is especially seen in the maximum pitch angle error. This error is decreased more than 0.4 degrees with gyro aiding.

The effect of gyro aiding on the other angles, roll and yaw, is seen again mostly on the error peaks. However, due to the slow and sinusoidal attitude dynamics of these angles, GPS outage case does not make any difference with the case with no GPS outages.

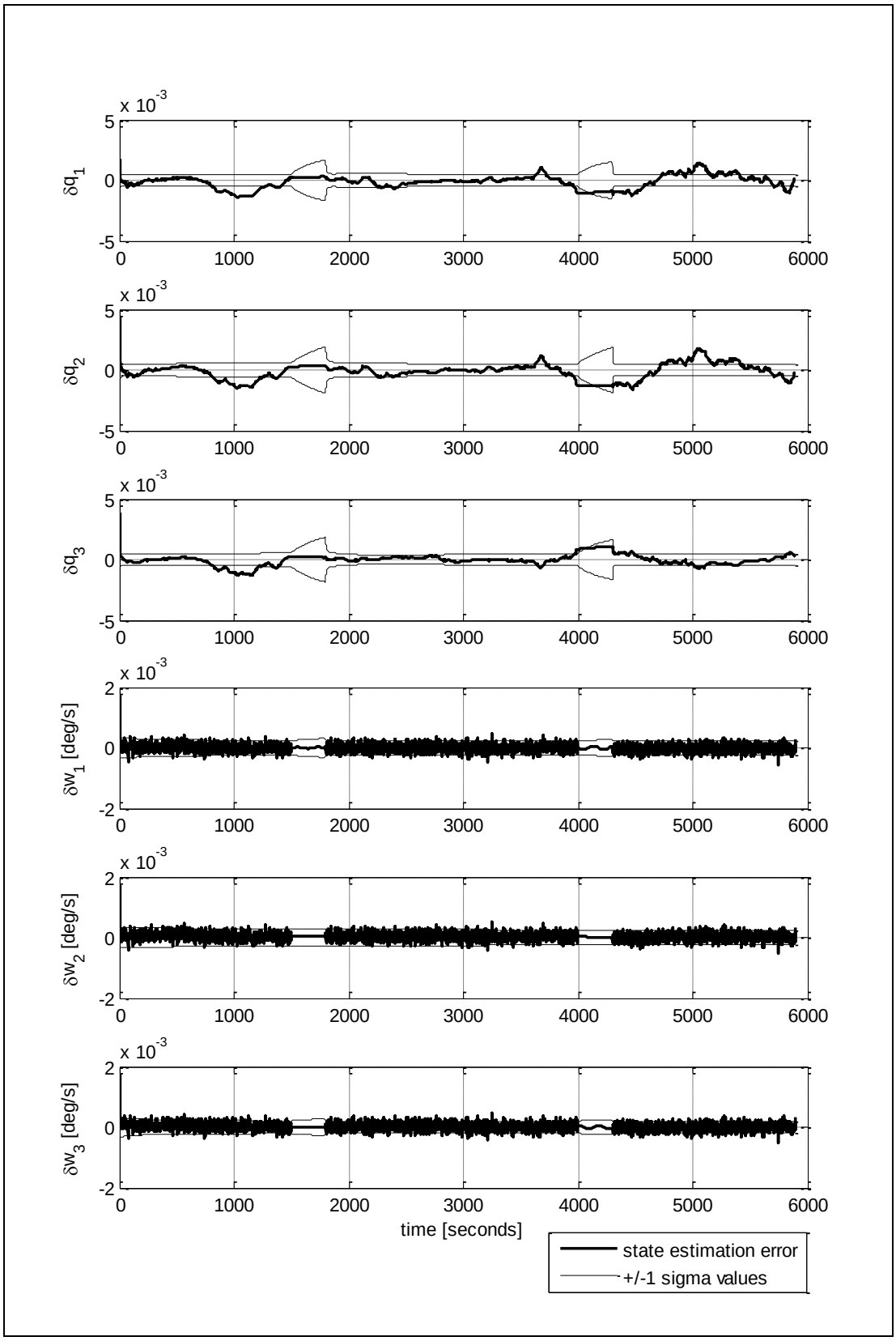

Figure 25: Kalman Filter State Estimation Error and Corresponding Standard Deviation for the GPS/Gyro Integrated Case under GPS Outages

8.3 LOW GPS SATELLITE VISIBILITY CASE

GPS satellite visibility is generally quite satisfactory in low Earth orbit satellites. However, for the middle or high orbit satellites no more than three GPS satellites are available in the measurements. The other reason to obtain small number of visible GPS satellites might be the antenna configuration. When all the antennas are pointing the same direction, it is possible to suffer from poor GPS availability. For such cases, it is intended to analyze the performance of the attitude filter under low GPS visibility. Tests are conducted for both the GPS only and Gyro integrated cases to examine the role of gyroscopes when the GPS visibility is low. For these tests, it is assumed that measurements from only 3 GPS satellites are available throughout the flight.

The results obtained are presented in Table 10 and Table 11.

Table 10: Performance Parameters Obtained with GPS only Case under Low GPS Visibility

	Roll	Pitch	Yaw
RMS [degrees]	0.1225	0.0954	0.0893
3 sigma [degrees]	0.2404	0.1686	0.1992
Maximum Error [degrees]	0.4044	0.2235	0.3272

Table 11: Performance Parameters Obtained with GPS/Gyro Integrated Case under Low GPS Visibility

	Roll	Pitch	Yaw
RMS [degrees]	0.1183	0.0864	0.0841
3 sigma [degrees]	0.2350	0.1500	0.1892
Maximum Error [degrees]	0.3732	0.1806	0.2961

After analyzing the results, it is observed that the reduction in the GPS visibility increases the benefit of gyro aiding. This improvement can be seen in Table 12.

Table 12: Benefits of Gyro Aiding in the Maximum Attitude Errors for the High and Low GPS Visibility Cases

	Max. Roll Error	Max. Pitch Error	Max. Yaw Error
5 Satellites Available	%6	%9	%8
3 Satellites Available	%7	%19	%9.5

The low GPS visibility effect analyzed in this thesis is only on the algorithm performances due to the lack of real measurements. However, in reality, for a Middle/High user satellite, the ADOP values of the measurements are quite high due to the visible GPS satellite geometry. In other words, the uncertainty on the GPS measurements is significantly higher. Therefore, using the same measurements with the LEO case is actually not suitable when analyzing the performance differences.

The other impact of low GPS visibility which is not examined in this thesis is the effect on the integer ambiguity solution and the technique used for it. For the most of the integer ambiguity resolution algorithms, at least 4 satellites in view are necessary. It is not suitable to use such an algorithm for a case with low GPS visibility. For such cases, there are resolution algorithms using also gyro measurements [26]. Therefore, under the poor GPS availability, gyros are needed not only for the attitude accuracy improvement but also the fast and accurate solution of the integer ambiguities.

CHAPTER 9

CONCLUSIONS

The goal of this thesis has been to develope a GPS based attitude determination system for a spacecraft. As the estimation algorithm for attitude determination using GPS measurements, an extended Kalman filter was developed.

Orbit simulation was conducted in order to evaluate the algorithm performance. In the simulation, a stochastic GPS error model was developed considering the errors which have high impact on the attitude solution. Considering this, the multipath error and the receiver noise were modeled. The effect of antenna phase center variation was assumed to be negligible due to the selected antenna configuration.

The antenna configuration used in the simulations was selected as four antennas in a square shape with 1 meter inter-antenna distance. It was also assumed that all the antennas are pointing the same direction.

The system was also integrated with three-gyroscope assembly again by EKF. In order to achive a low cost system, the gyro error performances was selected based on a low cost MEMS gyro, namely Inertial Stellar Compass. A gyroscope error model was developed in order to model the gyro measurements. The performance improvement obtained with the gyro aiding was analyzed under different GPS visibility cases.

After the simulations tests, the maximum attitude error obtained by using the GPS differential range measurements was found as less than 0.4 degrees. The gyro aiding resulted in a small increase in the attitude accuracy, which was around 6% for roll angle, 9% for the pitch and yaw angles. During this test, it was assumed that measurements from five satellites are constantly available througout the flight. However, the improvement caused by the gyro aiding was especially observed for the cases with GPS outages and low GPS visibility.

The attitude accuracy when the GPS measurements are unavailable was examined by appliying 300 seconds of GPS outage. For the GPS only case, during the GPS outage period, the attitude and the angular velocity was propagated using the equations of the motion. Therfore, a small attitude error in the start of the outage period resulted in a high error after the propagation. The error increase was higher for the rapidly changing angles, i.e. angles with high angular velocities in the related axes. The maximum error obtained by using the GPS only algorithm at the end of the 300 second GPS outage was 0.3590, 0.6112 and 0.3616 degrees respectively. The error in the pitch angle was more than the others due to the high angular velocity in y-axis. For the GPS/Gyro integrated case, the attitude estimates were

updated only by the gyro measurements during the outage period. The improvement was observed for all the angles but especially in the pitch angle. The error at the end of the outage period became around 0.2 degrees in the pitch angle, which means 0.4 degrees of improvement. Therefore, it can be concluded that the gyro integration is essential for the cases with high angular velocities, such as spinning satellites. However, the improvement is small for the stabilized satellites.

Low GPS visibility is often a problem for the middle/high orbit satellites. It can be also considered as a problem for the satellites in which all the antennas are pointing the same direction. The impact of low GPS visibility on the attitude accuracy estimations was tested by assuming that only three GPS satellites are available. After this test, it was seen that the benefit of gyro aiding increases under the low GPS visibility condition.

APPENDIX A

DEFINITION OF CLASSICAL ORBITAL ELEMENETS

The orbital elements are the parameters required in order to fully specify the motion of a satellite. The main orbital parameters are:

- Semi-major axis
- Eccentricity
- Inclination
- Right ascension of ascending node
- Argument of perigee
- Time of periapsis passage

The first five of them are sufficient to completely describe the size, shape and orientation of an orbit. A sixth element is required to specify the position of the satellite on the orbit at a particular time.

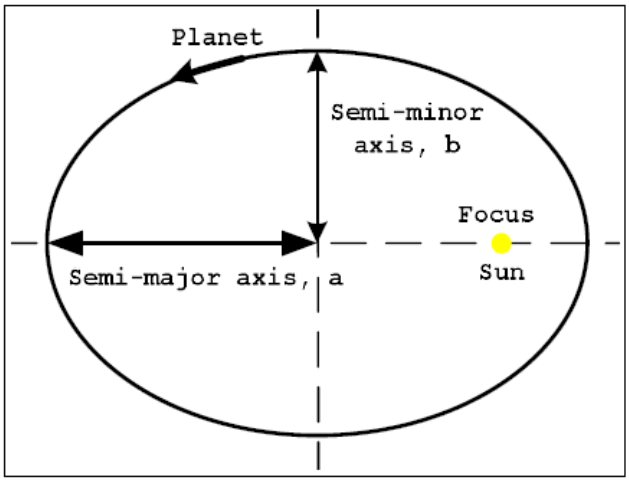

Figure 26: Geometry of an Ellipse

The semi-major axis, a, defines the size of an orbit, and it is half of the long axis of the ellipse.

The eccentricity, e, is a constant that defines the shape of an orbit. This parameter also identifies all the conic sections. Specifically, $e = 0$ is for a circle, $0 < e < 1$ for an ellipse, $e = 1$ for a parabola, and $e > 1$ for a hyperbola.

The inclination, i, specifies the orientation of an orbit, and it is defined as the angle between Earth's spin axis and the orbit normal vector.

The right ascension of ascending node, Ω, is the angle in the equatorial plane measured eastward from the vernal equinox direction to the ascending node of the orbit, which is the point where the satellite crosses through the equatorial plane in a northerly direction.

The rotation of the orbit within the orbit plane is defined by the argument of perigee, ω. This parameter describes the angle in the orbital plane between the ascending node and the periapsis point.

The time of periapsis passage describes the time when the satellite was at periapsis.

Although these six parameters are sufficient in order to describe the motion of a satellite on an orbit, there are also some additional parameters which can be used to identify the time of the periapsis passage. These are:

- True anomaly at epoch, ν_0
- Argument of latitude at epoch, u_0
- True longitude at epoch, l_0
- Mean anomaly, M

The true anomaly at epoch is used to identify the location of the satellite along the orbit. This is the angle in the orbital plane between the periapsis and the position of the satellite at a particular time, t_0, called epoch.

The argument of latitude at epoch is the angle in the orbit plane between the ascending node and the satellite position at a particular time.

$$u_0 = \omega + \nu_0 \tag{A.1}$$

The true longitude at epoch is the angle between the vernal equinox direction and the satellite position at a particular time. It measured eastward to the ascending node in the equatorial plane, and then to the satellite position in the orbital plane.

$$l_0 = \Omega + \omega + \nu_0 \tag{A.2}$$

Mean anomaly, M, is another parameter which is also describe the position of the satellite on the orbit. It can be calculated as:

$$M = 360\frac{\Delta t}{P} \qquad \text{A.3}$$

where P is the orbital period, and Δt is the time passed since the satellite passes the periapsis.

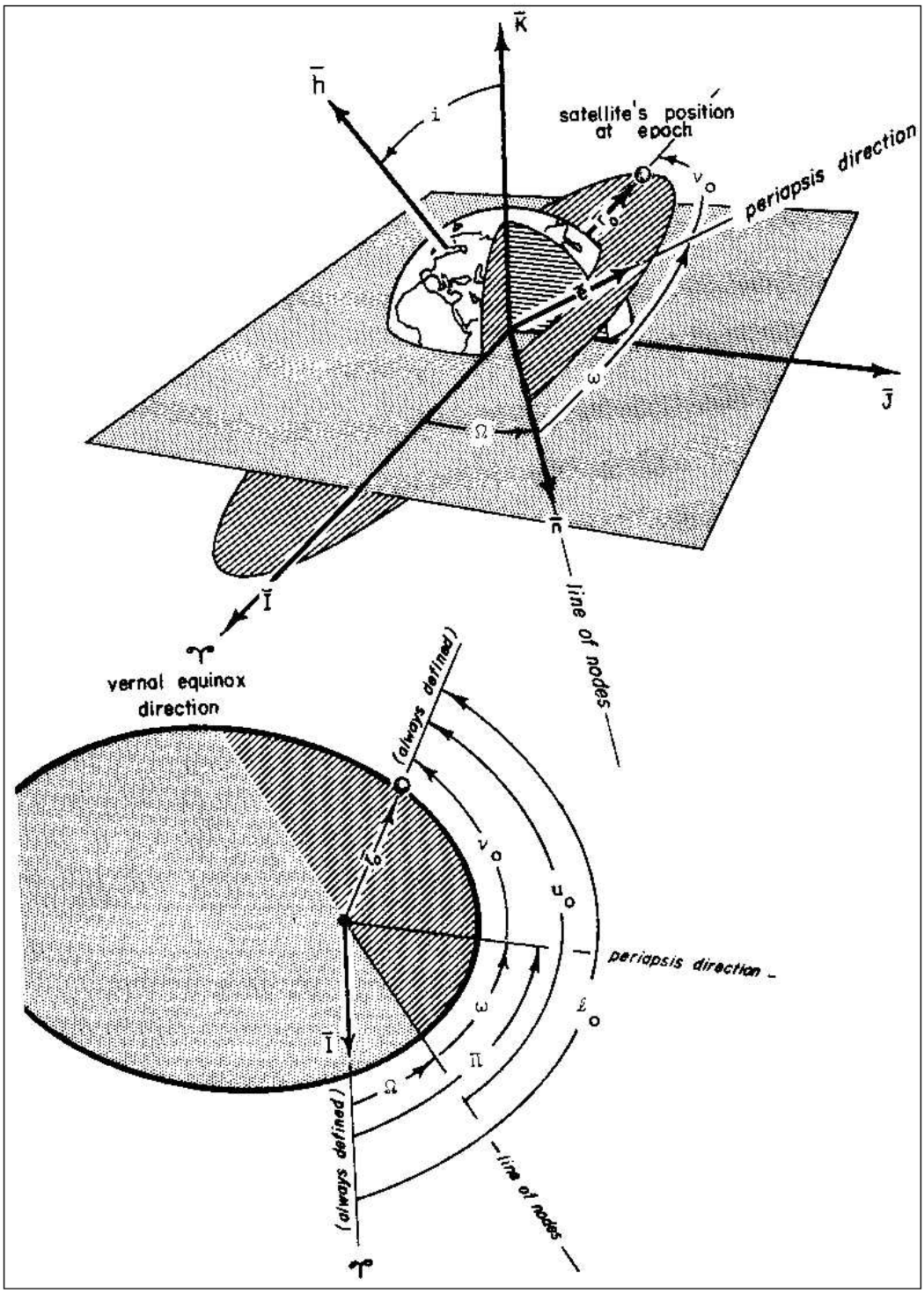

Figure 27: Classical Orbital Elements [30]

APPENDIX B

CALCULATION OF ECI COORDINATES FROM ORBITAL ELEMENTS

In order to calculate the position and velocity of a satellite with respect to ECI reference frame, position and velocity firstly should be expressed in the Earth Centered Orbital Coordinate System, and then transformation to the ECI coordinate system should be applied.

The position vector, r, can be calculated as follows:

$$r = \frac{a(1-e^2)}{1+e\cos\nu} \tag{B.4}$$

$$\boldsymbol{r} = r\cos\nu\,\boldsymbol{i_O} + r\sin\nu\,\boldsymbol{j_O} \tag{B.5}$$

where $\boldsymbol{i_O}$ and $\boldsymbol{j_O}$ are unit vectors along X_O and Y_O directions respectively.

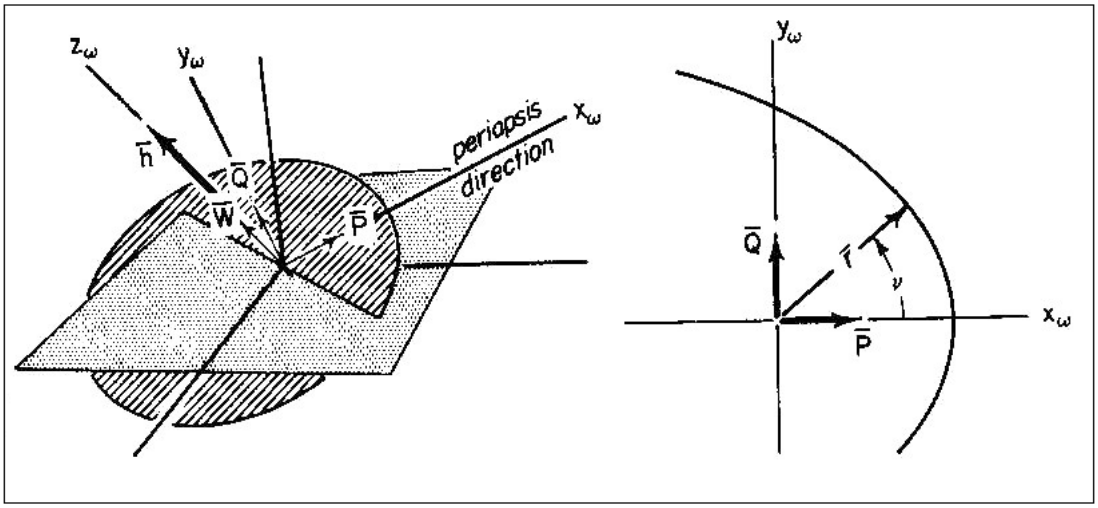

Figure 28: Representation of the Relation between the Satellite Position and Earth Centered Orbital Coordinate System [30]

The time rate of change of the position vector gives the velocity vector in Earth Centered Orbital coordinate system. It should be noted that this frame is an almost inertial reference frame. After the differentiation, the equation used to calculate the velocity vector is found as:

$$\mathbf{v} = \sqrt{\frac{\mu}{a(1-e^2)}}[-\sin\nu\, \boldsymbol{i_O} + (e + \cos\nu)\boldsymbol{j_O}] \quad \text{B.6}$$

Then the transformation of these position and velocity vectors to the ECI frame is applied.

$$r^I = R_O^I r^O \quad \text{B.7}$$

$$\mathrm{v}^I = R_O^I \mathrm{v}^O \quad \text{B.8}$$

where R_O^I is the transformation matrix from the Earth Centered Orbital coordinate system to the ECI coordinate system, and it can be calculated as:

$$R_I^O = R_z(\omega)R_x(i)R_z(\Omega) \quad \text{B.9}$$

$$R_O^I = \left(R_I^O\right)^T \quad \text{B.10}$$

APPENDIX C

CALCULATION OF ORBITAL ELEMENTS FROM ECI COORDINATES

In order to determine the orbital elements by using the satellite position and velocity of a satellite with respect to the ECI reference frame, the three vectors below should be determined firstly.

1. The specific angular momentum vector, **h**, which can be found with the following equation:

$$\boldsymbol{h} = \boldsymbol{r} \times \mathbf{v} \tag{C.11}$$

   The angular momentum vector is perpendicular to the satellite orbit plane.

2. The node vector, **n**. This vector lies in the intersection of the equatorial plane and the orbital plane and in the direction of ascending node. This vector can be calculated as:

$$\boldsymbol{n} = \boldsymbol{K} \times \boldsymbol{h} \tag{C.12}$$

3. The eccentricity vector, **e**. This vector from the Earth center toward the periapsis with a magnitude equal to the eccentricity of the orbit. It can be calculated as:

$$\boldsymbol{e} = \frac{\mathbf{v} \times \boldsymbol{h}}{\mu} - \frac{\boldsymbol{r}}{r} \tag{C.13}$$

,where **r** and **v** is the satellite position and velocity vectors with respect to the ECI frame, **K** is the unit vector along the Earth spin axis, μ is the Earth's gravitation parameter.

Then the orbital parameters can be calculated by using these three vectors:

Eccentricity: $e = |\boldsymbol{e}|$

Semi major axis: $a = \frac{h^2}{\mu(1 - e^2)}$

Inclination: $\cos i = \frac{\mathbf{h} \times \boldsymbol{K}}{h}$

Right ascension of ascending node: $\cos \Omega = \frac{\mathbf{I} \times \boldsymbol{n}}{n}$

Argument of perigee: $\cos \omega = \frac{\mathbf{n} \times \boldsymbol{e}}{n \cdot e}$

True anomaly at epoch: $\cos \nu_0 = \frac{\mathbf{e} \times \boldsymbol{r}}{e \cdot r}$

where **I** is the unit vector towards vernal equinox direction.

The calculation of some of the additional orbital elements is given as:

Argument of latitude at epoch: $\cos u_0 = \frac{\mathbf{n} \times \boldsymbol{r}}{n \cdot r}$

True longitude at epoch: $l_0 = \Omega + \omega + \nu_0$

APPENDIX D

STATE SPACE LINEARIZATION

Considering a nonlinear model with continuous time measurements:

$$\dot{x}(t) = f(\mathrm{x}, \mathrm{t}) + w(t) \tag{D.14}$$

$$\mathrm{z}(t) = h(\mathrm{x}, \mathrm{t}) + v(t) \tag{D.15}$$

In order to obtain the error system model, the nonlinear equations given are linearized around the current estimate $\hat{x}$ using a linearized first-order Taylor series expansion.

$$f(x,t) \cong f(\hat{x},t) + \left.\frac{\partial f(x,t)}{\partial x}\right|_{\hat{x}(t)} [x(t) - \hat{x}(t)] + h.o.t \tag{D.16}$$

$$h(x,t) \cong h(\hat{x},t) + \left.\frac{\partial h(x,t)}{\partial x}\right|_{\hat{x}(t)} [x(t) - \hat{x}(t)] + h.o.t \tag{D.17}$$

In this study, the error state is described as:

$$\delta x(t) = x(t) - \hat{x}(t) \tag{D.18}$$

$$\delta \dot{x}(t) = \dot{x}(t) - \dot{\hat{x}}(t) \tag{D.19}$$

Applying that $\dot{\hat{x}} = f(\hat{x}, t)$, the equation above becomes:

$$\delta \dot{x}(t) = [f(\mathrm{x}, \mathrm{t}) + w(t)] - f(\hat{x}, t) \tag{D.20}$$

Inserting Equation D.16 and ignoring the higher order terms (h.o.t.), the equation above becomes:

$$\delta \dot{x}(t) = \left.\frac{\partial f(x,t)}{\partial x}\right|_{\hat{x}(t)} \delta x(t) + w(t) \tag{D.21}$$

The linearization for the measurement model is performed with the same method:

$$\delta \mathrm{z}(t) = \mathrm{z}(t) - h(\hat{x}, t) = [h(\mathrm{x}, \mathrm{t}) + v(t)] - h(\hat{x}, t) \qquad \text{D.22}$$

Inserting Equation D.17 and ignoring h.o.t., the measurement residual equation becomes:

$$\delta \mathrm{z}(t) = \left.\frac{\partial h(x,t)}{\partial x}\right|_{\hat{x}(t)} \delta x(t) + v(t) \qquad \text{D.23}$$

APPENDIX E

LINEARIZED ERROR PROPAGATION EQUATIONS

The nonlinear quaternion and inertial angular velocity propagation equations is given in Equation 5.19 and Equation 5.27 respectively. After inserting the related terms of transformation matrix, R_L^B, the equations becomes:

$$\dot{q}_1 = \quad 0.5[q_0\omega_1 + q_2\omega_3 - q_3(\omega_2 - \dot{u})]$$

$$\dot{q}_2 = \quad 0.5[q_0(\omega_2 + \dot{u}) - q_1\omega_3 + q_3\omega_1]$$

$$\dot{q}_3 = \quad 0.5[q_0\omega_3 + q_1(\omega_2 - \dot{u}) - q_2\omega_1]$$

$$\dot{\omega}_1 = K_1\left[\omega_2\omega_3 - \frac{12\mu}{r^3}(q_1q_2 - q_0q_3)(q_1q_3 + q_0q_2)\right] - \omega_3\frac{h_w}{I_1} \qquad \text{E.24}$$

$$\dot{\omega}_2 = K_2\left[\omega_1\omega_3 - \frac{6\mu}{r^3}({q_0}^2 + {q_1}^2 - {q_2}^2 - {q_3}^2)(q_1q_3 + q_0q_2)\right]$$

$$\dot{\omega}_3 = K_3\left[\omega_1\omega_2 - \frac{6\mu}{r^3}({q_0}^2 + {q_1}^2 - {q_2}^2 - {q_3}^2)(q_1q_2 - q_0q_3)\right] + \omega_1\frac{h_w}{I_3}$$

where, $\quad K_1 = \dfrac{(I_2 - I_3)}{I_1}, \quad K_2 = \dfrac{(I_3 - I_1)}{I_2}, \quad K_3 = \dfrac{(I_1 - I_2)}{I_3}$

The linearized system model (F) should be calculated as given before in Equation 6.4.

$$F(x,t) = \left.\frac{\partial f(x,t)}{\partial x}\right|_{\hat{x}(t)} \qquad \text{E.25}$$

$$F(x,t)=\begin{bmatrix}\frac{\partial\dot{q}_1}{\partial q_1} & \frac{\partial\dot{q}_1}{\partial q_2} & \frac{\partial\dot{q}_1}{\partial q_3} & \frac{\partial\dot{q}_1}{\partial\omega_1} & \frac{\partial\dot{q}_1}{\partial\omega_2} & \frac{\partial\dot{q}_1}{\partial\omega_3}\\ \frac{\partial\dot{q}_2}{\partial q_1} & \frac{\partial\dot{q}_2}{\partial q_2} & \frac{\partial\dot{q}_2}{\partial q_3} & \frac{\partial\dot{q}_2}{\partial\omega_1} & \frac{\partial\dot{q}_2}{\partial\omega_2} & \frac{\partial\dot{q}_2}{\partial\omega_3}\\ \frac{\partial\dot{q}_3}{\partial q_1} & \frac{\partial\dot{q}_3}{\partial q_2} & \frac{\partial\dot{q}_3}{\partial q_3} & \frac{\partial\dot{q}_3}{\partial\omega_1} & \frac{\partial\dot{q}_3}{\partial\omega_2} & \frac{\partial\dot{q}_3}{\partial\omega_3}\\ \frac{\partial\dot{\omega}_1}{\partial q_1} & \frac{\partial\dot{\omega}_1}{\partial q_2} & \frac{\partial\dot{\omega}_1}{\partial q_3} & \frac{\partial\dot{\omega}_1}{\partial\omega_1} & \frac{\partial\dot{\omega}_1}{\partial\omega_2} & \frac{\partial\dot{\omega}_1}{\partial\omega_3}\\ \frac{\partial\dot{\omega}_2}{\partial q_1} & \frac{\partial\dot{\omega}_2}{\partial q_2} & \frac{\partial\dot{\omega}_2}{\partial q_3} & \frac{\partial\dot{\omega}_2}{\partial\omega_1} & \frac{\partial\dot{\omega}_2}{\partial\omega_2} & \frac{\partial\dot{\omega}_2}{\partial\omega_3}\\ \frac{\partial\dot{\omega}_3}{\partial q_1} & \frac{\partial\dot{\omega}_3}{\partial q_2} & \frac{\partial\dot{\omega}_3}{\partial q_3} & \frac{\partial\dot{\omega}_3}{\partial\omega_1} & \frac{\partial\dot{\omega}_3}{\partial\omega_2} & \frac{\partial\dot{\omega}_3}{\partial\omega_3}\end{bmatrix} \quad \text{E.26}$$

After taking the partial derivatives, the F matrix can be found as:

$$F(x,t)=\begin{bmatrix}0 & \frac{\omega_3}{2} & \frac{-(\omega_2-\dot{u})}{2} & \frac{q_0}{2} & \frac{-q_3}{2} & \frac{q_2}{2}\\ \frac{-\omega_3}{2} & 0 & \frac{\omega_1}{2} & \frac{q_3}{2} & \frac{q_0}{2} & \frac{-q_1}{2}\\ \frac{(\omega_2-\dot{u})}{2} & \frac{-\omega_1}{2} & 0 & \frac{-q_2}{2} & \frac{q_1}{2} & \frac{q_0}{2}\\ F_{4,1} & F_{4,2} & F_{4,3} & 0 & K_1\omega_3 & K_1\omega_2-\frac{h_w}{I_1}\\ F_{5,1} & F_{5,2} & F_{5,3} & K_2\omega_3 & 0 & K_2\omega_1\\ F_{6,1} & F_{6,2} & F_{6,3} & K_3\omega_2+\frac{h_w}{I_3} & K_3\omega_1 & 0\end{bmatrix} \quad \text{E.27}$$

where

$$F_{4,1}=\frac{\partial\dot{\omega}_1}{\partial q_1}=-\frac{12\mu}{r^3}K_1[\,q_2(q_1q_3+q_0q_2)+q_3(q_1q_2-q_0q_3)] \quad \text{E.28}$$

$$=-\frac{12\mu}{r^3}K_1[\,2q_1q_2q_3+q_0({q_2}^2-{q_3}^2)]$$

$$F_{4,2}=\frac{\partial\dot{\omega}_1}{\partial q_2}=-\frac{12\mu}{r^3}K_2[\,q_1(q_1q_3+q_0q_2)+q_0(q_1q_2-q_0q_3)] \quad \text{E.29}$$

$$=-\tfrac{12\mu}{r^3}K_2[\,2q_0q_1q_2+q_3({q_1}^2-{q_0}^2)]$$

$$F_{4,3}=\frac{\partial\dot{\omega}_1}{\partial q_3}=-\frac{12\mu}{r^3}K_3[-q_0(q_1q_3+q_0q_2)+q_1(q_1q_2-q_0q_3)] \quad \text{E.30}$$

$$=-\frac{12\mu}{r^3}K_4[-2q_0q_1q_3+q_2({q_1}^2-{q_0}^2)]$$

$$F_{5,1} = \frac{\partial \dot{\omega}_2}{\partial q_1} = -\frac{6\mu}{r^3} K_2 [\ \ 2q_1(q_1 q_3 + q_0 q_2) + q_3({q_0}^2 + {q_1}^2 - {q_2}^2 - {q_3}^2)\ ] \qquad \text{E.31}$$

$$= -\frac{6\mu}{r^3} K_2 [\ \ 3{q_1}^2 q_3 + 2q_0 q_1 q_2 + {q_0}^2 q_3 - {q_2}^2 q_3 - {q_3}^3]$$

$$F_{5,2} = \frac{\partial \dot{\omega}_2}{\partial q_2} = -\frac{6\mu}{r^3} K_2 [-2q_2(q_1 q_3 + q_0 q_2) + q_0({q_0}^2 + {q_1}^2 - {q_2}^2 - {q_3}^2)\ ] \qquad \text{E.32}$$

$$= -\frac{6\mu}{r^3} K_2 [-3q_0 {q_2}^2 - 2q_1 q_2 q_3 + q_0 {q_1}^2 - q_0 {q_3}^2 + {q_0}^3]$$

$$F_{5,3} = \frac{\partial \dot{\omega}_2}{\partial q_3} = -\frac{6\mu}{r^3} K_2 [-2q_3(q_1 q_3 + q_0 q_2) + q_1({q_0}^2 + {q_1}^2 - {q_2}^2 - {q_3}^2)\ ] \qquad \text{E.33}$$

$$= -\frac{6\mu}{r^3} K_2 [-3q_1 {q_3}^2 - 2q_0 q_2 q_3 + {q_0}^2 q_1 - q_1 {q_2}^2 + {q_1}^3]$$

$$F_{6,1} = \frac{\partial \dot{\omega}_3}{\partial q_1} = -\frac{6\mu}{r^3} K_3 [\ \ 2q_1(q_1 q_2 - q_0 q_3) + q_2({q_0}^2 + {q_1}^2 - {q_2}^2 - {q_3}^2)\ ] \qquad \text{E.34}$$

$$= -\frac{6\mu}{r^3} K_3 [3{q_1}^2 q_2 - 2q_0 q_1 q_3 + {q_0}^2 q_2 - q_2 {q_3}^2 - {q_2}^3]$$

$$F_{6,2} = \frac{\partial \dot{\omega}_3}{\partial q_2} = -\frac{6\mu}{r^3} K_3 [-2q_2(q_1 q_2 - q_0 q_3) + q_1({q_0}^2 + {q_1}^2 - {q_2}^2 - {q_3}^2)\ ] \qquad \text{E.35}$$

$$= -\frac{6\mu}{r^3} K_3 [-3q_1 {q_2}^2 + 2q_0 q_2 q_3 + {q_0}^2 q_1 - q_1 {q_3}^2 + {q_1}^3]$$

$$F_{6,3} = \frac{\partial \dot{\omega}_3}{\partial q_3} = -\frac{6\mu}{r^3} K_3 [-2q_3(q_1 q_2 - q_0 q_3) - q_0({q_0}^2 + {q_1}^2 - {q_2}^2 - {q_3}^2)\ ] \qquad \text{E.36}$$

$$= -\frac{6\mu}{r^3} K_3 [3q_0 {q_3}^2 - 2q_1 q_2 q_3 - q_0 {q_1}^2 + q_0 {q_2}^2 - {q_0}^3]$$

APPENDIX F

SIMULINK BLOCKS

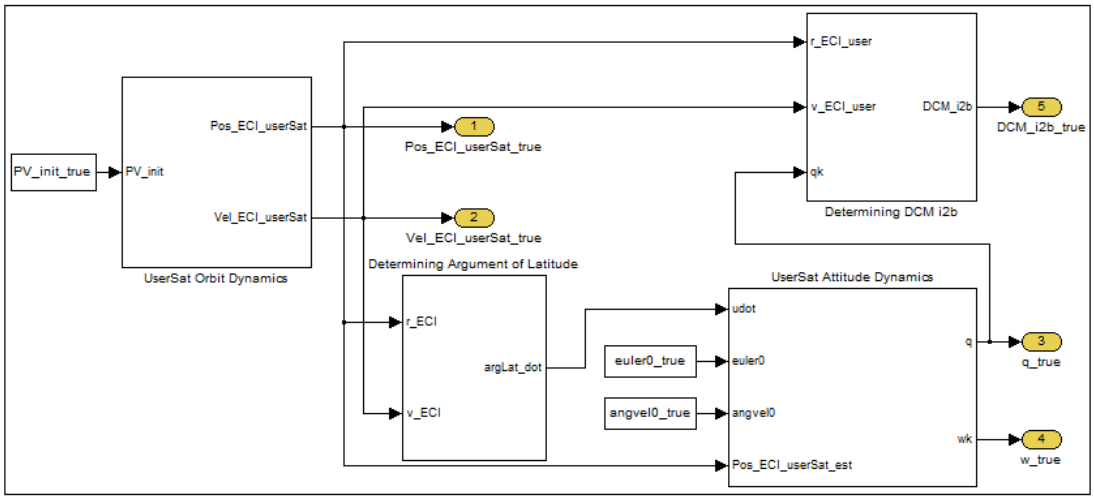

Figure 29: True Data Generation Simulink Model

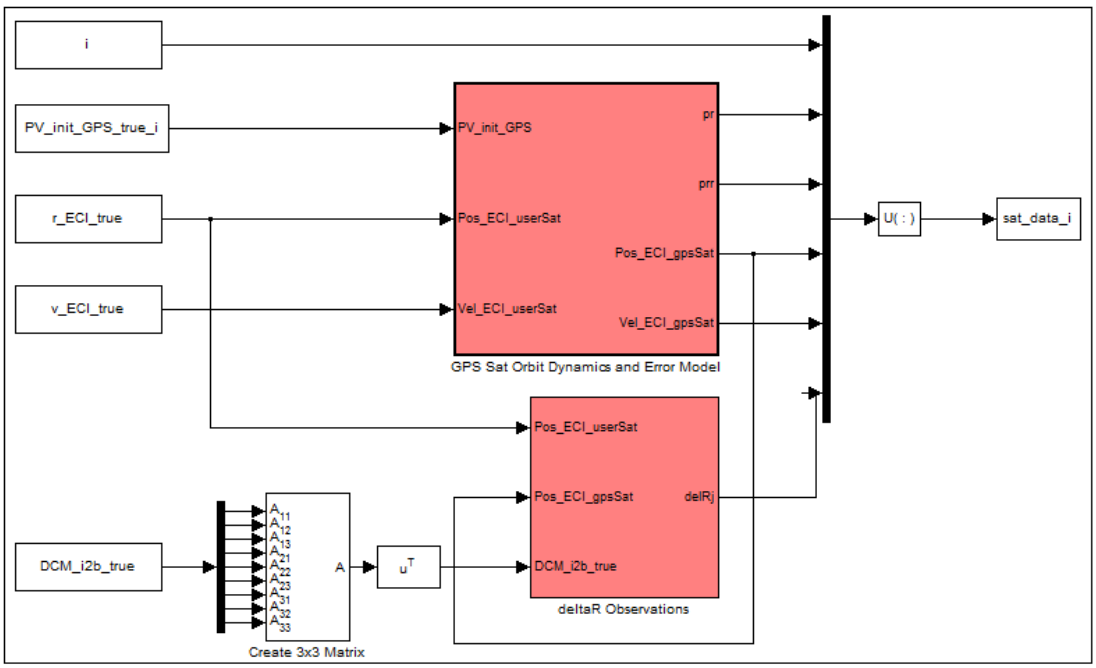

Figure 30: GPS Data Generation Simulink Model

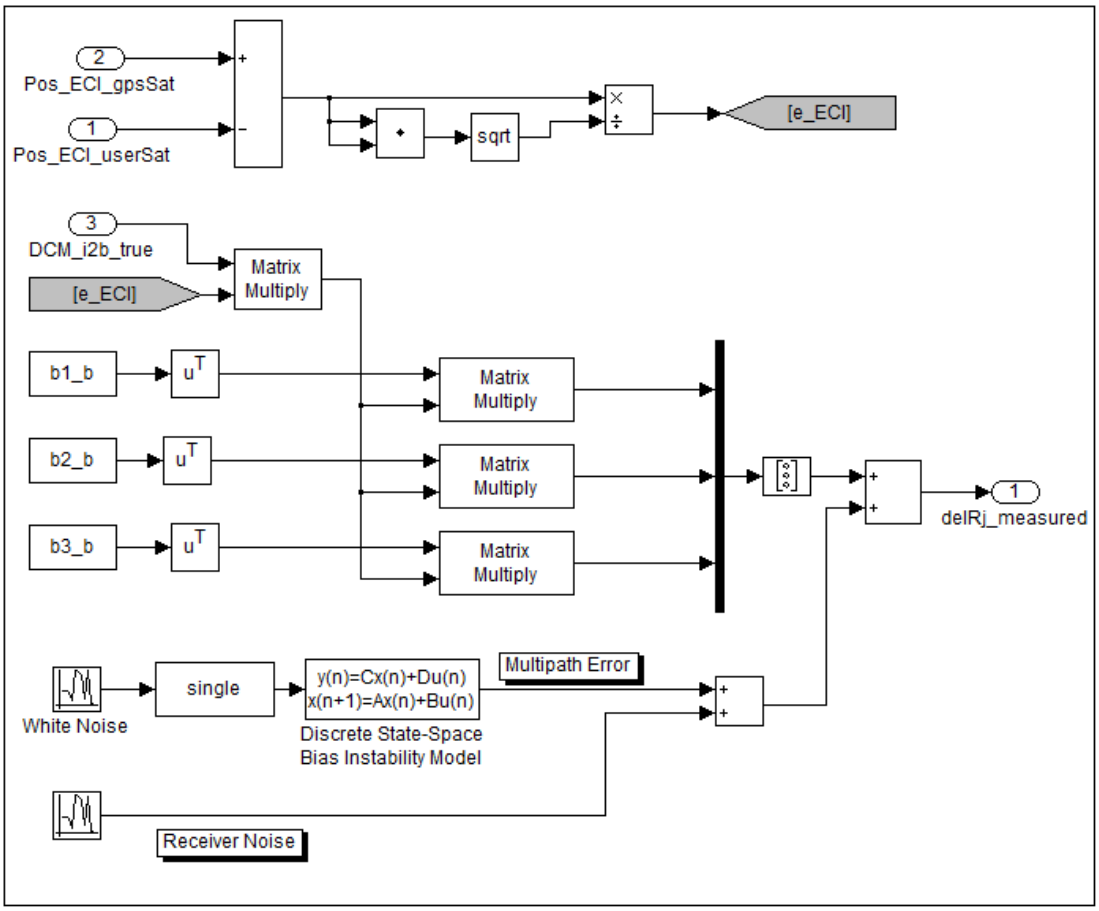

Figure 31: Delta Range Measurement Generation Simulink Model

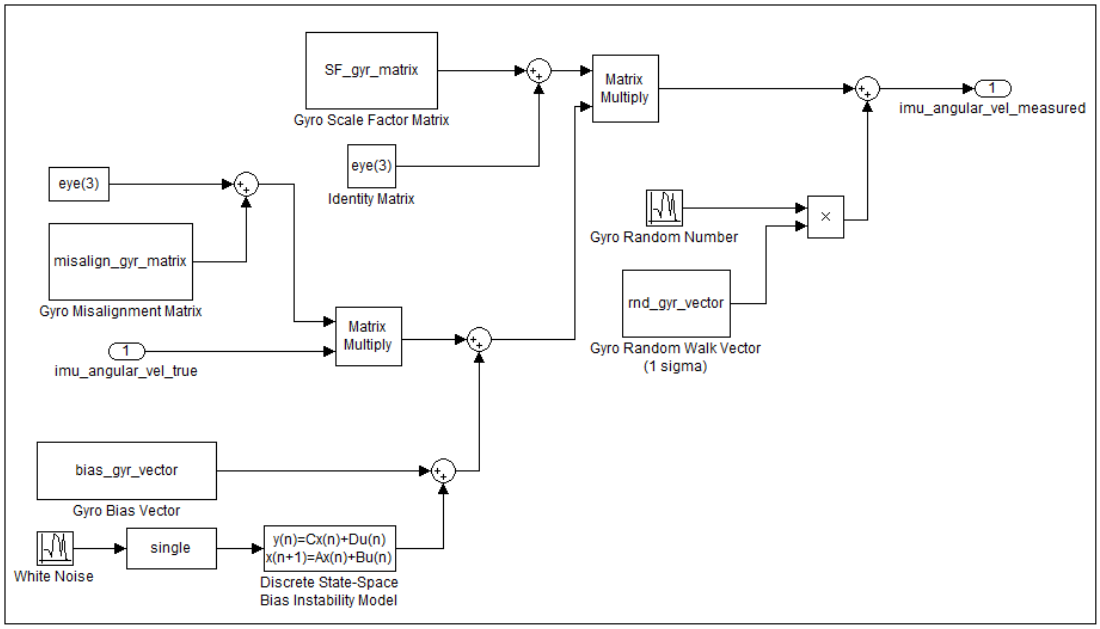

Figure 32: Gyro Error Model Simulink Model

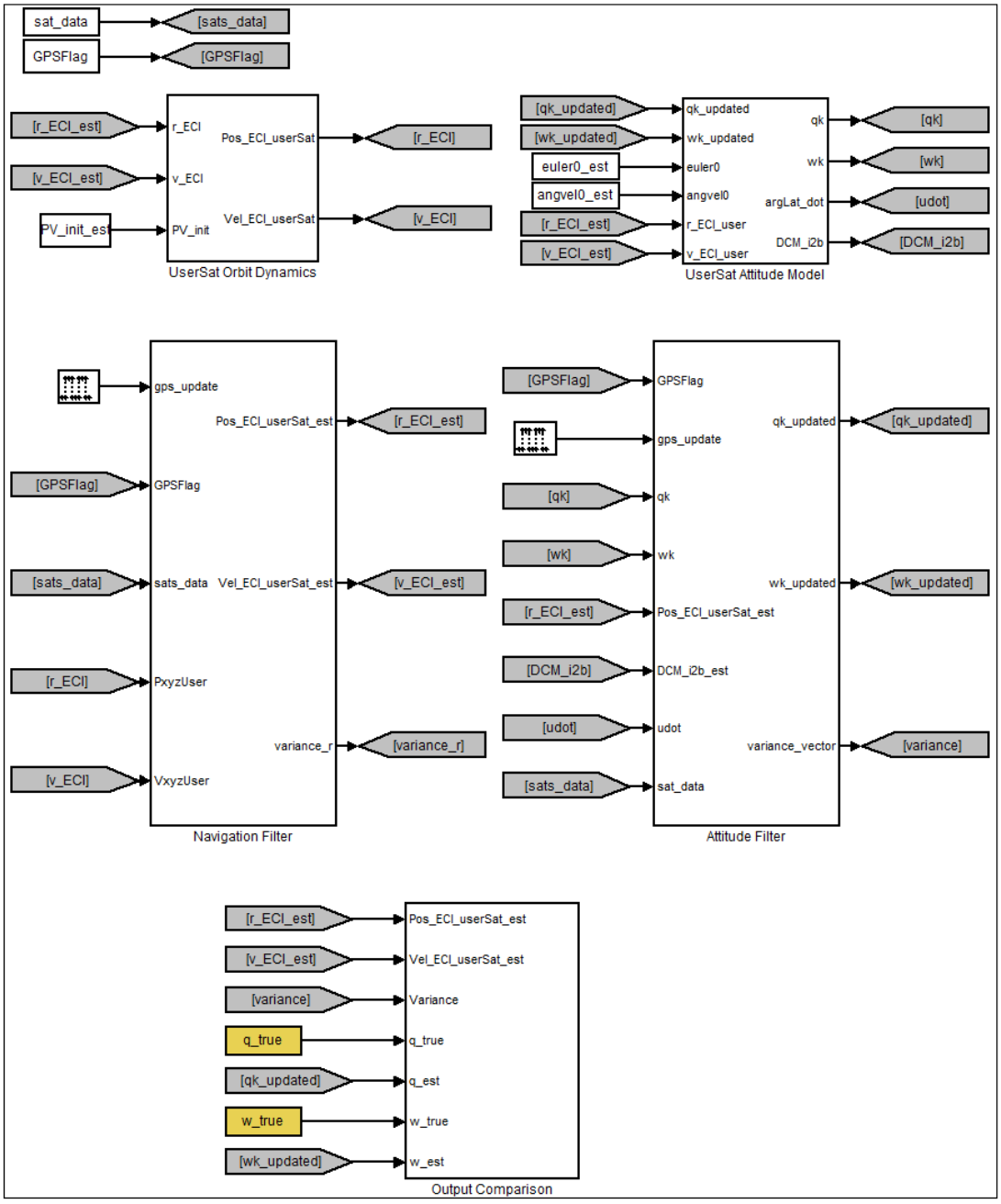

Figure 33: Attitude Estimation Simulink Model

APPENDIX G

NAVIGATION FILTER

A navigation filter is developed in order to estimate the user satellite position and velocity by using the pseudorange and pseudorange rate measurements from the GPS receiver. An EKF is conducted for this purpose. The Kalman filter equations given in Equations 6.9 - 6.13 are used.

The state vector is selected as three position and three velocity components of the user satellite with respect to the ECI frame.

$$\boldsymbol{\delta x} = [\delta \mathrm{x}\ \delta \mathrm{y}\ \delta \mathrm{z}\ \delta \dot{x}\ \delta \dot{y}\ \delta \dot{z}]^T \tag{G.37}$$

where

$$\boldsymbol{\delta x} = \hat{\boldsymbol{x}} - \boldsymbol{x} \tag{G.38}$$

The user satellite orbit dynamics equation given in Equation 5.14 is linearized in order to obtain the system model matrix (F). The linearization is performed as Equation 6.4.

$$F(x,t) = \begin{bmatrix} \frac{\partial \dot{x}}{\partial x} & \frac{\partial \dot{x}}{\partial y} & \frac{\partial \dot{x}}{\partial z} & \frac{\partial \dot{x}}{\partial \dot{x}} & \frac{\partial \dot{x}}{\partial \dot{y}} & \frac{\partial \dot{x}}{\partial \dot{z}} \\ \frac{\partial \dot{y}}{\partial x} & \frac{\partial \dot{y}}{\partial y} & \frac{\partial \dot{y}}{\partial z} & \frac{\partial \dot{y}}{\partial \dot{x}} & \frac{\partial \dot{y}}{\partial \dot{y}} & \frac{\partial \dot{y}}{\partial \dot{z}} \\ \frac{\partial \dot{z}}{\partial x} & \frac{\partial \dot{z}}{\partial y} & \frac{\partial \dot{z}}{\partial z} & \frac{\partial \dot{z}}{\partial \dot{x}} & \frac{\partial \dot{z}}{\partial \dot{y}} & \frac{\partial \dot{z}}{\partial \dot{z}} \\ \frac{\partial \ddot{x}}{\partial x} & \frac{\partial \ddot{x}}{\partial y} & \frac{\partial \ddot{x}}{\partial z} & \frac{\partial \ddot{x}}{\partial \dot{x}} & \frac{\partial \ddot{x}}{\partial \dot{y}} & \frac{\partial \ddot{x}}{\partial \dot{z}} \\ \frac{\partial \ddot{y}}{\partial x} & \frac{\partial \ddot{y}}{\partial y} & \frac{\partial \ddot{y}}{\partial z} & \frac{\partial \ddot{y}}{\partial \dot{x}} & \frac{\partial \ddot{y}}{\partial \dot{y}} & \frac{\partial \ddot{y}}{\partial \dot{z}} \\ \frac{\partial \ddot{z}}{\partial x} & \frac{\partial \ddot{z}}{\partial y} & \frac{\partial \ddot{z}}{\partial z} & \frac{\partial \ddot{z}}{\partial \dot{x}} & \frac{\partial \ddot{z}}{\partial \dot{y}} & \frac{\partial \ddot{z}}{\partial \dot{z}} \end{bmatrix} \tag{G.39}$$

After taking the partial derivatives, the F matrix can be found as:

$$F(x,t)=\begin{bmatrix}0 & 0 & 0 & 1 & 0 & 0\\ 0 & 0 & 0 & 0 & 1 & 0\\ 0 & 0 & 0 & 0 & 0 & 1\\ F_{4,1} & F_{4,2} & F_{4,3} & 0 & 0 & 0\\ F_{5,1} & F_{5,2} & F_{5,3} & 0 & 0 & 0\\ F_{6,1} & F_{6,2} & F_{6,3} & 0 & 0 & 0\end{bmatrix} \quad \text{G.40}$$

The derivations of the undefined parts are given in Equations G.42-G.50. For simplicity, the orbit dynamics equations in Equation 5.14 are modified as below:

$$\begin{aligned}\ddot{x} &= \mathrm{A}(1+\mathrm{B})\\ \ddot{\mathrm{y}} &= \mathrm{C}(1+\mathrm{B})\\ \ddot{\mathrm{z}} &= \mathrm{D}(1+\mathrm{E})\end{aligned} \quad \text{G.41}$$

where

$$A=\frac{-\mu x}{r^3}$$

$$B=-\frac{3}{2}J_2\left(\frac{R_e}{r}\right)^2\left(5\frac{z^2}{r^2}-1\right)$$

$$C=\frac{-\mu y}{r^3}$$

$$D=\frac{-\mu z}{r^3}$$

$$\mathrm{E}=-\frac{3}{2}\mathrm{J}_2\left(\frac{\mathrm{R_e}}{\mathrm{r}}\right)^2\left(5\frac{\mathrm{z}^2}{\mathrm{r}^2}-3\right)$$

$$F_{4,1}=\frac{\partial\ddot{x}}{\partial x}=\left(\frac{\partial A}{\partial x}+\frac{\partial A}{\partial r}\frac{\partial r}{\partial x}\right)(1+B)+A\left(\frac{\partial B}{\partial x}+\frac{\partial B}{\partial r}\frac{\partial r}{\partial x}\right) \quad \text{G.42}$$

$$=\left[\frac{-\mu}{r^3}+\frac{3\mu x}{r^4}\frac{x}{r}\right]\left[1-\frac{3}{2}J_2\left(\frac{R_e}{r}\right)^2\left(5\frac{z^2}{r^2}-1\right)\right]+\frac{-\mu x}{r^3}\left[0+\frac{3J_2}{\mathrm{r}}\left(\frac{R_e}{r}\right)^2\left(10\frac{z^2}{r^2}-1\right)\frac{x}{r}\right]$$

$$=\frac{-\mu}{r^3}\left[1-\frac{3}{2}J_2\left(\frac{R_e}{r}\right)^2\left(5\frac{z^2}{r^2}-1\right)\right]+\frac{3\mu x^2}{r^5}\left[1-\frac{5}{2}J_2\left(\frac{R_e}{r}\right)^2\left(7\frac{z^2}{r^2}-1\right)\right]$$

$$F_{4,2}=\frac{\partial\ddot{x}}{\partial y}=\left(\frac{\partial A}{\partial y}+\frac{\partial A}{\partial r}\frac{\partial r}{\partial y}\right)(1+B)+A\left(\frac{\partial B}{\partial y}+\frac{\partial B}{\partial r}\frac{\partial r}{\partial y}\right) \quad \text{G.43}$$

$$=\left(0+\frac{3\mu x}{r^4}\frac{y}{r}\right)\left[1-\frac{3}{2}J_2\left(\frac{R_e}{r}\right)^2\left(5\frac{z^2}{r^2}-1\right)\right]+\frac{-\mu x}{r^3}\left[0+\frac{3J_2}{\mathrm{r}}\left(\frac{R_e}{r}\right)^2\left(10\frac{z^2}{r^2}-1\right)\frac{y}{r}\right]$$

$$=\frac{3\mu xy}{r^5}\left[1-\frac{5}{2}J_2\left(\frac{R_e}{r}\right)^2\left(7\frac{z^2}{r^2}-1\right)\right]$$

$$F_{4,3} = \frac{\partial \ddot{x}}{\partial z} = \left(\frac{\partial A}{\partial z} + \frac{\partial A}{\partial r}\frac{\partial r}{\partial z}\right)(1+B) + A\left(\frac{\partial B}{\partial z} + \frac{\partial B}{\partial r}\frac{\partial r}{\partial z}\right) \quad \text{G.44}$$

$$= \left(0 + \frac{3\mu x}{r^4}\frac{z}{r}\right)\left[1 - \frac{3}{2}J_2\left(\frac{R_e}{r}\right)^2\left(5\frac{z^2}{r^2} - 1\right)\right] + \frac{-\mu x}{r^3}\left[J_2\left(\frac{R_e}{r}\right)^2\left\{-15\frac{\mathrm{z}}{r^2} + \frac{3}{\mathrm{r}}\left(10\frac{z^2}{r^2} - 1\right)\frac{z}{r}\right\}\right]$$

$$= \frac{3\mu xz}{r^5}\left[1 - \frac{5}{2}J_2\left(\frac{R_e}{r}\right)^2\left(7\frac{z^2}{r^2} - 3\right)\right]$$

$$F_{5,1} = \frac{\partial \ddot{y}}{\partial x} = \left(\frac{\partial C}{\partial x} + \frac{\partial C}{\partial r}\frac{\partial r}{\partial x}\right)(1+B) + C\left(\frac{\partial B}{\partial x} + \frac{\partial B}{\partial r}\frac{\partial r}{\partial x}\right) \quad \text{G.45}$$

$$= \left(0 + \frac{3\mu y}{r^4}\frac{x}{r}\right)\left[1 - \frac{3}{2}J_2\left(\frac{R_e}{r}\right)^2\left(5\frac{z^2}{r^2} - 1\right)\right] + \frac{-\mu y}{r^3}\left[0 + \frac{3J_2}{\mathrm{r}}\left(\frac{R_e}{r}\right)^2\left(10\frac{z^2}{r^2} - 1\right)\frac{x}{r}\right]$$

$$= \frac{3\mu xy}{r^5}\left[1 - \frac{5}{2}J_2\left(\frac{R_e}{r}\right)^2\left(7\frac{z^2}{r^2} - 1\right)\right]$$

$$F_{5,2} = \frac{\partial \ddot{y}}{\partial y} = \left(\frac{\partial C}{\partial y} + \frac{\partial C}{\partial r}\frac{\partial r}{\partial y}\right)(1+B) + C\left(\frac{\partial B}{\partial y} + \frac{\partial B}{\partial r}\frac{\partial r}{\partial y}\right) \quad \text{G.46}$$

$$= \left[\frac{-\mu}{r^3} + \frac{3\mu y}{r^4}\frac{y}{r}\right]\left[1 - \frac{3}{2}J_2\left(\frac{R_e}{r}\right)^2\left(5\frac{z^2}{r^2} - 1\right)\right] + \frac{-\mu y}{r^3}\left[0 + \frac{3J_2}{\mathrm{r}}\left(\frac{R_e}{r}\right)^2\left(10\frac{z^2}{r^2} - 1\right)\frac{y}{r}\right]$$

$$= \frac{-\mu}{r^3}\left[1 - \frac{3}{2}J_2\left(\frac{R_e}{r}\right)^2\left(5\frac{z^2}{r^2} - 1\right)\right] + \frac{3\mu y^2}{r^5}\left[1 - \frac{5}{2}J_2\left(\frac{R_e}{r}\right)^2\left(7\frac{z^2}{r^2} - 1\right)\right]$$

$$F_{5,3} = \frac{\partial \ddot{y}}{\partial z} = \left(\frac{\partial C}{\partial z} + \frac{\partial C}{\partial r}\frac{\partial r}{\partial z}\right)(1+B) + C\left(\frac{\partial B}{\partial z} + \frac{\partial B}{\partial r}\frac{\partial r}{\partial z}\right) \quad \text{G.47}$$

$$= \left(0 + \frac{3\mu y}{r^4}\frac{z}{r}\right)\left[1 - \frac{3}{2}J_2\left(\frac{R_e}{r}\right)^2\left(5\frac{z^2}{r^2} - 1\right)\right] + \frac{-\mu y}{r^3}\left[J_2\left(\frac{R_e}{r}\right)^2\left\{-15\frac{\mathrm{z}}{r^2} + \frac{3}{\mathrm{r}}\left(10\frac{z^2}{r^2} - 1\right)\frac{z}{r}\right\}\right]$$

$$= \frac{3\mu yz}{r^5}\left[1 - \frac{5}{2}J_2\left(\frac{R_e}{r}\right)^2\left(7\frac{z^2}{r^2} - 3\right)\right]$$

$$F_{6,1} = \frac{\partial \ddot{z}}{\partial x} = \left(\frac{\partial D}{\partial x} + \frac{\partial D}{\partial r}\frac{\partial r}{\partial x}\right)(1+E) + D\left(\frac{\partial E}{\partial x} + \frac{\partial E}{\partial r}\frac{\partial r}{\partial x}\right) \quad \text{G.48}$$

$$= \left(0 + \frac{3\mu z}{r^4}\frac{x}{r}\right)\left[1 - \frac{3}{2}J_2\left(\frac{R_e}{r}\right)^2\left(5\frac{z^2}{r^2} - 3\right)\right] + \frac{-\mu z}{r^3}\left[0 + \frac{3J_2}{\mathrm{r}}\left(\frac{R_e}{r}\right)^2\left(10\frac{z^2}{r^2} - 3\right)\frac{x}{r}\right]$$

$$= \frac{3\mu xz}{r^5}\left[1 - \frac{5}{2}J_2\left(\frac{R_e}{r}\right)^2\left(7\frac{z^2}{r^2} - 3\right)\right]$$

$$F_{6,2} = \frac{\partial \ddot{z}}{\partial y} = \left(\frac{\partial D}{\partial y} + \frac{\partial D}{\partial r}\frac{\partial r}{\partial y}\right)(1+E) + D\left(\frac{\partial E}{\partial y} + \frac{\partial E}{\partial r}\frac{\partial r}{\partial y}\right) \quad \text{G.49}$$

$$= \left(0 + \frac{3\mu z}{r^4}\frac{y}{r}\right)\left[1 - \frac{3}{2}J_2\left(\frac{R_e}{r}\right)^2\left(5\frac{z^2}{r^2} - 3\right)\right] + \frac{-\mu z}{r^3}\left[0 + \frac{3J_2}{\mathrm{r}}\left(\frac{R_e}{r}\right)^2\left(10\frac{z^2}{r^2} - 3\right)\frac{y}{r}\right]$$

$$= \frac{3\mu yz}{r^5}\left[1 - \frac{5}{2}J_2\left(\frac{R_e}{r}\right)^2\left(7\frac{z^2}{r^2} - 3\right)\right]$$

$$F_{6,3} = \frac{\partial \ddot{z}}{\partial z} = \left(\frac{\partial D}{\partial z} + \frac{\partial D}{\partial r}\frac{\partial r}{\partial z}\right)(1+E) + D\left(\frac{\partial E}{\partial z} + \frac{\partial E}{\partial r}\frac{\partial r}{\partial z}\right) \quad \text{G.50}$$

$$= \left(\frac{-\mu}{r^3} + \frac{3\mu z}{r^4}\frac{z}{r}\right)\left[1 - \frac{3}{2}J_2\left(\frac{R_e}{r}\right)^2\left(5\frac{z^2}{r^2} - 3\right)\right] + \frac{-\mu z}{r^3}\left[J_2\left(\frac{R_e}{r}\right)^2\left\{-15\frac{\mathrm{z}}{r^2} + \frac{3}{\mathrm{r}}\left(10\frac{z^2}{r^2} - 3\right)\frac{z}{r}\right\}\right]$$

$$= \frac{-\mu}{r^3}\left[1 - \frac{3}{2}J_2\left(\frac{R_e}{r}\right)^2\left(5\frac{z^2}{r^2} - 3\right)\right] + \frac{3\mu z^2}{r^5}\left[1 - \frac{5}{2}J_2\left(\frac{R_e}{r}\right)^2\left(7\frac{z^2}{r^2} - 5\right)\right]$$

The measurement residuals are calculated as differencing the measured and the estimated pseudorange and its rate:

$$\delta\rho = \rho - \hat{\rho} = \rho - |\boldsymbol{r_{rel}}| \quad \text{G.51}$$

$$\delta\dot{\rho} = \dot{\rho} - \hat{\dot{\rho}} = \dot{\rho} - \boldsymbol{V_{rel}} \cdot \boldsymbol{u_{r_{rel}}} \quad \text{G.52}$$

where $\boldsymbol{r_{rel}}$ and $\boldsymbol{V_{rel}}$ is the position and velocity of the GPS satellite with respect to the user satellite respectively. $\boldsymbol{u_{r_{rel}}}$ is the unit vector in the $\boldsymbol{r_{rel}}$ direction. The calculations of these parameters are performed as follows:

$$\boldsymbol{r_{rel}} = \boldsymbol{r_{GPS}} - \hat{\boldsymbol{r}}_U = (x_{GPS} - x_U)\boldsymbol{i} + (y_{GPS} - y_U)\boldsymbol{j} + (z_{GPS} - z_U)\boldsymbol{k} \quad \text{G.53}$$

$$\boldsymbol{u_{r_{rel}}} = \frac{\boldsymbol{r_{rel}}}{|\boldsymbol{r_{rel}}|} = \frac{(x_{GPS} - x_U)\boldsymbol{i} + (y_{GPS} - y_U)\boldsymbol{j} + (z_{GPS} - z_U)\boldsymbol{k}}{\sqrt{(x_{GPS} - x_U)^2 + (y_{GPS} - y_U)^2 + (z_{GPS} - z_U)^2}} \quad \text{G.54}$$

$$\boldsymbol{V_{rel}} = \dot{\boldsymbol{r}}_{\boldsymbol{GPS}} - \dot{\boldsymbol{r}}_{\boldsymbol{U}} = (\dot{x}_{GPS} - \dot{x}_U)\boldsymbol{i} + (\dot{y}_{GPS} - \dot{y}_U)\boldsymbol{j} + (\dot{z}_{GPS} - \dot{z}_U)\boldsymbol{k} \quad \text{G.55}$$

$\boldsymbol{i}$, $\boldsymbol{j}$, and $\boldsymbol{k}$ represents the unit vectors in the X_I, Y_I, and Z_I directions.

Bu using the measurement residuals in Equations G.51-G.52 , the measurement matrix (H) for the navigation filter is found as:

$$\mathrm{H} = \begin{bmatrix} \frac{\delta\rho}{\delta x} & \frac{\delta\rho}{\delta y} & \frac{\delta\rho}{\delta z} & \frac{\delta\rho}{\delta \dot{x}} & \frac{\delta\rho}{\delta \dot{y}} & \frac{\delta\rho}{\delta \dot{z}} \\ \frac{\delta\dot{\rho}}{\delta x} & \frac{\delta\dot{\rho}}{\delta y} & \frac{\delta\dot{\rho}}{\delta z} & \frac{\delta\dot{\rho}}{\delta \dot{x}} & \frac{\delta\dot{\rho}}{\delta \dot{y}} & \frac{\delta\dot{\rho}}{\delta \dot{z}} \end{bmatrix} \quad \text{G.56}$$

$$\mathrm{H} = \begin{bmatrix} u_{r_{rel,1}} & u_{r_{rel,2}} & u_{r_{rel,3}} & 0 & 0 & 0 \\ \frac{V_{rel,1}}{|r_{rel}|} & \frac{V_{rel,2}}{|r_{rel}|} & \frac{V_{rel,3}}{|r_{rel}|} & u_{r_{rel,1}} & u_{r_{rel,2}} & u_{r_{rel,3}} \end{bmatrix} \quad \text{G.57}$$

where $u_{r_{rel,1}}$, $u_{r_{rel,2}}$, and $u_{r_{rel,3}}$ represents the three components of the vector $\boldsymbol{u}_{\boldsymbol{r}_{\boldsymbol{rel}}}$,such that:

$$\boldsymbol{u}_{\boldsymbol{r}_{\boldsymbol{rel}}} = u_{r_{rel,1}}\boldsymbol{i} + u_{r_{rel,2}}\boldsymbol{j} + u_{r_{rel,3}}\boldsymbol{k}$$

After the error in the position and velocity is estimated using the developed EKF, the correction operation is performed as:

$$x = \hat{x} - \delta x \qquad \text{G.58}$$

REFERENCES

[1] Bak, T., "Spacecraft Attitude Determination - a Magnetometer Approach", Ph.D. dissertation, Department of Control Engineering, Aalborg University, Aalborg, Denmark, 1999.

[2] Lightsey, E. G., Madsen, J., "Three Axis Attitude Determination Using GPS Signal Strength Measurements", *Journal of Guidance, Control and Dynamics*, Vol.26, No.2, March-April 2003.

[3] Wang, C., "Development of a Low-cost GPS-based Attitude Determination System", M.S. thesis, Department of Geomatics Engineering, University of Calgary, Calgary, Alberta, 2003.

[4] Lightsey, E. G., "Development and Flight Demonstration of a GPS Receiver for Space", Ph.D. dissertation, Department of Aeronautics and Astronautics Engineering, Stanford University, Stanford, CA, 1997.

[5] Adams, J. C., "Robust GPS Attitude Determination for Spacecraft", Ph.D. dissertation, Department of Aeronautics and Astronautics Engineering, Stanford University, Stanford, CA, 1999.

[6] James, R. W., *Spacecraft Attitude Determination and Control*, Dordrecht: Kluwer Academic Publishers, 1990.

[7] Sevaston, G. E. et al., "GPS Based Attitude Determination for Spacecraft: System Engineering Design Study and Ground Testbed Results", *Guidance and Control*, vol. 7-11, February 1996, Breckenridge, CO.

[8] Lu, G., "Development of a GPS Multi-Antenna System for Attitude Determination", Ph.D. dissertation, Department of Geomatics Engineering, University of Calgary, Calgary, Alberta, 1995.

[9] Langley, R. B., "The Orbits of GPS Satellites", *Journal of GPS World*, Vol.2, No.3, March 1991.

[10] Petrovskyy, V., Tretyak, V., "Precise GPS Position and Attitude", M.S. thesis, Faculty of Engineering and Science, Aalborg University, Aalborg, Denmark, 2007.

[11] Farrell, J. A., *Aided Navigation: GPS with High Rate Sensors*, New York: McGraw-Hill, 2008.

[12] Geiger, A., "Modeling of Phase Center Variation and Its Influence on GPS Positioning", *GPS Techniques Applied to Geodesy and Surveying, Lecture Notes in Earth Sciences*, Vol. 19, Springer-Verlag, Berlin, 1988.

[13] Khanafseh, S., Langel, S., Pervan, B., "Overbounding Position Errors in the Presence of Carrier Phase Multipath Error Model Uncertainty", *Proceedings of IEEE/ION PLANS 2010*, 2010, pp. 575-584.

[14] El-Diasty, M., Pagiatakis, S., "Calibration and Stochastic Modelling of Inertial Navigation Sensor Errors", *Journal of Global Positioning Systems*, Vol.7, No. 2, pp. 170-182, 2008.

[15] Marreiros, J., P., "Performance Analysis of GPS Attitude Determination in a Hydrographic Survey Launch", M.S. thesis, Geodesy and Geomatics Engineering, University of New Brunswick, New Brunswick, Canada, 1997.

[16] Lightsey, E. G., Crassidis, J. L., "Real Time Attitude Independent GPS Integer Ambiguity Resolution", *AAS John L. Junkins Astrodynamics Symposium*, College Station, TX, May 2003.

[17] Abidin, H. Z., "On the Construction of the Ambiguity Searching Space for on-the-fly Ambiguity Resolution", *Journal of The Institute of Navigation*, Vol.40, No.3, 1993, pp. 321-338.

[18] Yoon, S., Lundberg, J. B., "An Integer Ambiguity Resolution Algorithm for Real-Time GPS Attitude Determination", *Journal of Applied Mathematics and Computation*, Vol.129, Issue 1, 15 June 2002, Pages 21‑41

[19] Titterton, D. H., Weston, J. L., *Strapdown Inertial Navigation Technology*, Stevenage, UK: IEE, 2004.

[20] Groves, P., *Principles of GNSS, Inertial, and Multisensor Integrated Navigation Systems*, US: Artech House, 2008.

[21] Yole Développement Report, "Gyroscopes and IMUs for Defense, Aerospace & Industrial", Lyon, France, 2012.

[22] Juang, J., Radharamanan,R., "Evaluation of Ring Laser and Fiber Optic GYROSCOPE Technology", Mercer University, School of Engineering, Macon, GA, USA.

[23] Miller,L.M., "MEMS for Space Applications", *Proceedings of SPIE*, Vol.3680, p. 2-11, May 1999.

[24] Brady, T.M, "Expanding the Spacecraft Application Base with MEMS Gyros", The Draper Technology Digest, Vol.16, 2012.

[25] Ling-juan, M. et al., "Derivation of Nonlinear Error Equation of Strapdown INS Using Quaternions", *Proceedings of the 41st SICE Annual Conference*, Vol.5, Osaka, August 2002.

[26] Han, S., Rizos, C., "Single Epoch Ambiguity Resolution for Real-Time GPS Attitude Determination with the Aid of One Dimensional Optical Fibre Gyro", *GPS Solutions: The Journal of Global Navigation Satellite Systems*, Vol.3, Issue 1, pp 5-12, July 1999.

[27] Andrei, C.O. et al.,"Ionosphere Effect Mitigation for SingleFrequency Precise Point Positioning", *Proceedings of the 22nd International Technical Meeting of The Satellite Division of the Institute of Navigation(ION GNSS 2009)*, Savannah, GA, September 2009, pp. 2508-2517.

[28] Sharaf, M.A., Selim, H.H., "Motion in cylindrical coordinates: applications to J2 gravity perturbed trajectories of space dynamics", *Contributions of the Astronomical Observatory Skalnaté Pleso*, Vol. 41, No. 1, pp. 54-62, 2011.

[29] Povero, G., "GNSS Introduction", class notes for 1.1, Master on Navigation and Related Applications, Politecnico di Torino, October 2009.

[30] Viola, N., "Basics on Geomagnetics and Satellite Orbits", class notes for 0.3, Master on Navigation and Related Applications, Politecnico di Torino, October 2009.